Ecosystem-based Approaches for Developing Resilience to Landslide Risk in Japan and Nepal

A Thesis submitted to
The Division of Sciences for Bioproduction and Environment
Graduate School of Bioresources and Environmental Sciences
and the committee on graduate studies of Ishikawa Prefectural University, Japan
In Partial fulfillment of the requirements for the degree of Doctor of Philosophy.

Submitted by
(.....)
Prakash Singh Thapa
Ph.D. Student
2023

Supervisors
I certify that I have read this thesis and that, in my opinion, it is fully adequate in scope and quality as a thesis for the degree of Doctor of Philosophy.

(.....)
Supervisor

(.....)
Supervisor

Approved for the University Committee on Graduate Studies

(.....)

TABLE OF CONTENT

ACKNOWLEDGEMENT

I want to express my deep appreciation and respect to my esteemed supervisors, Professor Dr. Seiji Yanai and Professor Dr. Hiromu Daimaru, from the Division of Sciences for Bioproduction and Environment at the Graduate School of Bioresources and Environmental Sciences at Ishikawa Prefectural University. Their guidance and active support throughout my research work, as well as their supervision in the classroom, laboratory, and fieldwork, have been invaluable. They have shown a remarkable level of trust in my abilities, and I am honored to have learned under their guidance.

I would also like to acknowledge Professor Dr. Toshihiko Momose, Professor Dr. Eiji Ichion, Professor Dr. Naoya Katsumi and former graduate student Mr. Kazeto Hanzawa for sharing their knowledge, data and experiences.

I am grateful to the JDS project for awarding me a full scholarship to pursue my studies at Ishikawa Prefectural University. This scholarship has provided financial support and the opportunity to immerse myself in a culturally diverse environment, enriching my overall educational experience. Thank you for this tremendous opportunity. I also extend my thanks to Ishikawa Prefectural University for awarding me a university grant to support my research activities during my study period, enabling me to access necessary resources and equipment to conduct my studies effectively. I am deeply thankful to all my previous teachers, senior officials in Nepal, JDS staffs in Japan and Nepal, for their invaluable support, cooperation, and facilitation in pursuing my academic aspirations. I would like to thank Ministry of Forests and Environment, Government of Nepal, for providing me with official leave to pursue my Ph.D. studies.

My genuine gratitude goes to my father and mother for being the pillars of strength in my life. Their unwavering support, encouragement, and sacrifices have been the driving force behind my success. Finally, I am heartily grateful to my wife (Bindu Ghimire) and son (Bipra Singh Thapa) for their unwavering support during the challenging period of beginning my studies amidst the Covid situation. Their constant encouragement, understanding, and sacrifices have been instrumental in accomplishing the Ph.D. during such trying times. Thank you.

EXECUTIVE SUMMARY

Landslides take the lives of people, destroy properties, and are a threat to communities. Large-scale landslides have multiple ecological impacts that affect not only the nearby area to the landslide but also distant downstream areas such as the river environment, fish habitat, and agricultural lands. Many engineering structures as well as nonstructural technologies have been in use for the management of landslides. Structural structures such as retaining walls, breast walls, and bolsters, are used. Non-structural measures utilized are hazard mapping, early warning systems, and ecosystem-based solutions. Ecosystem-based solutions are plantation and managing nature-based solutions, For the mitigation of landslide disasters, ecosystem-based solutions are getting attention in the global scenario.

In this study landslides and ecosystem-based solutions focusing on two landslides in Japan and one landslide in Nepal are studied in detail.

In Japan, the Sennindani and Hirose landslides were selected to understand the evolution of the landslide, downstream impacts of sediment transported, and restoration techniques used to manage these landslides. In Nepal, the Methum landslide was selected where the Landslide monitoring system was established. The effectiveness of the early warning system as soft structure for landslide risk mitigation was assessed.

The historical aerial photos of Sennindani revealed that the landslide activity in the area started at least 65 years ago. The volume of mass mobilized during smaller landslides in 2014 and the main event in 2015 were calculated at nearly 50,000 m^3 and 1.3 million m^3, respectively. The sediment from the 2015 landslide flowed along the Ozo River and ultimately joined the Tedori River downstream, causing increased turbidity in the Tedori River and affecting fish ecology, water recharge functions, and riverbed alterations. The irrigation canal network supplied the turbid water in the alluvial fan, causing sediment deposition in the paddy fields leading to reduced infiltration rates and a decrease in groundwater levels. Further, the spawning sites of Ayu fish along the Tedori River were destroyed, resulting in a decrease in the number of eggs laid, and the Tomiyo fish disappeared downstream of the alluvial fan in Kumada River. Chum salmon showed an unusually high movement towards the Tedori River during 2015 and 2016 and captured both near coastal and Tedori river mouth areas.

To restore the Sennindani landslide, various techniques were employed, including the use of soft structures and reforestation. Mortar was sprayed in 2015 to prevent soil erosion, and organic erosion inhibitors were applied in 2016 and 2017. Grass and tree seeds aided with

fertilizer and willow cuttings were broadcasted from 2017 to 2021, and organic erosion inhibitors were reapplied in 2020 and 2021. By 2022, green patches of planted grasses and trees had developed on the upper slope of the landslide. Hirose landslide occurred in 2021 in Hirose-town, Hakusan City, in Japan. Cedar trees were found to be effective in minimizing debris flow of this landslide. Cedar trees planted across the lower belt of the landslide acted as a barrier to stop debris flow and mitigate sediment spreading. The Methum landslide in Nepal posed a threat to settlements and agricultural lands, and a Landslide Early Warning System (LEWS) was used to monitor the landslide movement. The LEWS system monitored rainfall, land displacement, and soil moisture. This LEWS proved effective in some incidences of Methum landslide reactivation by providing alarms when the set thresholds were exceeded.

Ecosystem-based solutions for landslides, as studied in the Sennindani and Hirose landslides of Japan, evidenced that the use of plantation of native species can assist in the restoration of the landslide as well as in the mitigation of debris flow to longer distances. On the other hand, the landslide early warning system used in the case of the Methum landslide in Nepal depicted that this low-cost early warning system can be an effective tool to minimize landslide risk by generating early warnings. However, both need careful consideration while installing to mitigate the risk.

For this research study, we used aerial photographs, satellite images, airborne LiDAR data, UAV photographs, and SAR data for assessing the evolution of landslides and sedimentation. We conducted a cross-sectional analysis of secondary data to assess the potential effects of discharged sediments on the downstream environment, including long-term turbidity in rivers, alterations in fish habitats, and groundwater depletion. To analyze the spatiotemporal changes in the riverbed elevation and paddy fields, aerial photographs and Airborne Light Detection and Ranging data were assessed using the ArcGIS software.

In conclusion, it is essential to implement a combination of ecosystem-based solutions and early warning systems while considering the holistic approach to mitigate landslide risk and ensure community resilience against landslide disasters.

The main structure of the thesis is designed from introduction to conclusion and includes some auxiliary chapters. Chapter 1 provides a theoretical background on natural hazard-induced disasters, particularly landslides, and focuses on landslide management techniques with an emphasis on Eco-DRR. The objectives, both general and specific, of the thesis study

are also presented in this chapter. In Chapter 2, relevant terminology used in the dissertation is briefly defined. Chapter 3 provides detailed explanations of two case studies, namely the Sennindani landslide and Hirose landslide, which occurred in Japan. Chapter 4 describes the Geomorphological Assessment and discusses the effectiveness of the Landslide Early Warning System. Chapter 5 focuses on the role of forest ecosystems in landslide restoration and reduction of landslide risk, with lessons learned from the Hirose landslide and Sennindani landslide. Finally, Chapter 6 presents the conclusions of the overall study and provides recommendations for future research.

CHAPTER 1 INTRODUCTION

1.1 Background

Natural hazard-induced disasters have been increasing and intensifying in recent years (Panwar & Sen, 2019) due to the development and use of disaster-prone land due to rapid population growth and urbanization coupled with the effects of changing climate (*UN News*, 2021). Natural disaster events coupled with the changing climate pose an extreme risk to sustainable development over time (Khan et al., 2023). Mostly climate-related natural hazards like floods, landslides, droughts, and wildfires are on the rise, causing humans more suffering (*Annual Disaster Statistical Review 2016*, 2017, Mokhtari et al., 2023).

Landslides are becoming one of the most prominent disasters posing a direct threat to human safety, causing injuries or fatalities in sloppy parts of the world (Emberson et al., 2022). Landslides have caused an average of 13,601 deaths annually, affecting an average of 0.23 million people and resulting in annual economic losses of 0.26 billion US$ during 1991-2020 (Asian Disaster Reduction Center, 2022).

Landslides can have further significant impacts on the environment resulting in the loss of vegetation and habitat (Cui et al., 2012; Highland & Bobrowsky, 2008) while destructive forces of landslides can damage, destroy take the lives of many people, and damage properties demanding a heavy toll on the budget and hindering economic growth in Asian countries (Zhang et al., 2021).

Landslide risk mitigation and management is challenging work in modern times with budget constraints while landslide events are increasing (Winter & Bromhead, 2012). Both engineering infrastructures also known as grey structures, as well as ecosystem-based (often referred to as nature-based solutions or green structures of revegetation measures), are applied for landslide mitigation (Swanston & Schuster, 1989; Bromhead, 1997; Rey et al., 2019; Adhikari & Tian, 2021).

Choices of an appropriate treatment structure depend on (a) engineering feasibility, (b) economic feasibility, (c) legal/regulatory conformity, (d) social acceptability, and (e) environmental acceptability (Popescu & Sasahara, 2009).

Engineering infrastructures such as retaining walls, Gabion walls, Debris flow barriers, check dams, drains, and bolsters are designed to stabilize slopes, protect vulnerable areas, and mitigate and control landslides (Kwong et al., 2004).

On the other hand, In Eco-DRR, natural ecosystems, and their services are used to reduce risks and impacts of disasters on communities, through conservation, restoration, and sustainable management (Estrella and Saalismaa, 2013).

Ecosystem-based approaches utilize vegetation and ecological processes such as soil bioengineering, afforestation/reforestation, water management, and grass plantation to enhance slope stability, reduce erosion, and increase the resilience of landscapes (Moos et al., 2018).

Ecosystem-based solutions are getting higher interest recently from both academic and governmental bodies as they offer multiple benefits beyond slope stabilization (Wamsler & Pauleit, 2016).

Ecosystem-based remedies can lower the susceptibility of communities and downstream ecology to disasters (Kato & Huang, 2021). Ecosystems can act as a buffer zone against natural hazards (Dhyani et al., 2018). Ecosystems also provide food materials and other substances in times of disaster and recovery. Ecosystem-based solutions a low-cost but provide co-benefits at the same time for longer durations. Implementing Ecosystem-based solutions requires site-specific assessment, considering factors such as soil conditions, climate, and vegetation suitability. ECO-DRR recently emerged as a promising disaster mitigatory measure but is not yet established as a long-term solution irrespective of its multiple benefits. Though ECO-DRR may provide a solution for mitigating disaster impacts with various benefits, it has yet to be thoroughly demonstrated as a long-term sustainable choice (Uy & Shaw, 2012). Many academics believe that Ecosystems as shields are not an ultimate complete solution and must be combined with other measures such as disaster planning and early warning systems (Feagin et al., 2010).

This study described the role of vegetation in the restoration and mitigation of landslides and their impacts through case studies in central Japan and presented the role of forest ecosystem to develop resilience against landslide disasters. This type of assessment focusing on Eco-DRR is rare in literature so this documentation of ecosystem-based solutions could be useful

for future planners and conservationists. Further, this study has presented the role of a landslide early warning system to mitigate the landslide disaster risk in Nepal. The combination of both Eco-DRR and Landslide early warning systems is speculated to reduce the landslide disaster risk significantly.

1.2 Objectives

General objectives:

To assess ecosystem-based approaches for developing resilience to landslide risk in Japan and Nepal.

Specific objectives:

I. To detect the evolutionary process, the downstream impacts, and ecosystem based-restoration techniques implemented for the Sennindani 2015 Landslide in Mt. Hakusan, Central Japan.
II. To evaluate the function of Cedar trees as Forest ecosystem in preventing landslide risk in the Hirose landslide, Central Japan.
III. To assess the geomorphological advancement of and effectiveness of the Landslide early warning system installed in Methum landslide Sankhu Watershed, Lalitpur Nepal

CHAPTER 2 LITERATURE REVIEW

2.1 Natural Hazards and Disaster

A hazard is referred to as a potentially destructive physical event, incident, or human action that could result in death or injury, property damage, socioeconomic problems, or environmental damage (UNISDR, 2004). Human-made hazards namely war, famine, fire, pollution, toxic release, industrial accident, laboratory leakage, and civil strife are also equally dangerous to humanity (Mohamed Shaluf, 2007). The primary focus of this article is on natural hazards, excluding any discussion of human-induced hazards. Furthermore, natural hazards of a biological nature, such as infectious diseases and epidemics, are also not addressed in this study. A natural hazard refers to a naturally occurring process or phenomenon that potentially causes harm, injury, damage, loss of life, socioeconomic damage or property destruction, or environmental degradation (UNDRR-ISC, 2020). These hazards are typically a result of natural processes and can occur with varying degrees of predictability.

Common examples of natural hazards (Geophysical and hydrometeorological) include Earthquakes, Floods, Volcanic Eruptions, Landslides, Wildfires, Droughts, etc. (Chaudhary & Piracha, 2021). These natural hazards depict varying natures based on geographical location, frequency, magnitude, and severity. Evaluating and understanding natural hazards becomes of utmost importance for developing effective strategies for risk reduction, disaster preparedness, and resilience in vulnerable areas.

Natural hazards are inevitable, and the loss of property due to natural disasters has been increasing in the past few decades but Natural hazards do not always result in a disastrous event (Carlowicz, 1996). A natural hazard can be called a disaster when a significant loss to humans, property, the economy, or the environment is perceived, and the coping capacity of the community gets exceeded. UNISDR 2009, mentioned that several factors are responsible for contributing to the transformation of natural hazards into disasters such as magnitude and intensity, exposure, vulnerability, and resilience.

2.1.1 Intensity

The magnitude, intensity, and physical strength of the hazard is one of the crucial factors to make the transition to disaster. The magnitude of a severe physical event reflects its size, whereas intensity relates to the extent and concentration of impacts or additional consequences (Alexander, 1995; Felbermayr & Gröschl, 2014).

A natural hazard becomes a disastrous event when it leads to significant human, material, economic, or environmental losses and exceeds the capacity of the affected community or society to cope effectively (Lindell & Prater, 2003). This transition from a natural hazard to a disaster occurs when the impact of the event overwhelms the preparedness, response, and recovery capabilities of the affected area. Preparedness refers to the actions and steps undertaken ahead of time to guarantee an efficient response to the consequences of hazards (Keim, 2008).

It is important to note that the distinction between a natural hazard and a disaster is not solely based on the characteristics of the event itself but also on the context and vulnerability of the affected population and infrastructure.

2.1.2 Exposure

Exposure refers to the presence of all the living as well as non-living components such as people's property, infrastructures, or other assets which exist in hazard zones and thus may be impacted negatively in locations and, as a result, they are susceptible to damage, loss, or destruction (UNISDR, 2009). Living elements are mainly living communities such as Human populations, plants and vegetation, wildlife and animals, aquatic biodiversity, and insects.

Non-living elements refer to the physical components of the environment that can be affected or damaged by the hazard such as man-made infrastructures (buildings, roads, power lines, bridges, etc.) and natural resources such as agricultural lands, water bodies (lakes, river, reservoirs), topography and geology, etc.

These elements play a very important role in understanding the ecological, biological, and environmental impacts and consequences of natural disasters. (Lavell et al., 2012)

Thus, exposure is a product outcome of locality and the character of the neighboring construction and natural environment. For instance, a household living at a riverside poorly

constructed house and adjacent to a sewerage outfall will be more exposed to flooding (Pelling, 2001).

2.1.3 Vulnerability

The term vulnerability refers to the likelihood of a particular feature or element in a locality being exposed to a stressor (natural hazard) that it is sensitive to (Zacharias & Gregr, 2005). In general, vulnerability is commonly described as the combination of elements that include exposure and sensitivity to disturbances or external stresses, and the capability to resist (Adger, 2006).

The vulnerability status of the population and the built environment in the affected area is a significant factor to analyze the impacts of hazards. For instance, the communities and infrastructure poorly prepared are more susceptible to the destructive effects of natural hazards. For example, downstream people living near the riverbank can receive flood hazards. If the houses are constructed poorly in earthquake-prone areas, there is ample chance of suffering. On the other hand, the socio-economic conditions of the affected society can make the area suffer from severe disasters such as poor people suffering more than rich people. Marginalized communities will suffer more due to limited access to resources than well-off communities. Countries with weak governments, institutions, and policies suffer more than countries with strong governance, institutions, and policies.

2.1.4 Resilience

Resilience is characterized as the ability of a system, community, or society that may face hazards to adjust, resist, or transform itself to achieve and sustain an acceptable level of functionality and organization. In a simplistic way, resilience is the capacity of a system to endure deformation or disturbance up to the point where it no longer possesses the ability to recover or bounce back (Manyena, 2006). It entails developing capabilities and implementing steps to reduce vulnerabilities and improve the ability to recover and rebound in the face of adversity. It involves the ability of a society or a system to be prepared and to revive from the damaging impacts and influences of a disaster quickly and effectively. For instance,

communities that can claim damage to their agricultural crops following a debris flow or sedimentation event are more resilient than those that do not receive compensation for losses.

Thus, the combination of high exposure, high vulnerability, and low resilience increases the likelihood for a hazard to escalate into a disaster. By reducing exposure, mitigating vulnerability, and enhancing community resilience, the potential for hazards to turn into disasters.

2.1.5 Disaster

The United Nations defines a disaster as an abrupt and catastrophic occurrence that leads to significant disruptions in the operations of a community or society resulting in extensive human, material, economic, or environmental damage and losses that surpass the capacity of the affected community or society to manage using its available resources (UNISDR, 2004).

This definition emphasizes the magnitude of the event and the significant impact it has on multiple dimensions of a community or society. They can often lead to the displacement of people, the loss of essential services, and the need for immediate response and recovery efforts. The severity of a disaster is typically measured by the scale of its impact on the socioeconomic sector and the number of casualties or affected people it causes. Natural hazard-induced disasters can have severe impacts on various aspects of life, including infrastructure, housing, transportation, the economy, health, and the environment. In this study, the impacts of landslides as one of the Natural hazards/disasters are studied in detail.

2.2 Landslide

A landslide refers to the downward and outwards movement of a mass of soil, rocks, debris, or other materials down a slope or hillside (Varnes, 1978). It is a sudden and often rapid event that can occur due to various factors, such as gravity, slope instability, and external triggers like rainfall, earthquakes, or volcanic activity (Song et al., 2021).

Landslides can occur in different forms, including:

1. Rockfalls: Rockfalls involve the detachment and rapid descent of individual rocks or boulders from a cliff or steep slope.
2. Slides: Slides occur when a cohesive mass of soil or rock moves along a well-defined surface, such as a failure plane or a bedding plane.
3. Flows: Flows refer to the movement of loose or water-saturated material, such as mud, debris, or volcanic ash, down a slope. They can be further classified as debris flows, mudflows, or lahars depending on the specific material involved.

2.3 Landslide Evolution

Landslide evolution refers to the process by which a landslide develops, progresses, and changes over space and time (Xie et al., 2020). It involves the various stages and factors that contribute to the initiation, movement, and eventual stabilization of a landslide. The evolution of a landslide can be divided into several phases (Skempton & Hutchinson, 1969; Hungr et al., 2014) such as pre-failure phase, initiation phase, acceleration phase, transportation phase, stabilization phase and reactivation phase.

2.4 Geomorphological Precursors

Different types of precursors remain active that indicate whether a sloped surface is sliding over time and/or whether that slope has a high risk of triggering a mass failure. Among them, Geomorphological precursors are visible slope characteristics depicting alterations over the temporal evolution process of landslide. Geomorphological precursors are specific landforms or features that indicate the potential occurrence of a landslide e.g., Cracks, eroded surfaces, Scarp extensions, rupture, and erosion ditches. These precursors are often observed and studied in order to identify areas at risk of landslide activity. While the presence of these precursors does not guarantee an imminent landslide, they provide valuable information for landslide hazard assessment (Lan et al., 2023).

2.5 Triggering Factors

Landslides can be triggered by various factors that contribute to the instability of slopes. These triggering factors can be natural or human-induced (Song et al., 2022). Understanding

these factors is crucial for assessing landslide risks and implementing mitigation measures. Some of the common triggering factors of landslides are Heavy rainfall, earthquakes, Volcanic activity, Geology steep slopes, and soil characteristics, and Human activities.

2.6 Impacts of landslide on Downstream Ecosystems

Landslides can have significant impacts on downstream ecological systems, particularly those associated with rivers, streams, and aquatic habitats (Geertsema et al., 2009; Turner, 2018). Here are some of the impacts:

1. Sedimentation: When a landslide occurs, it can result in the rapid movement of soil, rocks, and debris downstream. This sedimentation can smother aquatic habitats, covering the streambed and affecting the availability of light, oxygen, and nutrients for aquatic plants and animals. Sedimentation can also alter the structure and composition of the stream channel, leading to changes in flow patterns and the loss of habitat diversity.
2. Water Quality Degradation: This sediment-laden water can impact water quality by increasing turbidity, reducing clarity, and impairing the ability of aquatic organisms to find food and navigate (Kondratyeva et al., 2020).
3. Habitat Destruction: Landslides can cause physical damage and destruction to riparian vegetation, wetlands, and other habitats along riverbanks and streams (Schuster & Highland, 2007).
4. Long-term Recovery: The impacts of landslides on downstream ecological systems can persist for an extended period (Tanyaş et al., 2021). Recovery and restoration of affected habitats may take years or even decades.

2.7 Landslides in Japan

Japan is a country that is prone to landslides due to its mountainous terrain, frequent seismic activity, and heavy rainfall (Shinohara & Kume, 2022). Japan is known to experience significant landslide problems due to its geographical characteristics and geological conditions. Here are some reasons why Japan faces landslide challenges:

1. Mountainous Terrain: Japan is a mountainous country, with approximately 75% of its land covered by mountains. The steep slopes and hilly terrain make certain areas prone to landslides, particularly during heavy rainfall or seismic activity (Parvin et al., 2022).
2. Rainfall Patterns: Japan has a diverse climate, including a rainy season and frequent typhoons. These weather patterns result in intense and prolonged rainfall, saturating the soil and increasing the risk of landslides (Dolojan et al., 2021).
3. Geological Instability: Japan is located on the Pacific Ring of Fire, a region known for its seismic activity. The collision of tectonic plates and the presence of numerous active faults contribute to the geological instability, leading to both earthquakes and subsequent landslides (Chen et al., 2017; Valagussa et al., 2019).
4. Volcanic Activity: Japan has several active volcanoes, such as Mount Fuji and Mount Aso (Yano et al., 2019). Volcanic eruptions can trigger landslides, as the loose volcanic ash and debris can easily be mobilized on steep slopes.
5. Human Activities: Human activities, including deforestation, urbanization, and improper land-use practices, can exacerbate landslide risks. Improper construction practices and inadequate slope stabilization measures can also contribute to landslides (Kadomura, 1980).

2.8 Landslides in Nepal

Nepal, like Japan, is a country that is prone to landslides due to its mountainous terrain, geological characteristics, and monsoon climate (Amatya, 2020). Here are some key points about landslides in Nepal:

1. Geographical Vulnerability: Nepal has 80% mountainous landscape and is located in the central part of the young Himalayan range, which is a highly active tectonic region with fragile geology. The collision of the Indian and Eurasian plates has resulted in the formation of rugged mountain ranges with steep slopes. The geology of Nepal includes various rock types and formations, including weak and unstable formations, which contribute to landslide susceptibility (Adhikari & Tian, 2021).

2. Monsoonal rainfall: Nepal experiences a monsoon climate with ca. 1600 mm average annual precipitation, characterized by heavy rainfall during the summer months (June to September) (Dahal & Hasegawa, 2008).
3. Seismic Activity: Nepal is situated in a seismically active zone, prone to earthquakes. The devastating earthquake in 2015 caused significant landslides throughout the country (Dahal, 2022).
4. Vulnerable communities: Many communities are located in hilly and mountainous areas in a scattered way. Population pressure and rapid urbanization have led to increased settlements on slopes, often in landslide-prone areas in the mid-hills (K.C., 2013).

2.9 Landslide Risk Reduction and Management

Landslide risk reduction and management involve a range of measures aimed at minimizing the potential impacts of landslides and enhancing the safety of communities and infrastructure (Dai et al., 2002; Anderson & Holcombe, 2013; Margottini et al., 2013). some key strategies and approaches in landslide risk reduction and management are Hazard Mapping and Risk Assessment, Land-use Planning and Zoning, Engineering Measures , Vegetation Management (Ecosystem-based solutions), Early Warning Systems , Public Awareness and Education , Emergency Preparedness and Response. Here are some key strategies and approaches in landslide risk reduction and management.

2.10 Landslide Early Warning System

A landslide early warning system is a crucial tool for monitoring and detecting potential landslide events in advance. It provides timely alerts and information to communities, authorities, and relevant stakeholders, allowing them to take necessary actions to minimize the impact of landslides.

Implementing a landslide early warning system requires collaboration among various stakeholders, including government agencies, researchers, local communities, and technology providers. By providing timely and accurate information, early warning systems can save lives, reduce damage, and improve overall resilience to landslides (Dikshit et al., 2018; Abraham et al., 2022; Thapa et al., 2023).

2.11 Traditional Engineering Structures (Grey Structures)

Traditional engineering structures for landslide treatment, also known as grey structures, are physical infrastructure measures designed to mitigate and control landslides. These structures aim to stabilize slopes by modifying slope geometry and reinforcing the slope, redirecting or controlling sediment flow using drainage, and protecting vulnerable areas using retraining structures (Chen & Liew, 2002; Popescu & Sasahara, 2009) Some common types of grey structures used for landslide treatment are Retaining Walls, Gabion Walls, Rockfall Protection Barriers, Debris Flow Barriers, Catchment Ditches and Drains, Check Dams (Sabo Dams). Checkdams are popularly known as Sabo dams in Japan. Check dams help trap sediment, reduce water velocity, and promote sediment deposition, reducing erosion and the potential for downstream landslides (Piton et al., 2017). The selection and design of grey structures depend on the specific site conditions, the type of landslide, and the desired outcome of the treatment.

2.12 Ecosystem-based Solutions (Green Structures/vegetation-based)

Ecosystem-based solutions, often referred to as green structures or revegetation measures, are nature-based approaches for landslide mitigation and management (McVittie et al., 2018; Sandholz et al., 2018; Teich et al., 2022). These solutions utilize vegetation and ecological processes to enhance slope stability, reduce erosion, and increase the resilience of landscapes (Punetha et al., 2019). Some common examples of ecosystem-based solutions used for landslide mitigation:

1. Afforestation and Reforestation: Planting trees and establishing forests in landslide-prone areas can help stabilize slopes by increasing root strength and soil cohesion. Tree roots bind the soil together, reducing the risk of slope failure. Afforestation and reforestation also enhance water absorption and regulate surface runoff, reducing soil erosion and landslide susceptibility (Sukhwani et al., 2022).
2. Soil Bioengineering: Soil bioengineering involves using live plants and organic materials to create natural structures that stabilize slopes. Techniques such as brush layering, live fascines, and root wads are used to promote vegetation growth and reinforce the soil. These living structures provide slope stability, dissipate water energy, and prevent erosion.

3. Riparian Vegetation and Buffer Zones: Establishing riparian vegetation and buffer zones along watercourses and drainage channels helps to stabilize the banks and prevent soil erosion.

Ecosystem-based solutions for landslide mitigation offer multiple benefits beyond slope stabilization. They contribute to biodiversity conservation, improve water quality, enhance ecosystem services, and provide aesthetic value. Implementing these solutions requires site-specific assessments, considering factors such as soil conditions, climate, and vegetation suitability. Combining green structures with traditional engineering measures and early warning systems can provide a holistic approach to landslide risk reduction and management.

CHAPTER 3 LANDSLIDES IN JAPAN

3.1 Evolution of Sennindani Landslide 2015 in Mt. Hakusan

3.1.1 Introduction

Landslides can occur in any terrestrial environment with sloped terrains triggered by earthquakes, volcanoes, heavy rainfall, snowmelts, changes in the underlying foundation of the slope, and/or anthropogenic interventions (Bennett et al., 2016; Du et al., 2017). Although, historically, shallow (above bedrock) landslides have commonly occurred in mountainous regions (Bellugi et al., 2021), recently the number of large-scale landslides has increased globally (Ogita et al., 2017). In the case of large-scale landslides, the large slope moves as a mass through the landslide surface as a part of or all of it, and, as a result, the damage caused by these large-scale landslides can be extensive, resulting in significant economic losses as well as injuries and casualties (Kjekstad and Highland, 2009). Annually, landslide-risk reduction and management require significant financial investments. However, landslide risk can be mitigated if there is sufficient information available about the precursory phenomena associated with the potential occurrence of a landslide. Landslide precursor events are small-scale surface deformations and hydrologic anomalies that precede large-scale sliding activity and are crucial to immediate disaster-prediction practices and accurate evacuation measures (Lan et al., 2022). These events can include various indications, such as small cracks appearing on the surface of the terrain, the observation of changes occurring in the direction of surface water flow, changes in ground movement, and changes in vegetation cover. By observing these changes, it is possible to identify when a landslide is more likely to occur and to take effective measures to mitigate the risk of its occurrence. Previous research has highlighted that the timely detection of the precursory phenomena is crucial to reducing landslide risk (Yang et al., 2020). Evidence of prominent precursors can be monitored by time-sequential on-site geodetic measurements and/or using temporal remote sensing data. However, on-site geodetic measurements are usually very difficult to perform in hazardous landslide sites and/or inaccessible areas, particularly over long periods of time. Therefore, in the case of inaccessible landslide areas, the use of remotely sensed data to monitor precursory phenomena can be one of the most effective techniques. By combining multiple sources of remote sensing data, it is possible to obtain a more comprehensive understanding of the precursors that can cause landslides (Borrelli et al., 2019; Giordan et al., 2020). The present study aims to assess the geomorphological precursors for a snowmelt-

triggered landslide with the combined use of aerial photographs, InSAR data, airborne LiDAR data, and precipitation records in a difficult-to-access site.

General Setting of the Study Site

A deep-seated earthflow (latitude: 36°11′59.27" N, longitude: 136°47′18.81" E; Fig. 1) occurred in May 2015 in the upper reach of the Ozo River, which is a tributary of the Tedori River, within an old landslide terrain (called the Sennindani (dani-valley) Landslide or 2015 Landslide) on Mt. Hakusan. The average annual precipitation (ca. 3000–3600 mm) that occurs is concentrated in the area (Wang et al., 2007; Dang et al., 2014) with a high amount of snowfall that can reach 7–12 m; most of the snow melts in the spring to summer months (April to August) and flows downhill by forming water networks.

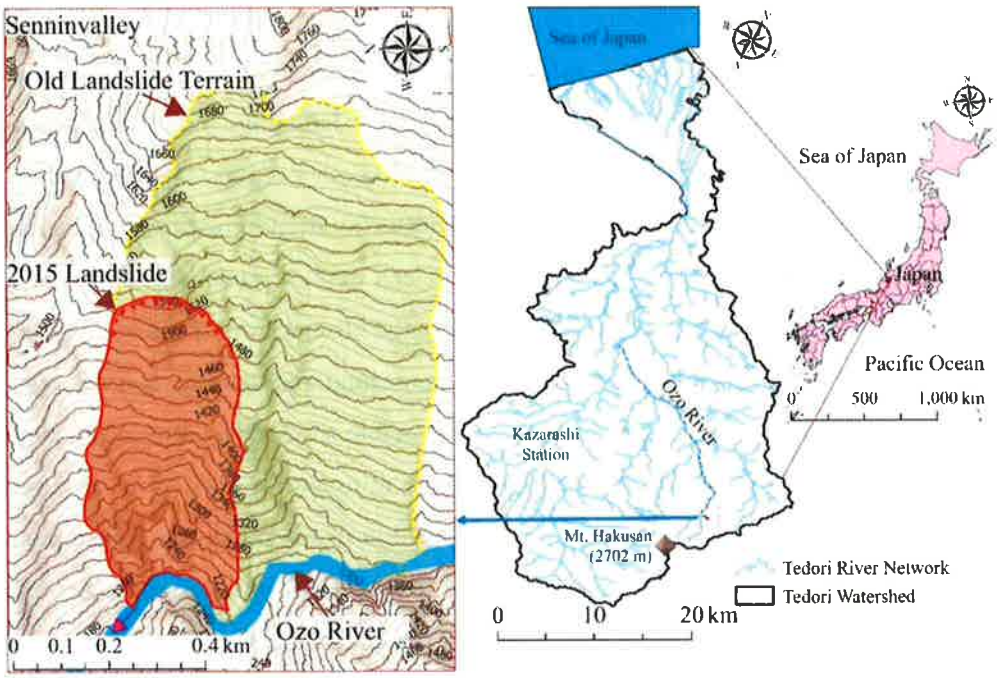

Figure 1 : Location of the study area showing the 2015 Landslide, Ozo River, and its adjoining topography (old landslide terrain) within Senninvalley.

The geology of the area consists of Jurassic and Cenozoic sedimentary rocks (mudstone and sandstone; Tedori Group) overlain with Cretaceous to Cenozoic rhyolitic tuff (Nohi Rhyolite) (Fujii and Hori, 2003) and Quaternary lava deposits from the Hakusan Volcano. The 2015 Landslide is located at the bottom of a large and old landslide and appears to be a reactivation of the lower part of the large landslide terrain.

The 2015 Landslide has a maximum length of 800 m and a width of 300 m (Fig. 2). The elevation of the crown of the landslide is approximately 1560 m and the lowest depositional area (Ozo River) has an elevation of 1200 m. The maximum elevational difference observed was approximately 400 m. Fig. 2 depicts the Sennindani Landslide, the adjoining landslide topography (potentially old landslide terrain), and the Ozo River located at the bottom of the slope.

Figure 2 : 2015 Landslide overview showing the maximum horizontal length and width of the landslide (photo credit: Ishikawa Forest Management Office, 2016).

3.1.2 Methods and Materials

This section provides a comprehensive overview of the primary methods and methodology employed in this research study.

3.1.2.1 Data Acquisition

For this study, aerial photographs, meteorological data, PALSAR data, and airborne LiDAR-derived DEMs were acquired. The details of the data used are presented in Table 1.

Table 1: Description of the data/records acquired for this study.

Data Used	Year/Duration	Source
Aerial photographs	1961, 1977, 2008, 2014	Geospatial Information Authority of Japan (GSI) and Ministry of Land, Infrastructure, Transport and Tourism (MLITT), Japan
Precipitation	2012–2016	Water Information System, MLITT, Japan
Snow depth	2012–2016	Water Information System, MLITT, Japan
Temperature	2012–2016	Japan Meteorological Agency (JMA), Japan
Airborne light-detection and ranging (LiDAR)-derived DEM	September 2014, November 2014, May 2015, October 2016	MLITT, Japan
Phased array type L-band synthetic aperture radar (PALSAR) data measured by the Advanced Land Observation Satellite (ALOS)	July 2008, July 2009, July 2010, August 2010	Japan Aerospace Exploration Agency (JAXA)

3.1.2.2 Methodology

Aerial-Photo Interpretation

In this study, geomorphic changes occurring in the landslide were detected and mapped from multi-temporal aerial photos (Fig. 4) taken by GSI Authority in Japan (1961 and 1977) and MLITT, Japan (2008 and 2014). The 1961 and 1977 aerial photographs used in the study were obtained from the Geospatial Information Authority of Japan (GSI), and the 2008 and 2014 aerial photographs were obtained from the MLITT, Japan. The images were taken at flying heights ranging from 4300 to 4192 m with a scale ranging from 1:15,000 and 1:40,000.

SAR Data Analysis

ALOS PALSAR data (Table 1) were acquired focusing on the 2015 Landslide area for the years 2008, 2009, and 2010. Interferometric analysis of the multitemporal PALSAR data (Jebur et al., 2015) was performed using ENVI SARscape v5.6 software to understand the land-displacement activity surrounding the 2015 Landslide in 2008–2010. For the

interferometric analysis, we used the DInSAR displacement workflow tool of EnviSARScape software. The displacement measurement obtained from the interferometric analysis was expressed as the relative movement of the ground surface towards the satellite (approaching) or away from the satellite (leaving) along the direction of the radar irradiation emitted from the satellite.

LiDAR Data Analysis

Multi-temporal LiDAR-derived DEMs were analyzed to clarify the development of the landslide prior to and following the 2015 event. LiDAR-derived DEMs were utilized to extract the morphological features prior to and following the 2015 Landslide. The resolution of all the post-processed DEMs was 30 cm. This assisted us in obtaining the minute terrain changes with better accuracy. For the present research, the DEM for October 2008 was considered as the reference year. Then, we estimated the geomorphic changes occurring in successive periods, namely, October 2008–September 2014, September–November 2014, November 2014–May 2015, and May 2015–October 2016. Geomorphological changes (James and Robson, 2012) were extracted from the LiDAR-derived DEM using ArcGISPro 3.0.1 software (Williams, 2012). The elevational difference (ΔD) can be calculated using the Raster calculator tool (after-before) in the spatial analyst extension. Similarly, the sediment volume of landslides was calculated for particular polygon shapes (Small landslide 2014 in Fig. 5A and Landslide 2015 in Fig. 5B) using the CutFill tool in the Spatial Analyst extension of ArcGISPro 3.0.1 software.

Meteorological Dataset Analysis

Monitored precipitation records were obtained from the nearest meteorological station established by the Water Information System, MLITT, Japan. It is located (latitude: 36°10′06" N, longitude: 136°37′55" E, elevation: 520 m) at Kazarashi station (Fig. 1) in Hakusan city. Temperature data was collected from a meteorological station managed by the Automated Meteorological Data Acquisition System (AMeDAS) of the Japan Meteorological Agency (JMA), Japan. The station is located (latitude 36°16′26.16" N and longitude 136°53′49.96" E, elevation 500m) approximately 12.5 km away from the location of the 2015 landslide.

3.1.3 Results and Discussion

3.1.3.1 Temporal Changes in Geomorphology of Landslide

Interpretation of the Aerial Photos in 1961–2014

There was no evidence of major deformation in the 1961 aerial photograph, and most of the landslide area had vegetation cover in that year. However, at the bottom (western side) of the region, fresh, eroded small scars present close to the Ozo River were noticeable. Gullies within these scars did not appear to be much deeper. These scars present at the toe of the landslide under study are referred to as toe scars (TS) in the present study (Figure 3A). Other remarkable features visible are small, crack-like scarplets without vegetation in the upper slope of the landslide (eastern) topography represented as SC1 and SC2 (Figure 3A). The scarplet might have developed where a portion of the slope had moved downwards along a planar surface, resulting in the loss of vegetation.

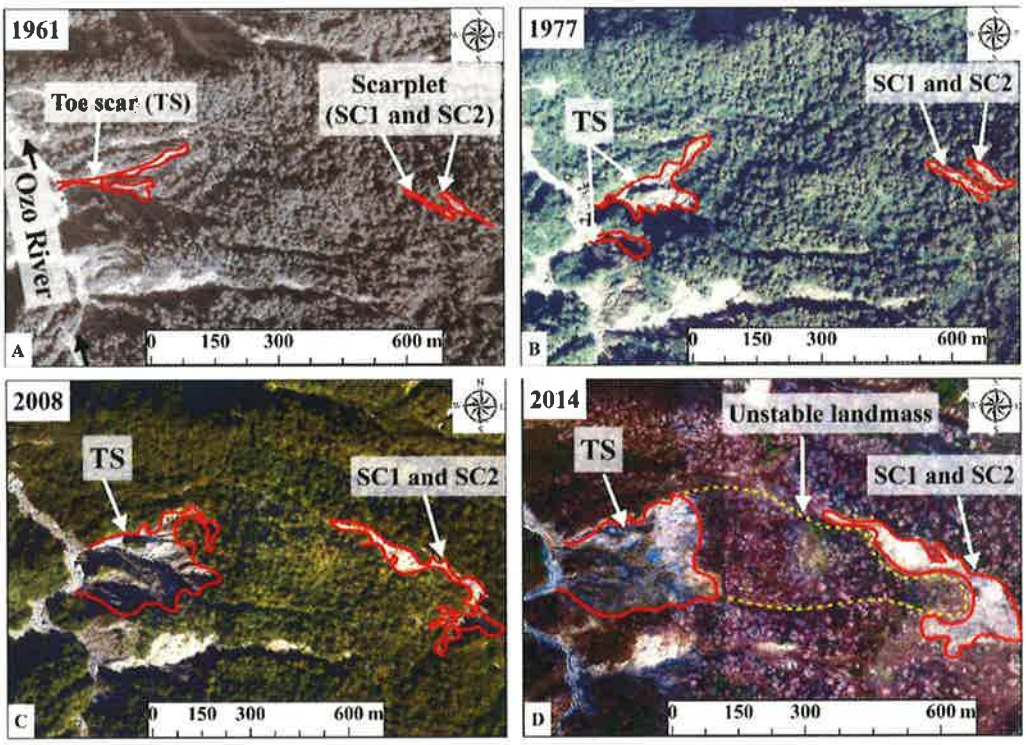

Figure 3: Aerial photographs: (**A**) 1961, (**B**) 1977, (**C**) 2008, and (**D**) 2014 showing toe scar (TS) and scarplets (SC1-left and SC2-right) advancements in the time-sequential photos.

The toe scar (TS) at the bottom of the landslide, observable in the 1961 photograph, appear to have widened in the 1977 aerial photograph (Figure 3B). The 1977 photo also shows that the pre-existing toe scar has expanded upward. Compared to the previous photo, the scarplets

(SC1 and SC2) in the upper part also seem to increase in size in 1977. The 1977 photo clearly indicates that the pre-existing scars have expanded toward the upslope.

The aerial photograph taken in 2008 (Figure 3C) shows that the separation of the two scarplets (SC1 and SC2) became more pronounced and progressed enough to appear as a single, larger scarplet. By 2008, the minor movement of the landmass can also be observed in the upper (eastern) area. Furthermore, the lower toe scar (TS) expanded upslope, eroding the surface. However, between the toe scar and scarplet, there seems to be an intact, vegetated scree slope.

The 2014 photo (Figure 3D) depicts the substantial expansion of a former TS in the bottom area and scarplet (SC1 and SC2) in the upper area. It seems that a shallow landslide (TS in Figure 3) occurred in the lower part of the present landslide. The eroded bottom advanced further, with noticeable gullies inside.

Previous researchers identified scarplets at various landslides from historical photographs and considered them as geomorphological precursors of large landslides (Chigira et al., 2013, Li et al., 2023). Geomorphic features, such as geological structures and landforms, can provide important clues to the potential for landslides (Chen et al., 2022). For example, areas with steep slopes, weak or erodible soil, areas with cracks or fissures on the slope, and areas with a history of landslides are more likely to experience landslides in the future (Dai et al., 2004). The presence of a smaller landslide at the bottom and the widening of the scarplet in the upper portion of the landslide suggest that the slope has been gradually destabilized and that the movement has been slow and gradual over time. The spatiotemporal expansion of TS, SC1, and SC2 are illustrated in Figure 4.

PALSAR Data Determine Land Displacement

InSAR data analysis results assisted us in determining the land displacement occurring in the landscape near the 2015 Landslide area. The displacement of the InSAR data analysis result is expressed in terms of approaching or leaving the satellite (relative to the direction of radar irradiation). The analysis of the ALOS PALSAR data for the periods of July 2008 and 2009 (Figure 4A) revealed that strong displacement approaching the satellite occurred in the southeastern area of the landslide. The analysis of the SAR data for July 2010 and August 2010 (Figure 4B) depicted strong displacement approaching the satellite exactly at the middle

to lower sections of the 2015 Landslide. This displacement was noticeable even after the 2015 Landslide and is described in supplementary Figures.

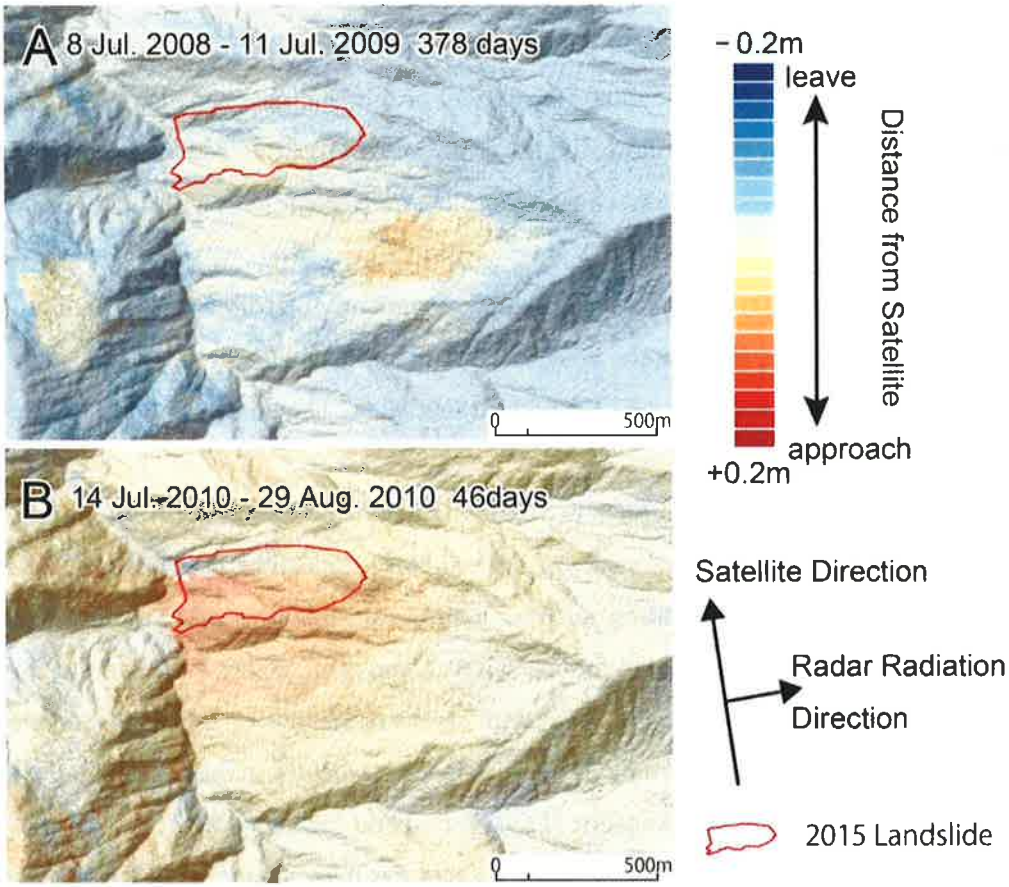

Figure 4 : Land displacement in the surrounding of the 2015 Landslide (maximum estimated from PALSAR 1 (JAXA; ascending) for three periods: (**A**) 8 July 2008–21 July 2009 and (**B**) 14 July 2010–29 August 2010. The background, shaded, topographical map was created from 2008 LiDAR-derived DEM with a 10 m contour interval.

The prevalence of displacement in the present landslide area was further supported by two sets of Interferometric analyses of PALSAR data between July 2008 and August 2010, which clearly showed land displacement in the area. This result is consistent with the results of the research conducted at the nearby landslide, which determined a horizontal displacement of 25 cm per year in the Jinnosukedani landslide area of Mt. Hakusan between the years 2006 and 2009 (Michinaka and Hiramatsu, 2010). The result of our study resonates with the results of a previous study that also identified a 1000 × 1000 m area, including the present 2015 Landslide, showing some movement (Yuya and Yoshihiro, 2017).

Geomorphological Precursors Derived from LiDAR

The DEM analysis for the period of October 2008 to October 2016 revealed the geomorphic changes that occurred in the 2015 Landslide area before and after the 2015 main event. The bluish color represents the degradation (erosion), while the reddish color represents the aggradation (deposition) of the land surface (Figure 5).

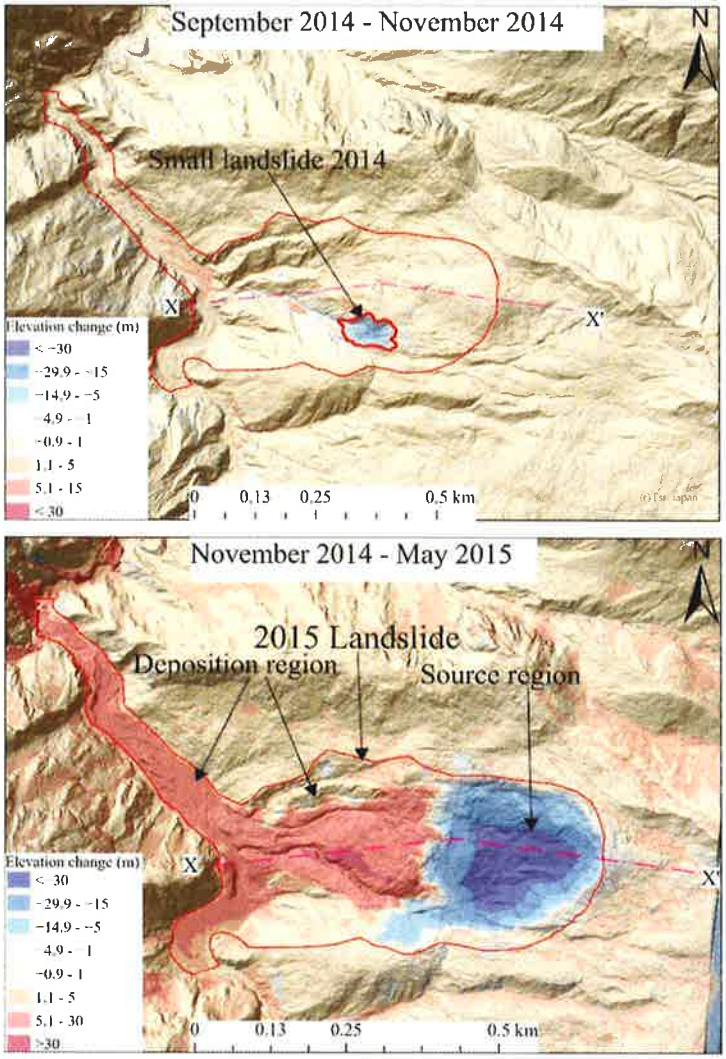

Figure 5: Geomorphological changes occurring (**A**) in September 2014–November 2014; (**B**) November 2014–May 2015. LiDAR derived DEMs analysis for a period of November 2014–May 2015 confirmed 2015 Landslide event While small landslide was detected between September 2014–November 2014 (Bluish color indicates degradation/erosion from source area and red color indicates aggradation/deposition in deposition region).

Figure 5A depicts the elevational changes that occurred between September 2014 and November 2014. During this period, a small failure with a volume of ca. 50,000 m^3 occurred

near the top of the eroded toe scar (Figure 5A). Following this period (probably due to the Small Landslide), upper landmass probably became unstable and resulted in a bulging-like scree slope.

The geomorphic changes that occurred between November 2014 and May 2015 are presented in Figure 5B, which reveals the occurrence of the 2015 Landslide. In Figure 5B, the bluish color indicates that a large-scale landslide (ca. 1.3 million m^3) occurred and deposited (reddish color) near the toe scar areas and valley floor of the Ozo River between November 2014 and May 2015. This 2015 Landslide occurred within just six months of the small landslide at the bottom. The slide occurred close to the crown-section (1560–1400 m) altitude and deposited at the bottom slope around the 1200–1400 m section of the landslide terrain.

From the available LiDAR-derived DEM analysis, we estimated the longitudinal profile for four periods. Fig. 9A presents the longitudinal profile (X–X') from the crown to the bottom of the 2015 Landslide for four different periods. When longitudinal sections along the crown to the toe of the landslide were assessed, it was evident that approximately 350 m of the crown part slipped and was transported along the lower landscape (450 m horizontal length) to accumulate the produced debris along the 500 m section of the Ozo River. The 2015 Landslide significantly changed the upslope morphology and a concave slope formed after the occurrence of the landslide (Figure 6A).

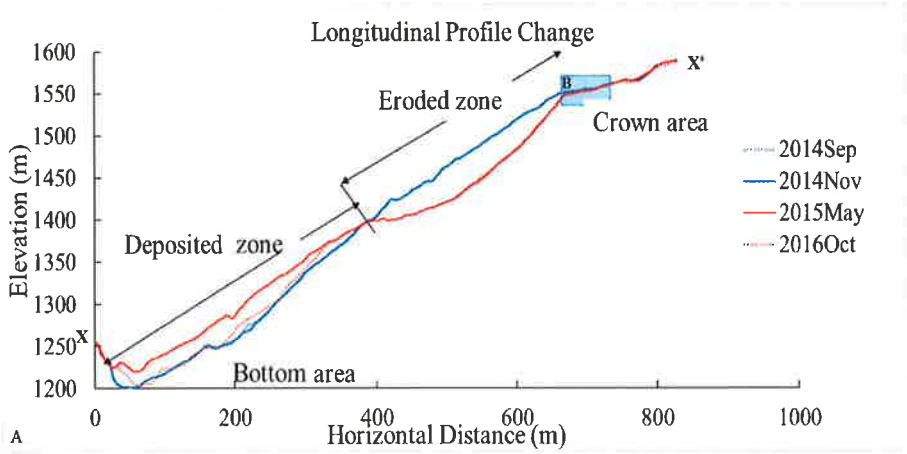

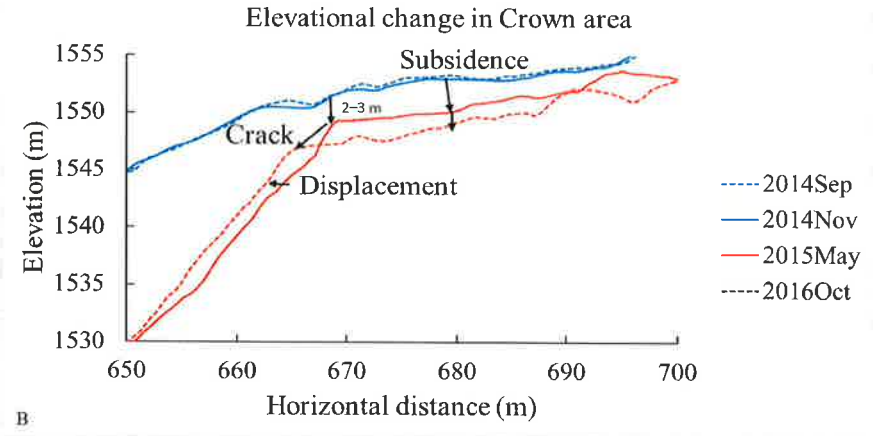

Figure 6 : Temporal longitudinal profiles derived from four periods from LiDAR-derived DEMs: (**A**) longitudinal profile of 2015 Landslide from crown to bottom toe areas (X–X'); (**B**) enlarged profile near the crown area (smaller rectangle B).

The crown area presented in the landslide profile (X–X') has been enlarged in Fig. 6B. The crown section, being the initiation area, had an altitude of approximately 1550 m until November 2014; however, following the landslide occurrence in May 2015, the land surface level decreased to an altitude of approximately 1548 m (Fig. 6B). The land surface subsided by approximately 2~3 m between November 2014 to May 2015 when the deep-seated 2015 Landslide occurred. The profile for October 2016 (Figure 6B) also seems further slightly lowered compared to its composition in May 2015.

From the above results it can be inferred that the formation of the Toe Scar (TS) in the landslide may have been caused by the cutting action of the Ozo River, which is a perennial tributary originating from Mt. Hakusan with a steeper slope. In the snowmelt season, the Ozo River experiences a significant increase in water flow, which might have caused the lateral erosion of its banks. The occurrence of continuous cutting due to the river's flow formed an inner gorge removing the toe support of the hillslopes, which is key to inducing landslides (Deng et al., 2021).

The small landslide in 2014 as presented in Figure 5A in the bottom area clearly evidenced that this shallow failure removed the bottom support creating instability along the scree slope. Thus, in addition to the toe cutting by Ozo river, the toe block was continuously pushed toward the Ozo River by the gliding of the landslide block behind it, and this instability is expected to continue for a longer period. Such topographic changes accompanied by

destabilization and the small, shallow landslide on the toe slope of a landslide are widely recognized as characteristics of active landslides (Miyagi et al., 2004).

Since the instability of the toe slope and displacement occurring along the head scarp are believed to be the most important indicators of landslide activity in Japan (Yagi et al., 2009), the precursor geomorphic features, such as small collapse occurring at the toe slope and growth of the head scarp, are important precursor features to predict future landslide hazards in the study area. The appearance of similar precursor phenomena was reported for deep-seated landslides in the Shizuoka Prefecture (Daimaru et al., 2013).

Meteorological Conditions Triggering the Landslide

The temporal variations in the meteorological factors, including precipitation, temperature, and snow depth, which were analyzed to determine the relationship between water availability and landslide occurrence (January 2012–August 2016), are presented in Fig. 7. In this period, the peak daily precipitation reached 85.6 cm in the month of December 2014 and the maximum snow depth recorded was 263 cm in February and March 2015, which is the highest reading for the 2012–2016 study period. In the year 2015, the temperature started gradually increasing from the month of February, and from April onwards snow melting was observed.

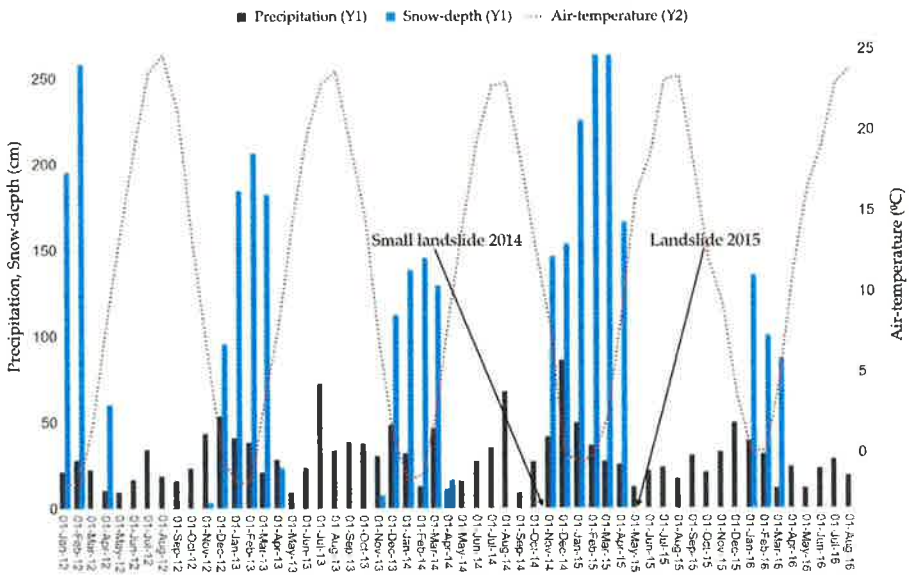

Figure 7 : Monthly precipitation, air-temperature, and maximum snow-depth levels in 2012–2016.

We assessed the changes that occurred from October 2014 onwards, as the Small Landslide occurred in the month of October 2014. The monthly precipitation and monthly maximum snow-depth levels from October 2014 to May 2015 are presented in Figure 10. In this period, the maximum snow-depth level in winter was the deepest in the 2012–2016 study period.

The monthly precipitation levels were 26.8, 41.2, and 85.6 cm for the months of October, November, and December 2014, respectively. The snow-depth levels measured were 146 and 153 cm in November and December 2014, respectively. However, no landslide occurred during those months, despite the heavy rainfall and snowfall. In January, February, March, and April 2015, precipitation levels were 49.4, 36.3, 26.8, and 25.2 mm, respectively. The snow-depth levels recorded were 225, 262, 263, and 166 cm in January, February, March, and April 2015, respectively. Figure 7 shows that in 2015, the temperature in the month of January was recorded nearly 0 degrees Celsius. However, it gradually started increasing since the month of February, and by the month of May, the temperature had increased to more than 15 degrees Celsius. This rise in temperature might have caused a sudden increase in the supply of water due to the melting of snow. The 2015 Landslide occurred in the month of May 2015 after the winter season when there was an abundant water supply due to the snow melting. The meteorological information suggest that snowmelt has greatly affected the occurrence of the 2015 collapse.

It was determined that the 2015 Landslide occurred in the month of May, which is snow-melt season. During this period (March onwards), snowmelt might have increased the water supply to and infiltration into the slope. Previous investigations show that many landslides have been shown to occur during snow melting (Osawa et al., 2018; Okamoto et al., 2018; Marui and Koizumi, 2014).

It is estimated that more than 1300 mm of water was supplied to the ground surface in the Sennindani Landslide. This significantly high levels of snowmelt water from deep snow cover accumulated during the 2014–2015 winter period is believed to be the major triggering factor of the 2015 event. Previous studies have reported similar cases of large-scale collapses caused by high levels of snowmelt water penetrating landslides that had already become destabilized (Matsuura et al., 1998; Nishii et al., 2013). Similarly, in the study area, the 2015 catastrophic collapse was likely caused by a record amount of snowmelt water supplied to a landslide that had been destabilizing for more than a few decades.

3.1.4 Conclusions

The 2015 Landslide occurred in a difficult-to-access landscape, making it infeasible for us to perform in situ geodetic observations over a long period of time. However, the combined application of remotely sensed data, such as aerial photographs, InSAR data, and LiDAR data helped us to monitor the changes in slopes over time. The results presented in this study help us to understand the precursory phenomena of the 2015 Landslide, which was reactivated within an old landslide block. The Sennindani Landslide has been exhibiting movement since 1961, but abundant water produced during the snowmelt season in the spring of 2015 most likely triggered the large landslide. The use of Lidar-derived DEMs has allowed us to quantify the mobilized mass material during the 2015 Landslide, as well as detect land subsidence in the crown area of the landslide, which has sunk nearly 2~3m, indicating instability. Additionally, InSAR analysis has revealed land displacement in the surrounding areas of the 2015 Landslide. The use of multitemporal remotely sensed data analysis provided the necessary information about the precursors, their advancement, volumetric information about landslide and the land displacement in the study area. While the Ozo River is causing erosion in the bottom area, it is believed that the 2015 Landslide was triggered by water released from snowmelt. Furthermore, the scarplets (SC1 and SC2) grew in shape at the head region (Eastern) of the present landslide terrain, which may probably advance into slope failure in the future. Therefore, to prevent or mitigate the risk of future landslides, it is essential to identify the stability of the old landslide terrain and determine the precursors and potential triggers that could cause further collapses in the 2015 Landslide upper slope and its adjoining topography.

3.2 Impact of the Sennindani Landslide 2015

3.2.1 Introduction

A landslide is a type of slope failure that is characterized by the rapid movement of soil and rock along a subsurface shear plane (Varnes, 1978). Landslides are triggered by heavy rainfall (Larsen and Simon, 1993), snowmelt (Kawagoe et al., 2009), and earthquakes (Sassa, 2005). Landslides near river tributaries that release debris into the river network can lead to downstream sedimentation (Hovius et al., 2000). In addition, collapsed sediment accumulates in river channels and becomes a continuous source of sediment for downstream areas (Benda, 1990). In downstream areas, transported sediment causes a short-term increase in sediment and debris deposition (Johnson et al., 2000). Furthermore, landslide sediments influence river morphology and processes by accelerating erosion, regulating (or blocking) river channels, and covering riverbeds (Korup, 2006). The short-term downstream impacts of landslides are sometimes serious and include the destruction of infrastructure, residential areas, agricultural land, and human casualties (Dadson et al., 2004; Petly, 2012; Guzzetti et al., 2012; Ministry of Land, Infrastructure, Transport, and Tourism, 2020; Esposito et al., 2021. In contrast, long-term impacts include groundwater depletion, river turbidity, disturbances in fish ecosystems, and changes in agricultural productivity (Schuster and Highland, 2007).

Much of the landslide research to date has focused on single systems or short-term impacts, such as damage to forest areas and farmlands, destruction of infrastructure, and human damage, whereas few studies have taken a comprehensive view of watersheds while studying the long-term impacts (Tanaka et al., 2017; Kobiyama et al., 2011; Kanbara and Imamori, 2020; MLIT, 2020; Bhat et al., 2021). The long-term environmental impacts of landslides on downstream landscapes (river turbidity, groundwater recharge, riverbed fluctuation, and loss of aquatic biodiversity) are also significant, but their relationships have scarcely been investigated. Understanding the relationship between landslides occurring in upstream mountainous regions and their impacts on downstream alluvial fans connected by a network of river channels is essential for mitigating similarly disastrous impacts of future landslides. In this context, we selected a watershed in central Japan to assess the long-term environmental impact of landslide-generated sediments on the downstream alluvial fan of the Tedori River watershed. It has been reported that a landslide that occurred in the headwaters of Hakusan in 2015 had a serious impact on the downstream system. Yanai et al. (2015, 2016) performed a detailed topographical analysis of landslides that occurred in the headwater area in the spring of 2015 using aerial photographs and air borne light detection and ranging

(LiDAR) derived digital elevation models (DEM). Tanaka et al. (2017) clarified that turbid water caused by an upstream landslide affects groundwater recharge in alluvial fans immediately after the landslide. However, these studies examined the effects within two to three years after landslide occurrence, and the long-term changes and effects on the river water, riverbed, groundwater, and fish habitats were not investigated. The lack of information on the long-term impacts of the 2015 landslide and its recovery duration has created a gap in our understanding of the potential changes that may have occurred after large amounts of sediment were transported downstream through the river network.

In this study, we conducted a thorough quantitative evaluation of the effects of sediment distributed downstream after 2015 landslide on various elements: (a) the status of river turbidity, (b) fluctuations in the riverbed, (c) changes in well water levels, (d) sediment accumulation in paddy fields, and (e) alterations in fish habitats. The findings of this study will be valuable for understanding the long-term impacts of downstream sediment efflux resulting from upstream landslides and for developing strategies for conservation, restoration, and mitigating disasters in an integrated manner at a watershed scale.

3.2.2 Methods

3.2.2.1. Overview of the study area

The study area included the Tedori watershed (807 km^2), encompassing both the upstream mountainous region, including Mt. Hakusan (elevation 2,702 m), where the Sennindani 2015 landslide occurred, and the downstream alluvial fan area (0–80 m) that stretches along the Sea of Japan coast starting from the Tsurugi town (Figure 1 A).

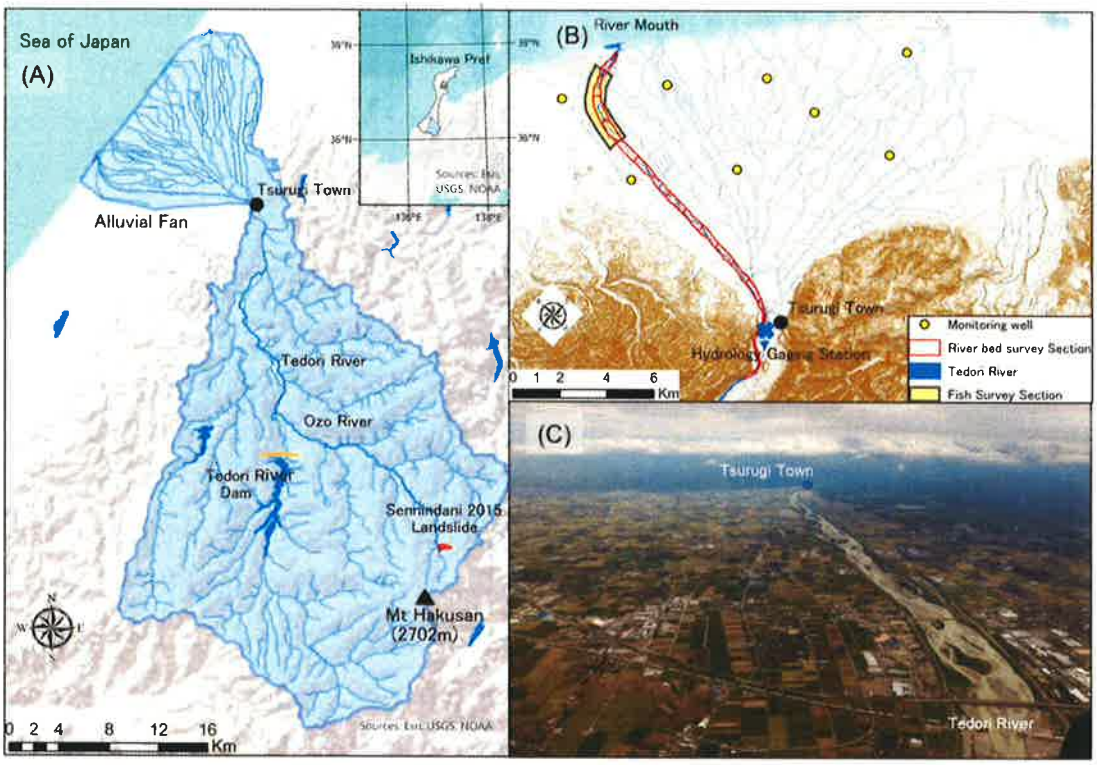

Figure 1. The study area (A) included the Tedori watershed extending from the Japan Sea to Mt. Hakusan, showing the Sennindani 2015 landslide. (B) The downstream alluvial fan showing the monitored well locations and section of the Tedori River studied for assessing fish ecosystem and sediment change in the riverbed. (C) Aerial view of the Tedori River section in the alluvial fan area.

The Tedori watershed includes the Tedori River system and its multiple tributaries, with a catchment area of 809 km^2 (743 km^2 in the upstream mountains starting from Tsurugi town, and 66 km^2 in the downstream alluvial fan areas). Annual precipitation is concentrated in mountainous areas (approximately 3300 mm), where snow cover can reach up to 7–12 m (Wang et al., 2007). Both the upstream and downstream areas are connected by a perennial Tedori River system (72 km).

There are no large storage dams between the landslide area and the alluvial fan, but many weirs and check dams prevent the remobilization and deposition of riverbed material. Flooding rarely occurs in this fan area, because levee structures have been constructed along the Tedori River. However, the Tedori River water is directly distributed to agricultural land in the alluvial fan through two main irrigation canals (named Shichika and Miyatake canal) and sub-canal networks.

The downstream alluvial fan (Figure 1B) starts at Tsurugi in the lower reaches of the Tedori River. The altitude of the alluvial fan top (Tsurugi town) was approximately 80 m, and the distance from the top to the end of the alluvial fan was approximately 16 km. The center of the fan is located at 36°30'44.74" N latitude and 136°33'41.47" E longitude, as shown in Fig. 1B. It has an area of 176.82 km^2, of which 42.6% is paddy fields, 2.9% is farmland, 34.2% is residential land, 15.0% is roads, and 5.3% is rivers, including canals (Ministry of Land, Infrastructure, Transport, and Tourism, 2011).

Numerous springs originate from alluvial fans, and several small streams originating from these springs are distributed throughout the area. One such stream is the Kumada River, which originates from spring-fed water, located 0.7 km south of the left bank of the Tedori River, approximately 4 km upstream from the mouth of the Tedori River, and flows for 4 km until it converges with the Tedori River near the Sea of Japan. The Kumada River is a habitat for the Tomiyo fish, a critically endangered and rare species of wild fish in the Ishikawa prefecture of Japan.

Sennindani 2015 landslide

The Sennindani 2015 landslide (36°11'59'27" N, 136°47'18'81" E) occurred in May 2015 on the right bank of the Sennindani area along the Ozo River, which is a tributary of the Tedori River. The Ozo River converges with the main channel of the Tedori River nearly 22 km downstream. The landslide that occurred in May 2015 had a horizontal distance of 650 m from the crown to the deposition area and a width of 200 m in the middle of the landslide. The Sennindani 2015 landslide (Figure 2A) extended to an area of 64000 m^2 and produced approximately 1.3 million cubic meters of sediment, which accumulated over a 500-meter section along the channel of the Ozo River and was gradually transported downstream to the Tedori River (Yanai, 2018).

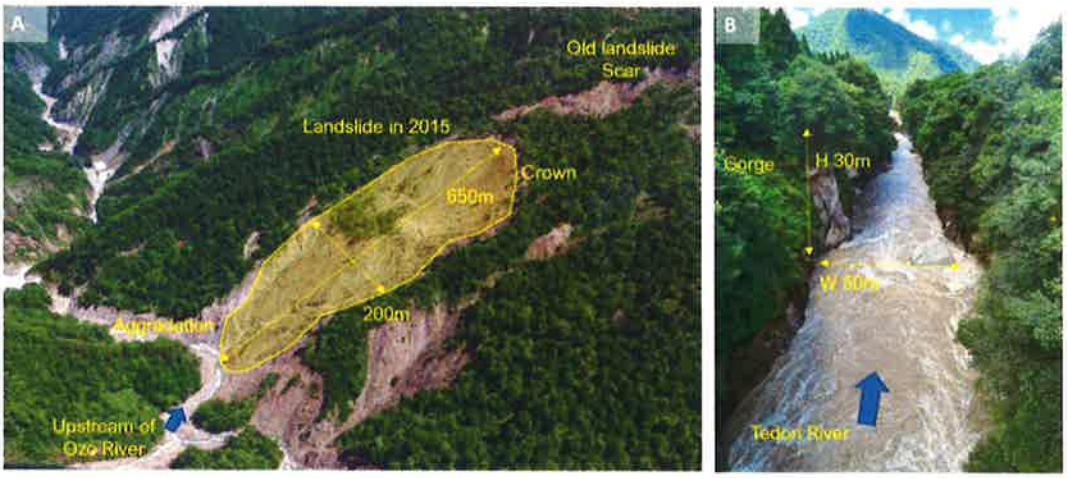

Photo credit: left photo (A) taken by Ishikawa Forest Management Office, 2016

Figure 2. Overview of the Sennindani 2015 Landslide and Tedori River: (A) a panoramic view of the 2015 landslide, showing the Ozo River (a tributary of the Tedori River) and old landslide scar, and (B) a gorge section of the Tedori River, almost 32 km downstream from the Sennindani 2015 landslide.

3.2.2.2. Research methodology

In this study, we evaluated the effects of the sediment produced by the Sennindani 2015 landslide, which was transported along the Tedori River and discharged to downstream alluvial fans. In this study, we analyzed pre- and post-landslide changes in the turbidity of the Tedori River, variations in the riverbed depth of the Tedori River, sediment accumulation in paddy fields, changes in well water levels in alluvial fans, and alterations in fish habitats and populations (Table 1). Various sources including government agencies, university libraries, and websites were accessed to gather both published and unpublished secondary data.

Table 1. Description of data/records and relevant sources used during the study.

Data	Year / Period	Source	Remarks/links
Fluvial erosion/deposition, LiDAR derived DEM data	2007, 2013, 2015, and 2021	LiDAR data obtained from the Kanazawa office of Rivers and National Highways, Hokuriku Regional Development Bureau, Ministry of Land, Infrastructure, Transport, and Tourism (MLITT), Japan	16 km from river mouth to Tsurugi town, https://www.hrr.mlit.go.jp/kanazawa/chisui/index.html#chisui2
Tedori river flow rate and Turbidity	2008-2021	MLITT, Japan	The river flow rate and Turbidity were measured at Tsurugi hydrology gazing station at Tsurugi town https://www.hrr.mlit.go.jp/kanazawa/chisui/tedori_dakudo/tedori_dakudo.html
Well water level (alluvial fan area)	2008-2021	Living Environment Department, Ishikawa Prefecture	Ishikawa Groundwater Conservation Measures Survey Report https://www.pref.ishikawa.lg.jp/kankyo/shiryo/tika/tyousahoukokusyo.html
Fan sediment Deposition Thickness	2006-2021	Shichika District Water Supply Land Improvement project	Primary records (unpublished data)
Fish (Ayu)	2008-2020	Ishikawa Fisheries Research Center Business Report, 2020	4 km upstream from the mouth of the river https://www.pref.ishikawa.lg.jp/suisan/center/kenpo/reportindex1.html
Fish (Salmon)	2008-2020	Ishikawa Fisheries Research Center Business Report, 2020	1.8 km section from the mouth of the river https://www.pref.ishikawa.lg.jp/suisan/center/kenpo/reportindex1.html
Fish (Tomiyo)	2007-2021	Ishikawa Prefectural University report, 2021	Report by Ichion et al. 2021

Turbidity status of the Tedori River

To understand the changes in turbidity status, we analyzed the data on turbidity and river flow rate of the Tedori River, which were recorded by an automatic measurement system installed at the Tsurugi hydrology gazing Station of the Ministry of Land, Infrastructure, Transport, and Tourism (MLITT) (Figure 1B). River discharge (m^3/s) and turbidity (NTU) were automatically observed every minute from 2006 to the present. For this study, we accessed the data recorded for a period of 14 y, from 2008 to 2021 (Figure 3 and 4).

Fluvial (riverbed) sediment erosion/deposition

To assess river topography dynamics, we utilized LiDAR data for the years 2006, 2013, 2015, and 2021 in the form of point clouds obtained from the Kanazawa River and the National Highway Office under the MLITT. We utilized the 3D Analyst tool in ArcGIS Pro 3.0 (ESRI Inc.) to convert the point cloud data (x, y, and z data) into a LAS dataset, and subsequently used the las dataset to create 0.5 m mesh DEM data for each consecutive year. Using these DEM data, elevation differences and changes in volume were calculated for the 2006–2013, 2013–2015, and 2015–2021 periods, using the cut-and-fill and raster calculator of the spatial analyst tool (Figure 5 and 6). The Tedori River channel (within the alluvial fan) is divided into 17 sections of 1 km each from the top of the alluvial fan (Tsurugi town) to the mouth of the river (Sea of Japan), and the amount of sedimentation and erosion per unit area was estimated by dividing the area of each section by the area of the active channel section, excluding the forested sections on both banks of the river (Table 2).

Sediment dynamics in paddy fields

The sediment-laden water of the Tedori River after the 2015 landslide also spread to the paddy fields in the alluvial fan through the irrigational canal network. To assess the changes in secondary information regarding the deposited sediment thickness in the paddy field, measured at 42 locations (Figure 7) near the irrigation canals in the alluvial fan, was accessed from the Shichika district water supply land improvement for the period of 2006 to 2021. Sediment thickness was found to be unevenly distributed, ranging from 0–40 cm, at 42 locations. The sediment thickness difference was interpolated to the entire alluvial fan using

the interpolation tool of the spatial analyst in ArcGISPro 3.0 (ESRI Inc.) and is presented in Figure 7.

Well-water level in the alluvial fan

We selected eight water wells in the alluvial fan (Figure 7) to assess fluctuations in water levels post- and pre-landslide. The water levels in these eight wells are measured every 3 h using hydraulic sensors, and the Ishikawa Prefectural Government publishes the results annually on its website (Ishikawa Prefecture, 2022). Such measurements have been ongoing since 1974, but we used 14 y of data (2008–2020) to study the impact of the 2015 landslide on water-level changes in the alluvial fan region (Figure 8). Furthermore, we calculated the average water level in the wells for seven years using water level records from 2008 to 2014 for each well. The average annual water levels of the monitored wells in 2015, 2016, 2017, and 2018 were calculated. Then, the difference between the seven-year average groundwater level and the average water levels for 2015, 2016, 2017, and 2018 was estimated. The maximum water level differences for 2015, 2016, 2017, and 2018 were interpolated using the inverse distance weighting (IDW) method and the IDW conversion tool of the spatial analyst in ArcGISPro 3.0 (ESRI Inc.), as shown in Figure 9.

Effects on fish and their habitats

Among the downstream ecosystems, fish are the most vulnerable to sediment-laden flows in the Tedori River. Thus, we focused on three fish species with different life cycles and habitats in the Tedori River: (i) Ayu (*Plecoglosus altivelis)*, a bilateral migratory fish; (ii) chum salmon (*Oncorhynchus keta)*, an anadromous migratory fish; and (iii) Tomiyo (*Pungitius sp.1)*, a freshwater fish. Ayu is a vital freshwater fish species in Japan, prized not only as a food source but also for its economic value and popularity among anglers. (Fujita et al., 2022). In this study, we examined data from the Ishikawa Prefectural Water Surface Experiment Station's Ayu spawning surveys (Supporting Information S1), which reported the number of Ayu eggs found in their spawning sites along the Tedori River between 2007 and 2020 (Figure 10).

The second species selected for this study was the Tomiyo fish, which inhabits the Takeyabu Canal, a tributary of the Kumada River that originates from the spring water supplied by the Tedori River. To evaluate the impact of the sediment-laden flow of the 2015 landslide on the Tomiyo fish habitat and their population in the Kumada River, we analyzed data previously published by researchers from the Ishikawa Prefectural University. The data spanned 16 y, covering the period from 2006 to 2021 (Figure 11) (Supporting Information S1).

The third most notable species selected was the chum salmon, which is one of the most abundant fish in Japan and an important fishery resource in northern Japan. Every autumn (October–November), they migrate upstream of the Tedori River from the coastal areas of the Sea of Japan. We evaluated the effect of turbid water on chum salmon by analyzing data published by the Ishikawa prefectural government on changes in the number of coastal catches and Tedori River catches for the 2006-2021 period (Figure 12).

3.2.3 Results and Discussion

3.2.3.1 Results

The following sections present the findings of this study that compared the impact of sediment carried by water on downstream ecosystems before and after a landslide occurred.

Turbidity fluctuations in the Tedori River

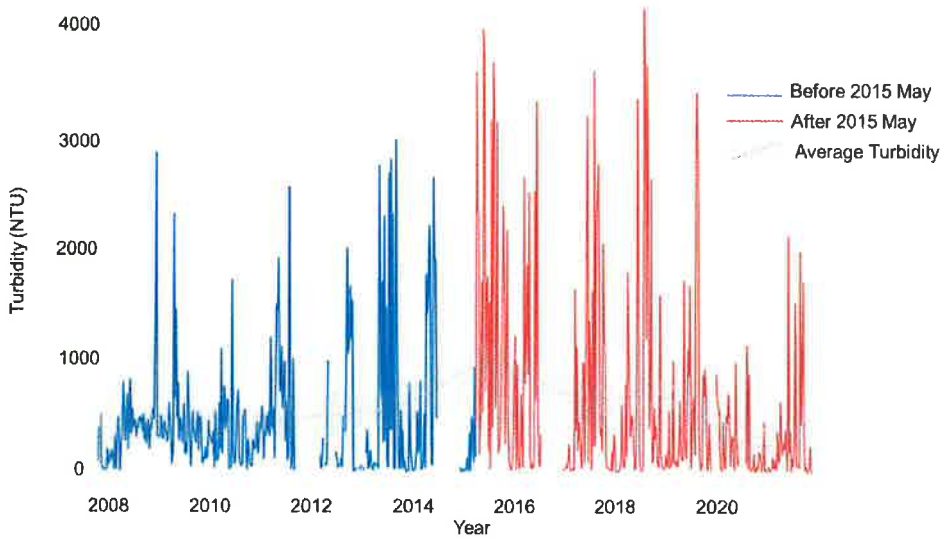

Figure 3. Weekly changes in maximum turbidity in the Tedori River over time (average turbidity is shown at the 95% confidence interval).

According to Figure 3, the highest turbidity levels recorded in the Tedori River on a weekly basis between 2008 and 2014 averaged around 500 NTU over the course of seven years. Furthermore, the maximum turbidity level during this period did not exceed 3000 NTU. Despite 2014 being a wet year, the turbidity levels frequently approached but never exceeded 3000 NTU. However, following the Sennindani landslide in May 2015, which generated a significant amount of sediment, the turbidity rose rapidly to record levels. On May 3, 2015, the turbidity exceeded 3600 NTU and reached a peak of 4012 NTU on June 21, 2015. While the turbidity levels decreased slightly during winter, there were frequent instances of levels exceeding 1000 NTU. The highly concentrated turbid water continued to flow in 2016, with turbidity levels exceeding 2000 NTU beginning from the snowmelt in April and rising to 3300 NTU by the month of July. Subsequently, the automatic measuring instrument malfunctioned, and data collection was temporarily suspended until February 2016. Between 2017 and 2018, high concentrations of turbid water persisted, and in August 2018, the highest recorded turbidity level of 4200 NTU was measured. The average turbidity between 2015 and the end of 2018 was 859 NTU, nearly 1.9 times higher than that before 2015. Since 2019, the turbidity levels have shown a decreasing trend, and in 2020, the highest recorded value was 1138. In 2021, several floods caused the concentration to rise to over 2000 NTU, but the average value remained low (approximately 84 NTU) throughout the year.

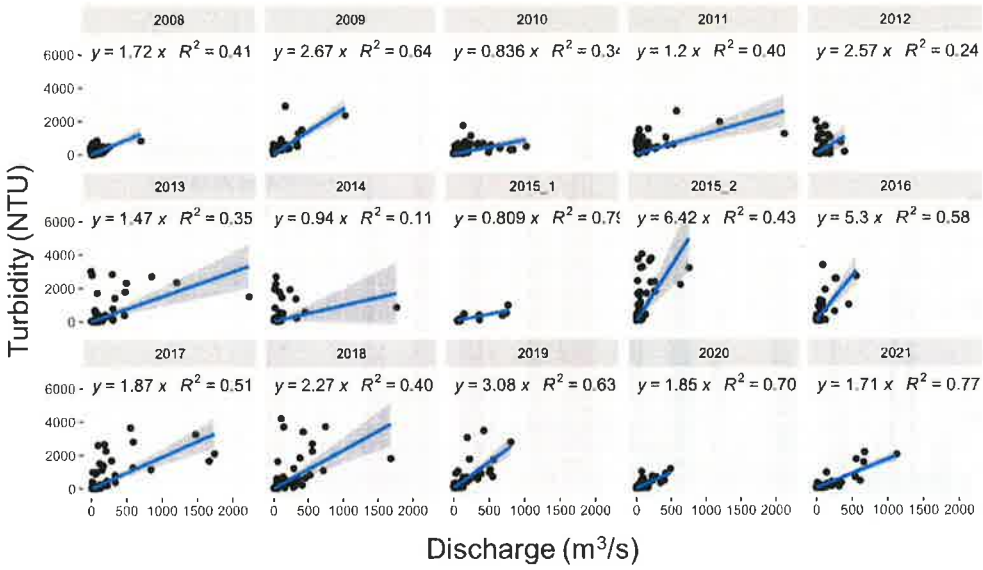

Figure 4. Changes in the relationship between discharge and turbidity for each fiscal year from 2008–2021. Sub figures for 2015 (before (2015_1) and after (2015_2) the landslide in May) are separately presented.

Figure 4 depicts the relationship between annual maximum weekly turbidity and discharge from 2008 to 2021. High turbidity tends to occur at the time of flooding; therefore, there is a general tendency for a high correlation between discharge and turbidity. From 2008 to 2014, the slope of the linear regression ranged between 0.836 and 2.67, and the turbidity of the river water remained below 2000 NTU even when the discharge exceeded 2000 m^3/s. In 2012, the slope of the regression line was steeper, but both the water discharge and turbidity were <2000 NTU, and the coefficient of determination (R^2) was less (0.24). However, from May 2015 to December 2016, despite low discharge (<1000 m^3/s), maximum turbidity (>4000 NTU) was observed, and the slope of the regression line had higher values ranging between 5.3–6.42, respectively. In the years 2017, 2018, and 2019, the slope of the regression line was 1.87, 2.27, and 3.08, respectively, and the turbidity was found to be approximately 4000 NTU. The water discharge fluctuated between 800 m^3/s to 1600 m^3/s and the turbidity remained below 4000 NTU during this period. This may have occurred in response to large floods. During 2020-2021, the slope of the regression line reduced to 1.7–1.8, which was similar to the level before 2014, and the R^2 value showed a high correlation of 0.7 or more.

Fluvial erosion and sediment changes in the Tedori River section

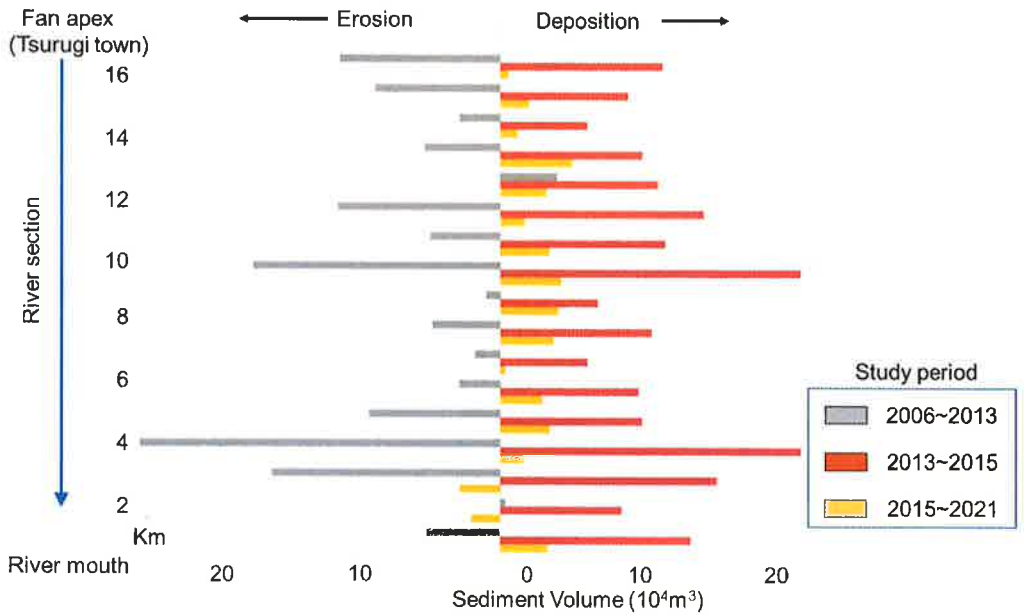

Figure 5. Erosion/sedimentation volume changes in 17 sections (each with 1 km length shown in Figure 1B) of the Tedori River for the three periods between 2006–2021.

The erosion and sediment deposition volumes for 17 sections of the Tedori River (alluvial fan) were calculated from the LiDAR data for three time periods (2006–2013, 2013–2015, and 2015–2021), as shown in Figure 5. Of the 17 sections studied between 2006 and 2013, all showed a negative erosion trend before the landslide, except for section 2 near the river mouth and section 13 upstream, which exhibited a positive trend. In particular, sections 3, 4, and 10 were remarkably eroded, exceeding 200,000 m^3. Between 2013 and 2015, positive sedimentation (i.e., sediment accumulation) occurred in all 17 sections. During this period, sections 4 and 10 exceeded a sediment volume of 200,000 m^3, and a few other sections exceeded 100,000 m^3. Finally, between 2015 and 2021, a mostly positive trend was observed in sedimentation, although the sediment quantity ranged from 20,000 to 50,000 m^3. In addition, downstream sections 2 and 3 demonstrated negative sedimentation values.

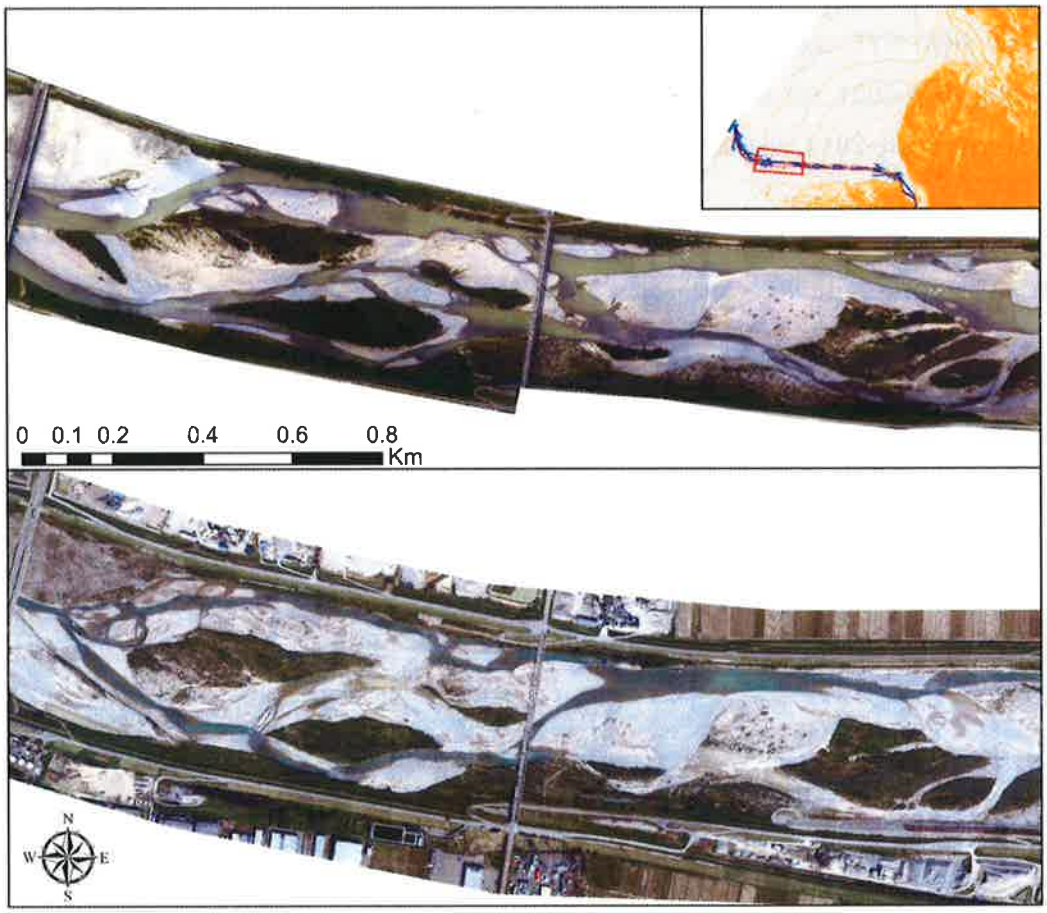

Figure 6. Spatiotemporal changes in section 4 where the largest changes in erosion and sediment volume were observed: (A) Aerial photograph in September 2013 and (B) Aerial photograph in September 2015.

In 2013, the streams appeared to be braided on both banks and a wide riverbed and gravel belt could be seen more vividly on the western side of the middle bridge (Figure 6A). Additionally, a riverside forest belt stranded in a green-striped pattern in the central part developed near the westward bridge. However, in 2015, the area of the gravel belt spread further and the gaps between the striped distributions of the gravel piles were buried by sediment (Figure 6B). In addition, the braided segments of the river were pushed parallel to the northern bank of the river channel.

From the analysis of the LiDAR-derived DEMs and aerial photographs, it was found that there was a large difference in the sedimentation tendencies for each period. Large fluctuations occurred in all 17 sections, from the apex of the fan to the fan tip.

Table 2. Average sedimentation and annual riverbed variation between fan areas during the three periods.

Period	2006-2013	2013-2015	2015-2021
Mean sediment Volume per section (m^3)	−74373.75	119190.32	21886.98
Mean sediment accumulation rate in the period (m^3/m^2)	−0.37	0.58	0.11
Mean annual accumulation rate (m^3/m^2)	−0.05	0.29	0.02

Table 2 shows the amount of riverbed fluctuation per unit area obtained by dividing the amount of sedimentation/erosion in the section by the active channel area (Supporting Information S2). The average sedimentation volume in the section from 2006 to 2013 was almost 74,000 m^3; however, from 2013 to 2015, sedimentation reached approximately 120,000 m^3. Since then, the sedimentation trend continued till 2021, at an average of 22,000 m^3. Sedimentation thickness from 2006 to 2013, 2013 to 2015, and 2015 to 2021 was 0.37 m, 0.58 m, and 0.11 m, respectively. The periodic sedimentation thicknesses were converted to a yearly scale, which revealed that the riverbed was lowered by 0.05 m per year before the 2015 landslide, while it abruptly rose by 0.29 m immediately after the landslide and has continued to rise by 0.02 m since then till 2021.

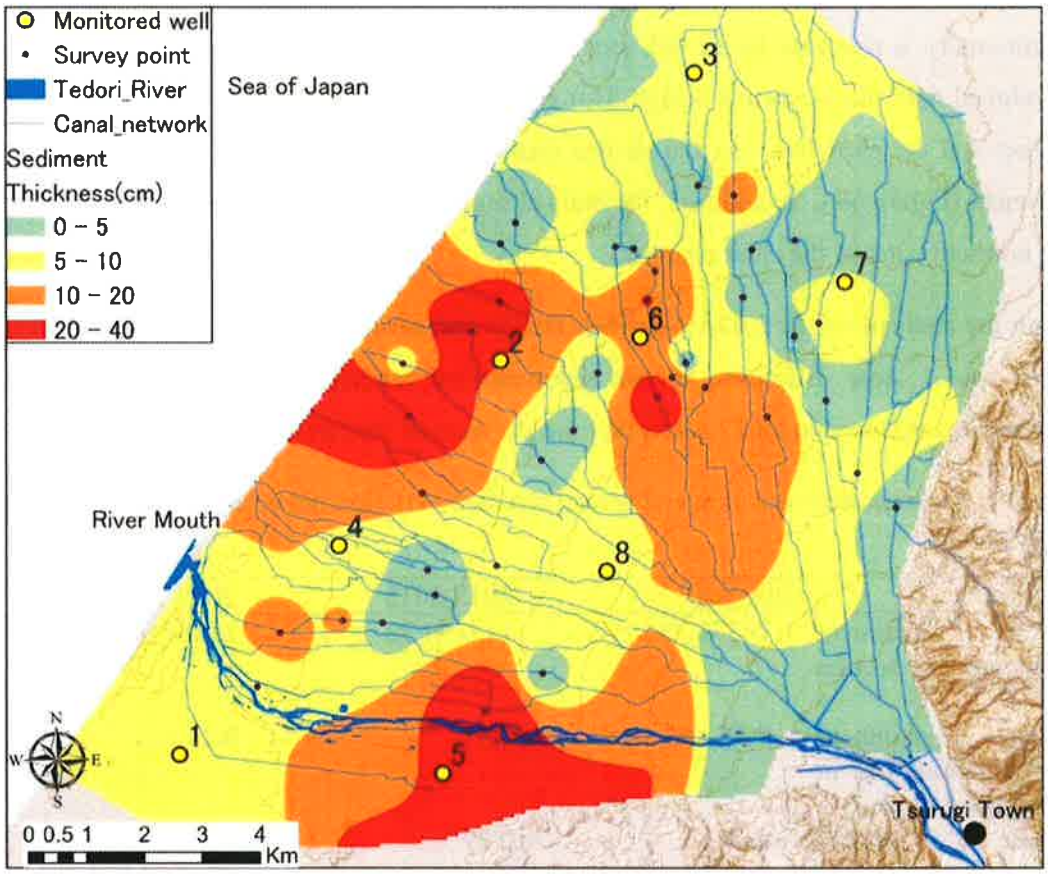

Figure 7. Location of monitored well, sediment thickness survey point, irrigation canal network, and distribution of sediment thickness after the 2015 landslide in the entire alluvial fan.

A positive relationship was revealed between the layout of the canal network and the diffusion and distribution of the sediment. The distribution trend in the figure shows that sediments up to 10–40 cm thick were deposited along the central part of the alluvial fan, which diverged slightly downstream of Tsurugi at the top of the alluvial fan. In addition, the left bank of the Tedori River, which flows along the west side of the alluvial fan and the end of the central part of the fan near the coast, also have areas with large sediment deposit thicknesses. In contrast, patches of thin sedimentary layers were distributed on the east, north, and west sides of the alluvial fan. Sediment deposits tend to be widely distributed throughout the alluvial fan along the main canals (there are seven main canals), and supply water to the paddy fields on the south side of the alluvial fan on the left bank.

Fluctuation in the water levels of the monitored wells

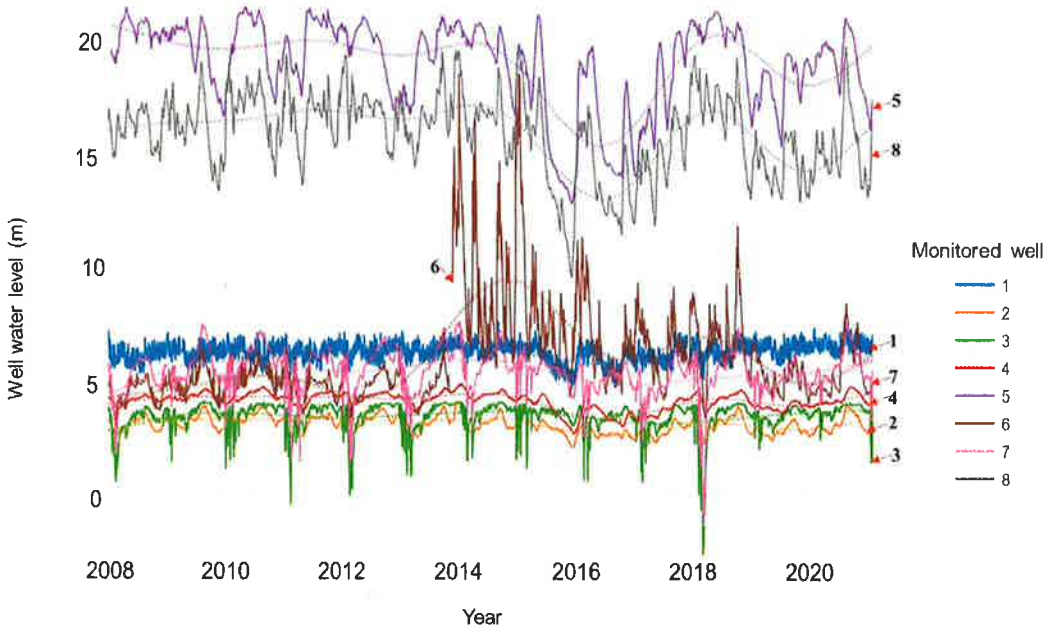

Figure 8. Mean water level variation over time in eight monitored wells in the alluvial fan (2008 to 2020).

The water level records of the monitored wells from 2008 to 2020 are presented in Figure 8. The water level in each well differed depending on the altitude and depth of the well. For instance, consider Well 5 in Figure 8, which exhibits a distinct pattern. Despite some variations before 2015, the water level remained steady at approximately 20 m. However, a sudden decline in water level has been noticed since May 2015, with the lowest water level dropping to 15 m during the summer of 2016, experiencing a decline of >5 m. Subsequently, the water level gradually recovered, and at the end of 2017, it returned to its previous height of 20 m. Subsequently, it declined until 2019, although the decrease was minimal. Thereafter, it gradually increased to its initial level by the end of 2020. A similar pattern was noted in Well 8, where there was a sharp decline in the spring of 2015, followed by a partial recovery, and then a further decline, which persisted until the end of 2017. The other monitored wells (1, 2, 3, 4, and 7) exhibited comparable phenomena, where the reduction in the water level was minimal. However, there was a high degree of synchronization between the attenuation and minimum water level periods. Figure 8 illustrates that among the monitored wells, only Well 6 exhibited a distinct variation in groundwater level. The level increased significantly

from 2013 to 2016 and remained elevated thereafter. The sensor used to measure the groundwater level in Well 6 was replaced in 2014, and its detection ability differed from that of the other sensors.

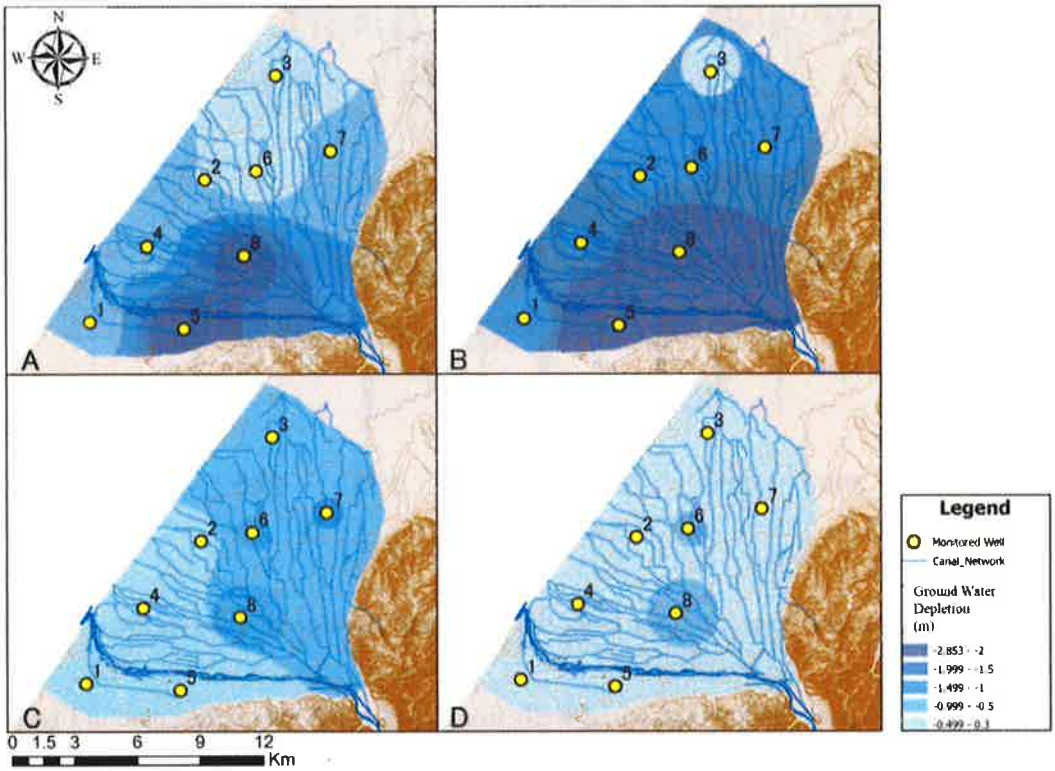

Figure 9. Visual representation of the distribution of maximum groundwater level depleted in A) 2015, B) 2016, C) 2017, and D) 2018. Dark blue areas indicate a significant drop in the water level of the monitored wells.

In 2015, Wells 5 and 8, located in the upper area of the alluvial fan, exhibited a significant drop in the water level, as shown in Figure 9. In addition, the western and eastern areas of the alluvial fan and the vicinity of the Japan Sea coast experienced a drop in water level of 1 m or less. However, the northern side of the alluvial fan was less affected. Compared to 2015, the area affected by the drop in the water level expanded in 2016. By 2017, the affected area had undergone a complete change, with the most notable drop in water level observed in the eastern half of the alluvial fan. The decrease in the water level in the central part of the alluvial fan was <2 m. In 2018, a water level drop was only observed in the form of smaller patches scattered throughout the alluvial fan, and the affected area was significantly reduced compared to previous years.

Effects of sediment on fish and their habitats

Effects on Ayu spawning sites

Ayu spawning in the Tedori River typically occurs between October and November. The box plots in Figure 10 show the changes in the number of Ayu eggs based on the survey results of the Ayu spawning sites from 2007 to 2020. From 2007 to 2011, the maximum number of eggs was approximately 200×10^6, while the median was in the range of 36×10^6 to 75×10^6 per section. In 2012, spawning sites with a maximum of 657×10^6 eggs and a median of 130×10^6 eggs were observed. In 2013 and 2014, high-density spawning numbers of up to 225×10^6 and 352×10^6 eggs were observed (in 2014, there was a plot of zero and the median value was low). However, in 2015 and 2016, when turbid water flowed, almost no eggs were observed in the spawning sites (in 2016, only 0.2×10^3 eggs were laid). Even in 2017, the number of eggs was less, but as time passed, it increased from 80×10^6 to 192×10^6, from 2018 to 2020. Based on this boxplot, the number of eggs laid at the spawning sites was at almost the same level in 2019 as in 2013; therefore, it can be inferred that it took almost five years to recover from the effects of turbid water after the 2015 landslide.

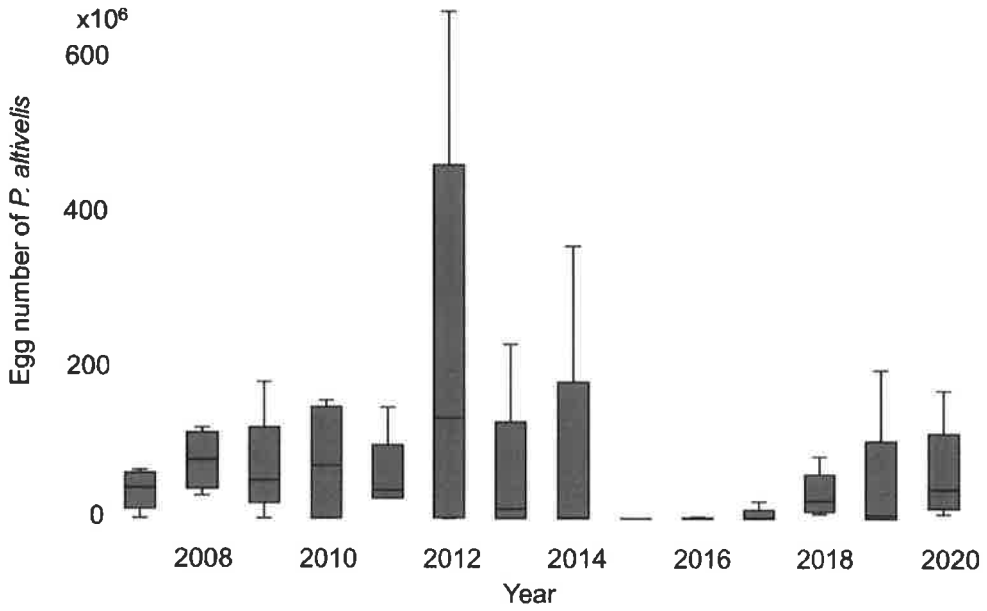

Figure 10. Annual change in the spawning of Ayu at a fixed point at the mouth of the Tedori River.

Sedimentation effect on Tomiyo fish habitats

Since 2015, spring water flowing in Takeyabu Canal (which is a spring-fed stream), a tributary of the Kumada River, has disappeared. The water level decreased significantly. The drop in water level had a severe adverse impact on the Tomiyo population, as they completely relied on the canal as their spawning habitat. This significantly affected the Tomiyo population, which used the canal as a spawning habitat.

Figure 11 shows the total number of Tomiyo fish captured annually (March to July) in the cage nets set in the Takeyabu irrigation canal during the study period. Between 2006 and 2011, this number fluctuated between 250 and 617. In 2012 and 2013, the number of fish caught was the highest (around 1,000), since the start of the measurement, but in 2014, it dropped sharply to 328. In 2015, this number increased to 615. However, between 2016 and 2017, only 3 to 17 fish remained. Since 2018, the number of fish gradually recovered, reaching 189–380, and increased to 1308 in 2021, the highest number recorded during the study period. The right side of the figure shows a dry riverbed with exposed riverbed gravel and puddles, in which a limited number of Tomiyo fish remained in 2016.

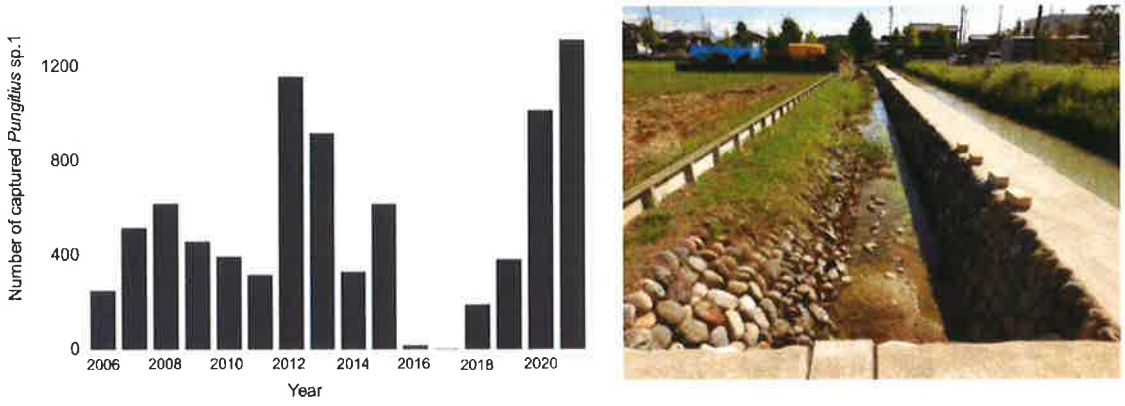

Figure 11. Left: Changes in the number of Tomiyo caught in the Kumada stream section over 16 y. Right: Depleted waterways of spring water (Photo taken by Ichion in the Takeyabu Irrigation Canal section of the Kumada River in 2016).

Effects on the anadromous migration of Chum Salmon

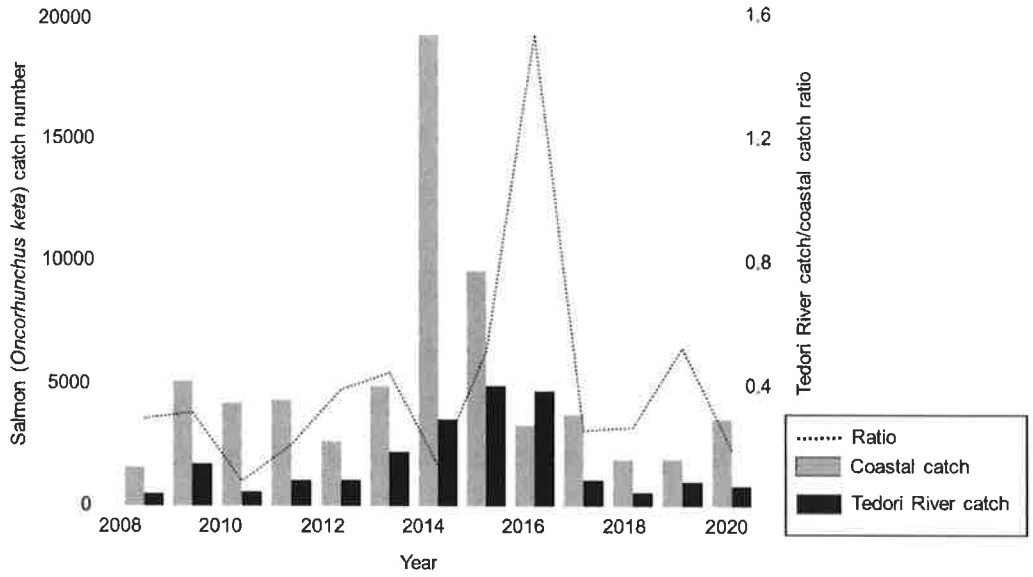

Figure 12. Changes in River catches and coastal catches of Salmon (for Tedori River catches, fishing was conducted in a 1.8 km upstream section from the river mouth). The dashed line indicates the ratio of the number of salmon caught along the coast to the number of salmon that migrated upstream into the Tedori River.

In autumn, salmon, which spawn during this season, approach the coast of Ishikawa Prefecture from the Sea of Japan, and some migrate upstream to the Tedori River. Figure 12 shows the number of salmon caught along the coast and in the Tedori River as well as the ratio between them, based on data collected by the Ishikawa Prefecture Fisheries Research Center. The number of salmon caught along the coast averaged around 3,000 per year between 2008 and 2013 but never exceeded 5,000. However, nearly 20,000 salmon were caught along the coast in 2014. In 2015, the number was approximately 10,000, and from 2016 to 2020, it fluctuated between 1,800 and 3,500. No significant decrease in the number of salmons was observed during this period. In 2014, when the number of salmon caught along the coast was significantly higher, the number caught in the Tedori River was 3,500; in 2015, it reached a maximum of 4,900. The number caught in 2016 was similar to that of the previous year, and from 2017 onwards, it fluctuated between 1,000 and 500. The highest number of salmon caught to date was in 2015, followed by 2016, when there was significant turbidity in the Tedori River due to sediment transportation caused by the Sennindani 2015 landslide. This ratio fluctuated between 0.14 and 0.5, from 2008 to 2014. However, in 2015 (0.5) and 2016 (1.41), the number of salmon caught in the Tedori River exceeded that caught along the coast. Since then, there have been years, such as 2019, when the ratio was slightly

higher (0.52); however, it mostly fluctuated between 0.2 and 0.3. The number of salmon caught in the river in 2015 and 2016 showed a prominent trend of increase.

3.2.3.2 Discussion

Changes in sedimentation-induced river turbidity

Previous research has shown that sediments from large-scale landslides in mountains can pose major hazards downstream, including land subsidence, increased flooding, and river channel avulsion. These topographic effects can occur well beyond the site of slope failure (Korup et al. 2006). In this study, we present the impact of landslides in an alluvial fan nearly 40 km downstream of the landslide.

When the deep-seated Sennindani 2015 landslide occurred on Mt. Hakusan, the turbidity of the Tedori River increased significantly after May 2015. Nearly 35 m thick layer of sediment was deposited along a 500 m section of the Ozo River (Yanai, 2018). This large amount of sediment was gradually transported downstream, creating turbid water in the Ozo River that persisted for an extended period of time.

The Ozo River flows in a narrow V-shaped channel and confluences with the Tedori River just below the Tedori River dam (153 m height) (Figure 1A). Since the Tedori River catchment area is large, many other active landslides occur in the upstream tributaries of the Tedori River on Mt. Hakusan; however, the Tedori River dam at the confluence point also stores sediment carried by other tributaries. However, the Ozo River confluence is just below the Tedori River dam (Figure 1A); therefore, all sediment flowing through the Ozo River channels into the Tedori River. Therefore, the Ozo River is considered to be one of the main sources of sediment supply in alluvial fans. The Tedori River channel has a gorge topography with a depth of 30 m and a steeper slope downstream that stretches for 20 km. It is believed that most of the transported sand in the river was not stored in the channel but rather carried towards Tsurugi town.

The turbidity of the Tedori River rose sharply, reaching a maximum of 4000 NTU, more than six months after the landslide. The turbidity of the Tedori River increased by at least two times the average turbidity before the landslide. In general, when landslides occur near rivers, the river becomes highly turbid (Lin et al. 2011), and the level of turbidity decreases over

time. Six years after the landslide collapsed, the sediment-laden flow gradually decreased. As a limitation, this study has acquired turbidity data from a single hydrological station, potentially overlooking other sources of sediment such as surface erosion of different land use and channel scouring of Tedori river. To improve accuracy, future research endeavors should incorporate multiple turbidity monitoring stations along different sections of the river. As sediment production and transportation along the Ozo River receded, the downstream sediment supply also declined. One factor is thought to be a decrease in slope erosion owing to vegetation recovery. The Kinki Chugoku Forest Management Bureau took action to reclaim the Sennindani 2015 landslide area by implementing countermeasures and commencing revegetation activities in 2017 (Kinki Chugoku Forest Management Bureau, 2021).

In the alluvial fan area, there was a remarkable increase in sediment deposition after the 2015 landslide. Time-series LiDAR data revealed that the riverbed rose by 0.29 m immediately after the landslide in 2015. The phenomenon of riverbed heightening continued until 2021 but at a lower rate. Hai et al. (2014) investigated the long-term changes in the Tedori River channel and observed a lowering of the riverbed by 0.5–3.5 m from 1950 to 1991, resulting in a loss of 12.7×10^6 m^3 and identified continuous sediment extraction as the main cause of this deterioration during that period. Hai et al. (2019) stated that sediment extraction and dam construction had a significant impact on the morphological characteristics of the lower Tedori River.

Similarly, riverbed degradation (Figure 5) occurred in all 17 sections before the landslide, whereas deposition was observed after the landslide in 2015 and declined gradually. Although the data acquisition interval was three years, from 2013 to 2015, it is considered that the sedimentation occurred in 2015. Yanai et al. (2016) reported that the amount of sedimentation has increased in a sediment trap pond installed near the irrigation canal of the Tedori River since the spring of 2015. Later, during 2015–2021, a slight decline in deposition was observed, indicating that the sediment remaining in the channel continued to move and flow down to the Sea of Japan.

Effect of sedimentation on groundwater recharge

Sediments transported from the upstream landslide flowed across the river channel and were diverted to paddy fields in the alluvial fan through an irrigational canal network. It has been reported that 50% of the groundwater was supplied from the riverbed of the Tedori River and 50% was contributed by paddy fields in alluvial fans (Takase and Fujihara, 2019). First, our study revealed that after the landslide, the riverbed received sediment deposition of up to 0.58 m in the alluvial fan area. As shown in Figure 7, the sediment originating from the landslide was thickly deposited on the riverbed, and it is thought that this added muddy layer blocked infiltration into the ground by burying gravel and stones along the channel. Yoshioka et al. (2020) used a two-member mixing model based on Sr concentration and isotopic composition (Hydrogen-H, Oxygen-O, Strontium-Sr) to confirm that the contribution of groundwater recharge from the Tedori River during the turbid water flow period decreased, particularly along the left bank of the river. Their results coincide with the results of our study, as shown in Figure 7, where the deposition was highest on the left bank of the Tedori River, and there was significant groundwater depletion in the same area (Figures 9A and 9B).

Second, this study found that paddy fields, which are the major land-use type of alluvial fans, received sediment deposition up to 0.40 m after the landslide. It is supposed that the deposition of fine-grained sediment inhibited another infiltration route into the ground, reducing groundwater recharge, and consequently causing a long-term decrease in groundwater level. Tanaka et al. (2017) conducted a survey to assess water reduction in paddy fields before (2014) and after (2016) the occurrence of turbid water and clarified that the paddy field infiltration rate decreased from 12.4 mm/d in 2014 to 7.9 mm/d in 2016.

The groundwater levels in Wells 5 and 8 on the left bank of the Tedori River, as shown in Figure 9, exhibit a significant decline. This decline in the water level is believed to be a direct result of reduced infiltration in the area (Yoshioka et al. 2016). The reduction in infiltration may be attributed to the supply of fine-sized sediments, which can obstruct the pores on the soil surface in paddy fields. However, farmers plowed and puddled paddy fields after harvesting to prepare for the following year's rice plantations. This human intervention may have mixed the previously accumulated sediment with the soil, leading to gradual recovery during the infiltration process. However, this study has not considered the aspect of polluting chemicals being supplied to water sources and paddy fields during sedimentation due to limited data availability.

Effects of sediment on fish and their habitats

The continuous supply of sediment to rivers can affect downstream water quality, leading to fish habitat degradation (Sidle et al., 1985). Fish are probably affected the earliest, as they depend on access to and water quality in rivers (Schuster and Highland, 2007). Landslides that release sediment often create a harsh aquatic environment for fish in the short term, but can completely alter their habitat in the long term. Suspended sediments in rivers reduce light penetration and algae production, and damage the gill membranes of fish, which can be lethal at high sediment concentrations and long exposure to sediments (Lazar et al., 2010). Sediments deposited in the gravel bed fill the gaps and reduce the dissolved oxygen supply to the fish eggs. Excess sediment can also damage habitats where juveniles feed and grow by creating unfavorable conditions for the growth of aquatic insects (Kemp et al., 2011). Geertsema et al. (2009) highlighted that storms and landslides are the dominant events causing physical habitat degradation in rivers.

We assessed sedimentation impacts on Ayu, Tomiyo, and Salmon fish, but the long-term sedimentation might have influenced many other aquatic species for which data was unavailable.

Ayu fish population has experienced a significant decline owing to the effects of turbid water; however, they had recovered to their original levels by 2020. The reasons for this dramatic decrease are not entirely clear. However, there are two possible explanations. One possible explanation is that turbid water is an unsuitable environment for them. When turbid water persists for an extended period, fish tend to avoid it and take refuge in other tributaries. According to a study conducted by Mori et al. (2018), when the turbidity level reached 200 mg/l, the Ayu moved away from their habitat. Moreover, algae such as diatoms, which are the main food source for Ayu fish, grow on the surface of stones and gravel in fast-flowing water, but turbid water fills the spaces between the gravel, making it difficult for algae to survive. Therefore, it is conceivable that Ayu might have left their original habitat and moved to a tributary with less turbidity. Another possible explanation for the decline in Ayu population is that turbid water has a significant impact on the formation of spawning beds. The necessary conditions for the spawning site of Ayu include shallow flowing water with small-sized sediments and gravels/pebbles, which provide a suitable substrate for the eggs to attach to. Previous researchers have recommended that the necessary parameters for Ayu spawning sites include the presence of pebbles or rough gravels, water flow velocity of 20–

120 cm/s, water depth of 10–60 cm, <5–10 mm sediment particle size, and 15 °C or less water temperature (Ishida 1962; Ishida 1990; Suzuki et al., 2011).

However, as shown in Figures 10 and 11, the shallow water and slow flow rate caused by upstream sediment deposition and the burial of pebbles and gravel caused a loss of suitable Ayu spawning environments. Eventually, sediment deposition and water turbidity decreased, causing fine sand to be transported downstream and resulting in the restoration of rapid water flow, which allowed the Ayu to return to the Tedori River for spawning.

The Tomiyo fish survey was conducted in the Takeyabu irrigation canal, which originates from spring water supplied by the Tedori River. In 2015, the Tomiyo fish population remained intact in the Takeyabu Canal, even when turbid water flowed into the Tedori River. However, in 2016 and 2017, the number of Tomiyo fish reached nearly zero. In 2016, the water levels of the Takeyabu irrigation canal and the upper reaches of the Kumada River significantly decreased, and little water remained in the channel. Tomiyo fish generally lay eggs from March to July; however, the water in this stream was depleted in early July 2016. The decreased water infiltration towards the spring from the Tedori River might have affected the water volume in the Kumada River basin, causing the disappearance of the Tomiyo population. As the groundwater level gradually recovered after 2018, the Tomiyo fish population also gradually recovered to its pre-2015 landslide status by 2021.

In contrast, the number of catches of the chum salmon in the river and coastal areas was higher in 2015 and 2016, than in previous years, in the same section of the river due to the impact of concentrated turbid water flow to coastal areas.

One possible reason for this is that turbid water may impair olfactory cues (Bandoh et al., 2011) at the time of upstream migration. Turbidity can interfere with these olfactory cues by masking the chemical signals (Yamamoto et al. 2009) that salmon use to find their way. As a result, salmon may become disoriented and move upstream in search of their home stream. Therefore, the maximum number of salmon may have aggregated near the coastal areas in search of their natal river and the lower segment of the Tedori River. Moreover, high concentrations of turbid water have been reported to act as a cover for salmon fish from predators (Gregory and Levings, 1998). Young salmon are more likely to be targeted by large predators such as mammals and birds. Turbid water is believed to reduce water transparency and minimize the rate of predation during anadromous migration.

Evaluating landslide sediment effects on watershed systems

Landslides that occurred upstream of the Tedori River on Mt. Hakusan produced a large volume of sediment, which quickly flowed downstream, significantly affecting the downstream systems in the alluvial fan. The Tedori River is a rapidly flowing river with no meandering sections in which sediments can accumulate, forming deep gorges that allow sediments to flow smoothly downstream. Consequently, a substantial amount of sediment deposition was observed in the alluvial fan, where the slope became gentler, and eventually, fine-grained turbid water flowed into the seacoast. This deep landslide occurrence, through sediment movement, serves as an indication of the fundamental connection between mountains and coastal areas at the watershed scale. Figure 13 schematically shows the relationship between mountains, rivers, alluvial fans, and coastal areas. A large amount of sediment flowed downward without stopping and was deposited in an alluvial fan. In addition, more fine-grained components migrated to the sea and diffused.

An extensive volume of sediment was transported by the Tedori River and deposited in the alluvial fan. Deposited sediments in the braided sections of the river channels in the alluvial fan areas buried stony substrates (stones and gravel), created a muddy layer, and resulted in the decreased infiltration of water from the riverbed to the ground, disrupting the groundwater recharge function. Consequently, the groundwater level decreased immediately after the landslide, reaching its lowest point in September 2015, but replenished to its original level in the winter. However, the sedimentation processes persisted in 2016, and this decline and recovery cycle of the groundwater level continued for the next three years until 2019. For aquatic organisms that inhabit river waters to sustain their life cycles, the continuous flow of turbid water can have a deleterious impact, resulting in the loss of spawning grounds and feeding habitats. In this study, we found that the Ayu lost their spawning habitat, and a significant decrease in the number of Tomiyo fish was observed due to the drying of spring water in the stream. However, as the turbidity level decreased and returned to its original level from 2020 onwards, the situation improved, but it took nearly five years to regain a conducive environment for aquatic habitats.

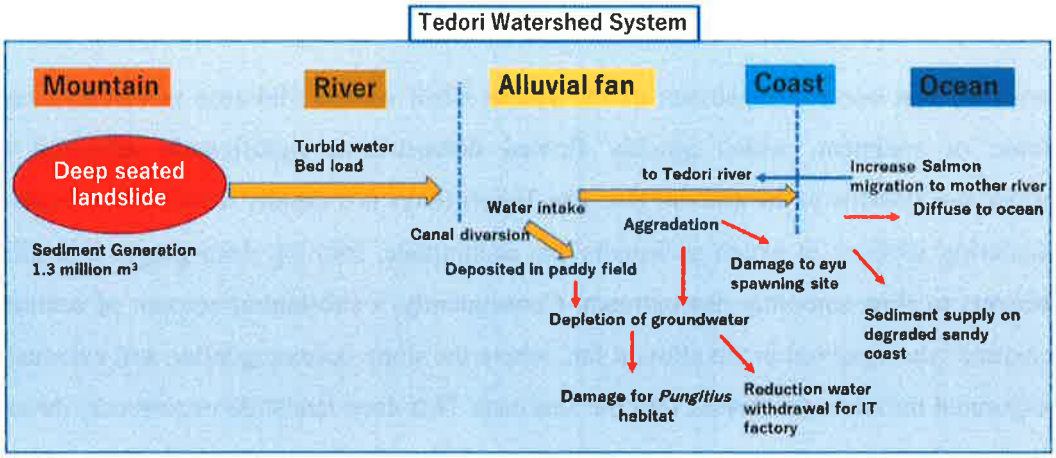

Figure 13. 2015 Landslide in the upstream Tedori River affects downstream ecosystems, both biotically and abiotically, at the watershed scale.

Sedimentation did not adversely affect the growth of crops in paddy fields in the alluvial fan area, although the sediment contained large quantities of alkaline components (Shichika irrigation land improvement district, unpublished material, Ishikawa Prefecture, 2017). Furthermore, it has been revealed that the sand from the Tedori River reaches Chirihama Beach along the Sea of Japan, 50 km to the east, and helps maintain the sandy beach (Sato et al., 2020).

It is also important to note that episodic phenomena such as landslides have a positive effect on the sediment balance of the entire watershed. In Japan, since World War II, many dams have been installed for water utilization and flood control in river basins. Although dams are believed to have a positive impact on the prevention of downstream damage (Rudolf-Miklau and Suda, 2013), they also negatively impact the biodiversity of rivers by reducing the flow velocity and sediment supply downstream (Ezcurra et al. 2019). The installation of the upstream Tedori River Dam also resulted in a significant reduction in the riverbed level in the Fan Top Tsurugi area. (Dang et al., 2014). The adverse effects of sedimentation from upstream landslide on both biotic and abiotic environments in downstream areas can be addressed by formulating an integrated approach to watershed management. Integrated watershed management approaches have proven their effectiveness in enhancing forest ecosystems, fostering community development, and making significant contributions to mitigating disasters such as floods, landslides, and soil erosion (Thapa et al.,2022).

3.2.4. Conclusion

The results of this study suggest that the transportation of sediment from landslides in upstream areas can cause various downstream effects over an extended period. The sediment transported into the Tedori River has been severely affected by turbidity for more than 20 mo. This turbidity had a serious impact on fish, such as the Ayu and Tomiyo, which almost disappeared from their habitats. The increased turbidity of rivers and coasts after the landslides caused an increase in salmon migration from the coast of Japan to the upstream (Natal River) of the Tedori River. The monitored well was affected by the landslide sediment for more than three years after the landslide and took nearly five years after the landslide to recover. Based on these findings, river turbidity, groundwater depletion, and fish ecosystem degradation were observed in the Tedori River as environmental effects of landslides. For the Ayu and Tomiyo, artificial ponds and hatcheries can be set up to protect endangered fish as a backup plan in the event of a similar disaster resulting in high turbidity. The irrigation canal should be diverted to the mainstream to control the inflow of sediments into it. This study discussed the impact of sedimentation on downstream alluvial fans from both biotic and abiotic environmental perspectives, making the findings and recommendations relevant to similar areas at high risk of large-scale landslides.

3.3 Assessment of Hirose Landslide 2021 to learn the protective role of Cedar Forest against debris flow.

3.3.1 Introduction

Recently as a consequence of climate change, mountain landslides are occurring more frequently every year throughout Japan. In the year 2017, a large-scale mountain collapse hit a Cedar (Cryptomeria japonica) plantation forest area in the Kitakyushu area, and the debris flow caused damage to downstream communities (Asada et al., 2020). Also in 2018, the Chugoku region experienced torrential rains causing mountain slope failures and mudslides resulting in large landslides (Kaibori et al., 2018). The sediment disasters have been increasing in recent years. Though erosion control and flood control structures have been constructed to minimize these disasters, the percentage of countermeasures constructed in collapse-prone areas is extremely low.

A landslide is a complex phenomenon in which weathered soil layers or base rock on a slope lose stability due to heavy rainfall, and snow melting, etc. It can be divided into two types of collapse: shallow landslide (landslide of topsoil with 2-3 m depth from the ground surface) and deep landslide (relatively large-scale failure in which not only the topsoil layer but also a deep layer of ground up to several tens of meters in depth becomes a collapsed earth mass). In the past, surface failures used to occur more frequently in Japanese mountains (Yanai and Igarashi, 1990), but deep failures have become more frequent in recent years (Jitozono and Shimokawa, 1998; Matsumura et al., 2012), and there is much urgency in elucidating their mechanisms and predicting their occurrences.

When the landslide occurs at a much deeper surface than the root systems of trees, the soil-binding effect of tree root systems in preventing such landslide (Kitahara, 2010) is not observed. However, it has been reported that when collapsed soil flows downstream as debris flow, its energy is reduced by trees growing along the transportation and deposition areas as a natural barrier, resulting in a shorter-flow distance (Mizuyama et al., 1990; Nonoyama et al., 2020). The purposes of this study are : (a) to illustrate the mechanism of deep-seated Hirose town landslide (hereafter known as Hirose Landslide), which occurred near human settlements and paddy fields in the spring season using aerial photos and Laser Imaging and Ranging (LiDAR) data, and, (b) to quantify the functions of Cedar trees to control debris flows. The learnings of this study can be referred to create effective ecosystem-based disaster risk reduction (Eco-DRR) approaches in landslide-prone areas.

3.3.2 Methods and Materials
3.2.2.1 Study site

The Hirose Landslide that occurred on 20th May 2021, is situated in Hakusan city in Ishikawa prefecture, central Japan with a geographical location of 136° 37′ 30.55″E and 36° 24′ 54.68″ N (Figure 1).

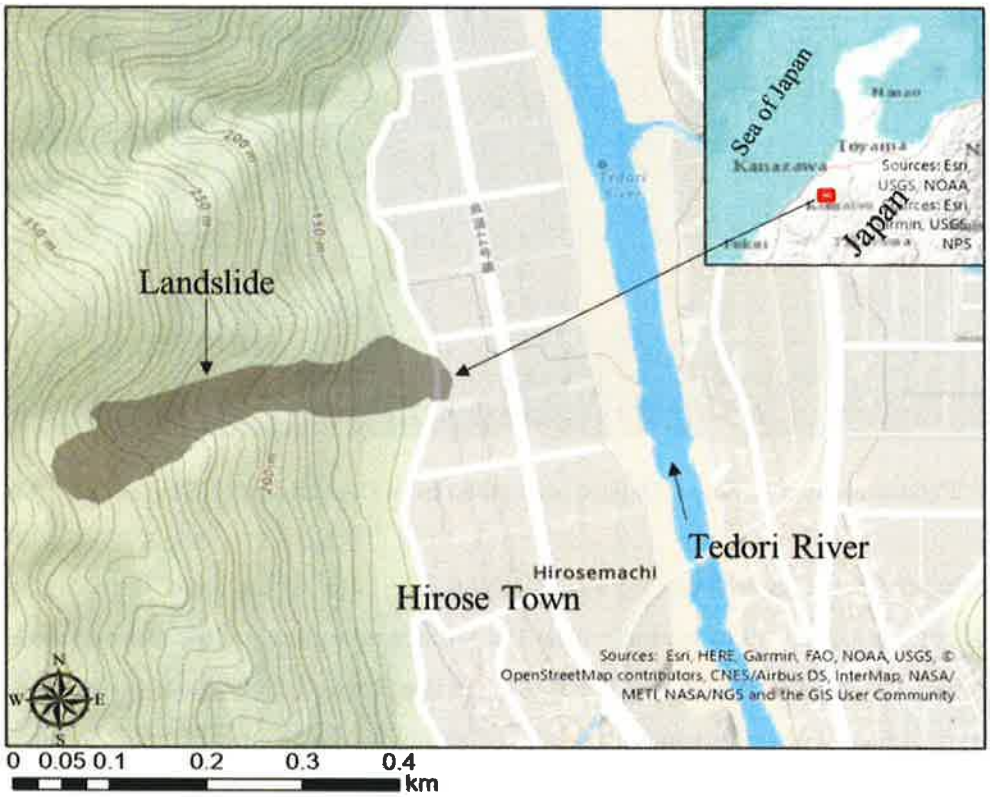

Figure 1: Study area showing location of Hirose Landslide (cited from ArcGIS online topographical basemap)

It has an elevation range of 125m-385m with the land surface generally inclining from east to west. The area is located near a Hirose town settled on a river terraces on the left bank of Tedori river, which is 72km long perennial river that originates from Mt. Hakusan (2702m) and confluences in the Sea of Japan. The nearest settlement has 34 households (Figure 2) living around and cultivating the alluvial fan for vegetables and paddies production.

Figure 2: Panoramic view of the collapsed area taken from the helicopter (Source: Seiji Yanai, 2021)

In this area, distinct river terraces are formed along the Tedori River. River terraces have a specific height less than 10 m having a clear flat surface along the middle to lower reaches of the Tedori River (Ishikawa Prefecture, 1987). In the Hirose Landslide area, the terraces form a flat surface with a horizontal distance of about 500 m from the Tedori River, and mostly used as paddies production land. On the left bank of the Tedori River, where the landslide occurred in 2021, a hill range with an elevation of 300-400m has developed continuously for 4-5km parallel to the river, and the mountain slope is steep with an average gradient of 30°. Furthermore, a distinct alluvial cone topography, with a width of 100 meters and a 15-degree slope, is continuously formed along the boundary between the river terrace and the hill slope. The tip of this cone overhangs the river terraces, forming a fan shape (Figures 1 and 2). The upper part of the slope has a steep valley-like topography.

According to the surface geological map of the National Land Survey Office (Ishikawa Prefecture, 1987), the geology of the area is mostly composed of rhyolitic pumice tuff and hornblende tuff, which is generally light greenish gray in color. The rhyolite is exposed in various places and is often white in color due to alteration. The altered rhyolite is used as a

ceramic ore. The ceramic stone which is the raw material for Kutani ware is mined at the Kawai Mine (Ishikawa Prefecture, 1987) located 3.5 km south of the Hirose Landslide area.

The existing vegetation on the hill-slope is Cedar plantations on the lower part of the slopes and dense secondary broadleaf forests on the upper part of the slopes. The planted Cedar Forest is about 60 years old, with an average diameter at a breast height (DBH) of 60 cm and a average height of 30 m, with some trees reaching 35 m. The trees are relatively well-grown and established in the Hirose Landslide surrounding. Secondary broadleaf forest at the upper slope to the ridge is composed mainly of Quercus serrata, and a variety of other broadleaf trees such as Japanese alder (Alnus hirsuta), Cherry (Prunus serrulate), azuki-nashi (Aria alnifolia), and Aburachan (Parabenzoin praecox), with medium diameter trees measuring 30 cm at breast height and 10 m or less in height. The forest-floor receives little light, and ferns grow in abundance throughout the landscape in the forest around the Hirose Landslide.

3.2.2.2 Methodology

Topographic assessment using LiDAR data

The topography before the collapse was reconstructed using airborne LiDAR data and aerial photographs taken in 2006, which were provided by the Kanazawa office of Rivers and National Highways, Ministry of Land Infrastructure, Transport, and Tourism. These LiDAR data consisted of original data and ground data of the ground surface. Since it was detected that the ground data did not represent detailed topography, the topographic analysis was conducted using the original data. First, the original text data were converted to a las file, using R software version 4.0.1 (R Core Team, 2021), and only the ground surface was extracted from the point cloud data using the lidR package.

Then, this point cloud data was used to create a 0.5m mesh DTM data and saved as a GeoTIFF file using the raster package function. Second, a detailed 1-meter contour topographic map of the post-collapse topography was utilized (provided by the Ishikawa Prefecture Forest Management Division, Ishikawa Prefecture, Japan), to create a 0.5-meter DEM file using ArcGISPro 2.8 and saved as a GeoTIFF file. These two GeoTIFF files were used to estimate the amount of topographic change, the amount of sediment produced, and deposited using the raster calculation tool and the CutFill tool in ArcGISPro 2.8.

The original data and the ground surface data were further used to estimate the number of trees that were grown in the collapsed area before the landslide. The CHM tool in the lidr package was used to differentiate the canopy data from the original data and the ground surface data, by determining the vertices to obtain the height of each single tree as point data. Further clipping with the polygon of the collapsed area, the number of trees that had been buried and deposited by the landslide were estimated.

Additionally, a drone (Mavic2 Zoom) captured imageries were used to measure the post-collapse microtopography and size (height) of driftwood. For capturing pictures, the collapsed area was divided into three sections. The shooting range and altitude were set using the GroundStationPro application, and the automatic shooting mode of drone was activated. Drone photography was conducted in June 2021, one month after the landslide. The photos taken were processed to create orthophotos, DTMs, and DSMs in the laboratory using ESRI's Drone2Map for further assessment.

In order to understand the sediment runoff prevention function of trees lost during the collapse, the Critical Turning Moment (Y) is calculated using the average height and DBH of the estimated lost tree. The 'Y' depends directly upon the size of the DBH. This 'Y' was assessed for each lost cedar tree by using an equation prepared for cedar trees by Shimada and Nonoda (2017) as below.

$$Y = 19.84X \quad \ldots\ldots\ldots\ldots\ldots\ldots\ldots\ldots \text{equation (1)}$$

Where, Y is the Critical turning moment (kNm)

and $X = H \times DBH^2$

Here, H = Tree Height, and $DBH = 0.3914 \times H^{1.407}$

DBH = Daimeter at Breast Height (cm)

However, since the LiDAR data was collected in 2006, there is a time lag of 15 years from 2021, the date of the landslide event. Therefore, we estimated the height of Cedar trees after 15 years by referring to the height growth curve of Cedar trees by Kotani and Sengi (2006) and DBH is calculated further to obtain the critical turning moment in 2021.

Field survey

Field surveys were conducted in May, June, and August 2021. A 10 x 10-meter quadrat was set up in the planted Cedar Forest growing in the vicinity of the site, and the DBH, height, and understory herbs of the trees within the quadrat were measured. Next, topographic measurements were taken in the collapsed area, and the size of driftwood was measured using a measuring staff. Soil samples were collected at the source head of the collapsed site.

For understanding the local resident's perception of the situation before and after the landslide, nearly half of the households (n=16 samples, out of 34 households) were interviewed. We collected their views by asking a few questions such as a) if there were any unusual events or signs noticed along the slope prior to the collapse; b) how much rainfall occurred in that period; c) is this landslide resulted from the activation of older collapse? and d) when was the Cedar plantation conducted? One of the residents, who were working in the agricultural fi eld directly below the collapsed site on the day of the landslide incident, shared noteworthy experiences regarding the Hirose Landslide event.

Laboratory analysis of soil sample to estimate sediment mobility index

For the clay layer contained in the collapsed sediment, the clay sample was taken back to the laboratory, 10 mL of 0.5 mol/L magnesium chloride solution was added to approximately 0.5 g of the clay sample, stirred well, and allowed to stand overnight (Mg saturation treatment). After stagnating, the magnesium chloride solution was removed by centrifugation (2,000 g, 15 min). Then, 10 mL of ultrapure water was added, stirred well, and centrifuged (2,000 g, 15 min) to remove the supernatant solution. This washing operation with ultrapure water was performed twice to remove excess magnesium that was not adsorbed on the clay sample. The same washing operation was then performed twice with ethanol to replace the solvent from water with ethanol. The Mg-type clay sample (solvent: ethanol) was prepared by the above operations. To this, 1 mL of ethanol was added, and the clay sample in suspension was applied to a preparate and dried at room temperature. Ethylene glycol was applied to this preparate and the dried sample (EG-treated), a sample heated at 300°C for 1 hour using a muffle furnace (heat-treated), and an untreated sample (Mg-saturated) were prepared for X-ray diff raction

(XRD). The XRD system used was a Rigaku MiniFlex with a copper tube sphere. The measurement conditions were as follows: tube voltage 30 kV, tube current 15 mA, measurement range 5 to 30°, step width 0.1°. The lattice spacing (nm) was calculated from the obtained diffraction angle (2θ) and X-ray wavelength ($\lambda = 0.15418$ nm) using the Bragg formula. The saturated water content ratio and liquid limit of the collapsed clay were measured, and the approximate mobility index, which was proposed by Ellen et al. (1987) as an index of the mobility of collapsed clay, was calculated. The approximate mobility index is expressed as the ratio of the saturated water content ratio to the liquid limit (Yamashita et al., 1992).

3.3.3 Results and Discussion

3.3.3.1 Results

General characteristics of Landslide

Figure 3 shows a plain view of the collapse that occurred in the Hirose area and the situation in each section from debris production (initiation) area to the toe (flow out) area (3A, B, C, D). The total length of the landslide terrain reached 575 m.

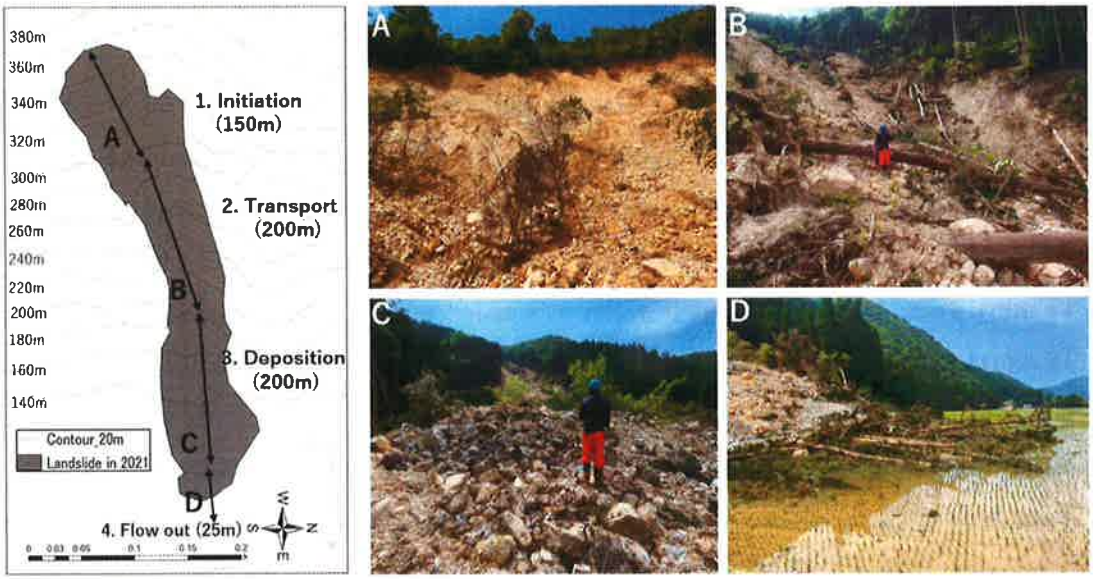

Figure 3: Landslide morphology and its classification: landslide topography with contours (20m) and sediment run-off distance (left); A) debris production (Initiation); B) middle section with toppled trees and driftwood (Transport); C) depositional area with debris

(Deposition); D) toe of landslide near paddy fi elds (Flow out). (Photo Source: Seiji Yanai, 2021)

The initiation area was 78 m wide and 150 m long between 280 and 360 m above sea level, with a collapse area of 1.1 ha. The length of the exposed bedrock is about 40m, and the slope is steep with an angle of over 40°. The base of the slope was flat and mortar-shaped, and medium-sized hardwood trees with roots had slid down and accumulated in the center forming a boardlike shape (40 m wide and 60 m long) (Figure 3, A). The lower part of the valley is a steep slope where collapsed sediments move (Transport zone), with an elevation of 180 to 280 m, a width of 50 m, a length of 200 m, and a slope of 35 to 40°. The central part of the valley was cut off like a slough, and highly viscous mud mixed with spring water and clay was flowing down. At the base of the valley, more than a dozen large-diameter Cedar trees (root diameter of 50 cm or more), which had fallen secondarily after the mudslide, were observed (Figure 3B). In the deposition area, huge gravels reaching 50 cm~2 m in diameter were deposited on an alluvial cone which lies at 120-180 m above sea level. The deposition area was 70 m wide, 200 m long, and with a slope of about 15°. The deposits had a lobed topography and were layered downstream (Figure 3, Photo C). Its terminus bordered a planted Cedar Forest, which was dammed up to a height of 5 m as the mudslide drifted the Cedar Forest at the terminus. Along its edge, many driftwoods were continuously deposited in overlapping rows for a length of 200 meters. There was a farm road as a separating boundary between the rice field and the forested area. The debris flow completely covered the road, forming a small hill-like terrain and depositing the debris. The debris flow of landslide overhung the paddy field side about 25 m from the end of the road. A few Cedar trees that had been toppled down and reached almost to the road with debris flow.

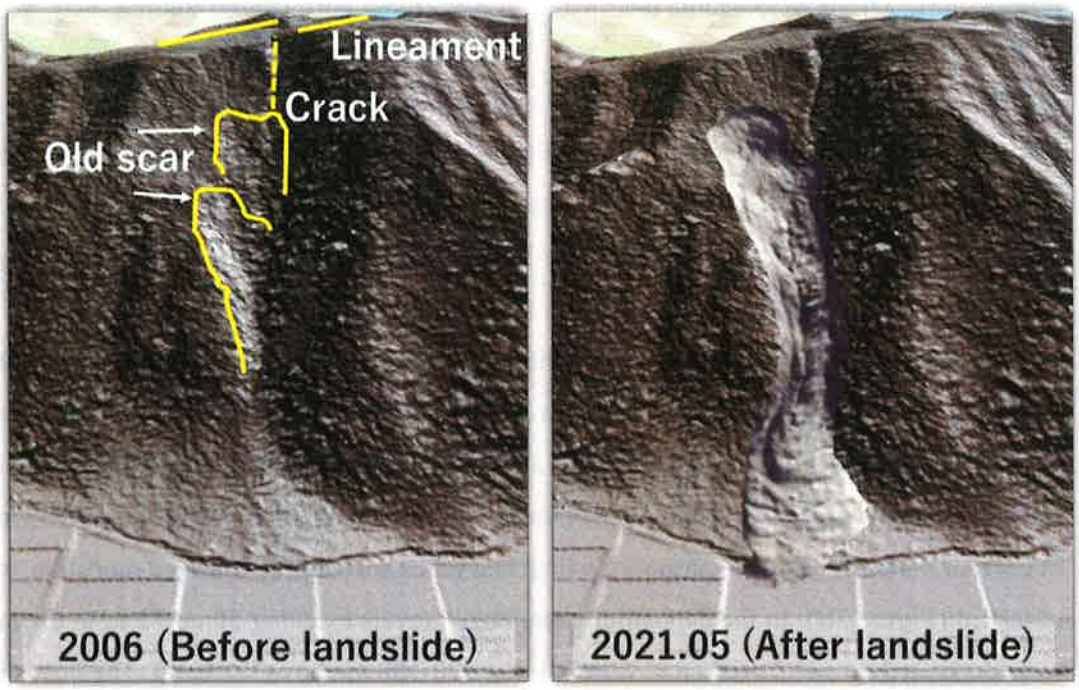

Figure 4: Comparison of geomorphological change before and after the landslide by LiDAR derived DEM analysis.

3.3.3.2 Terrain analysis using LiDAR data.

LiDAR data, taken in 2006, before the collapse were analyzed to reconstruct the pre-collapse topography. Figure 4 shows the shaded relief map created from the topographic survey before 2006 on the left and after 2021 the collapse on the right. The slope around the head scarp where the collapse occurred had a concave catchment topography with a steep slope before the collapse. In this zero-order valley, two previously collapsed slopes were identified in the middle to upper part of present landslide slope. The first one developed at an elevation of 300 m on the right side of the slope and was 150 m long and 50 m wide. The second is a 50m wide and 100m long collapse zone at an elevation of 340m above the slope. A clear alluvial cone with a radius of 110 m and an angle of 105° was formed at the bottom of the slope, and its end overhung the alluvial surface (terrace). The debris flow spread and deposited (Flow out zone) from the center of the cone, which was 150 m long and at a narrow angle of 45°.

Topographic change and sediment budget

Figure 5 (left) shows a plan view of the difference in elevation before and after the collapse, and the right shows the topographic changes before and after the collapse in the production (initiation) area (Line A), downstream sliding (transport) area (Line B), and deposition area (Line C). In the initiation area, the maximum elevation was depleted by 22 m, and the average elevation was reduced by about 15 m, indicating that arc-shaped slides occurred in the entire area. In the downstream area, the V-shaped valley topography was buried and flattened by about 6m. In the landslide flanks, the slopes were depleted by about 1 m. In the depositional area, the collapsed soil was deposited in a convex shape with a thickness of about 8 m over an area of about 80 m^2.

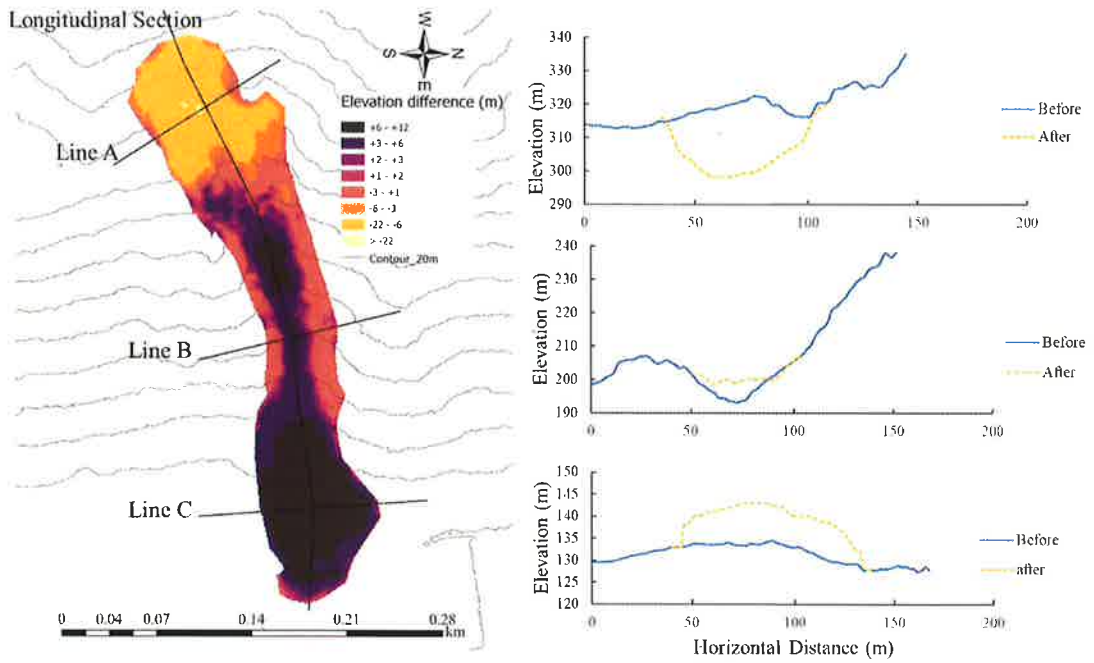

Figure 5: Topographic surface changes before and after collapse in three sections: Initiation section-Line A, Transport section-Line B, and deposition area-Line C.

The changes in the longitudinal topography before and after the collapse are shown in Figure 6. The slope before the collapse at an elevation of 300~350m is considered to be an old landslide block, and a concave break point can be recognized. In the present case, the upper slope above the transition line collapsed with a 15m-deep arc-shaped slip surface. In the downstream area from 160m to 300m elevations, sediments cover the slope, and as shown in Figure 5, Line B, the V-shaped valley floor is filled with sediments. Below the elevation of

160 m, the area is a depositional area, and the mudslide that flowed downstream overshooted the end of the alluvial cone and advanced further to the rice paddy field, and stopped. The volume of sediment produced by the landslide in the initiation area was 86,000 m^3 , while 22,000 m^3 was deposited in the transport area, 3000 m^3 was scoured from the valley walls in the transport area, and 63,000 m^3 was deposited in the deposition area. Out of the 89,000 cubic meters of sediment produced, 85,000 cubic meters were transported as debris and 4,000 cubic meters were discharged from the watershed with flowing water.

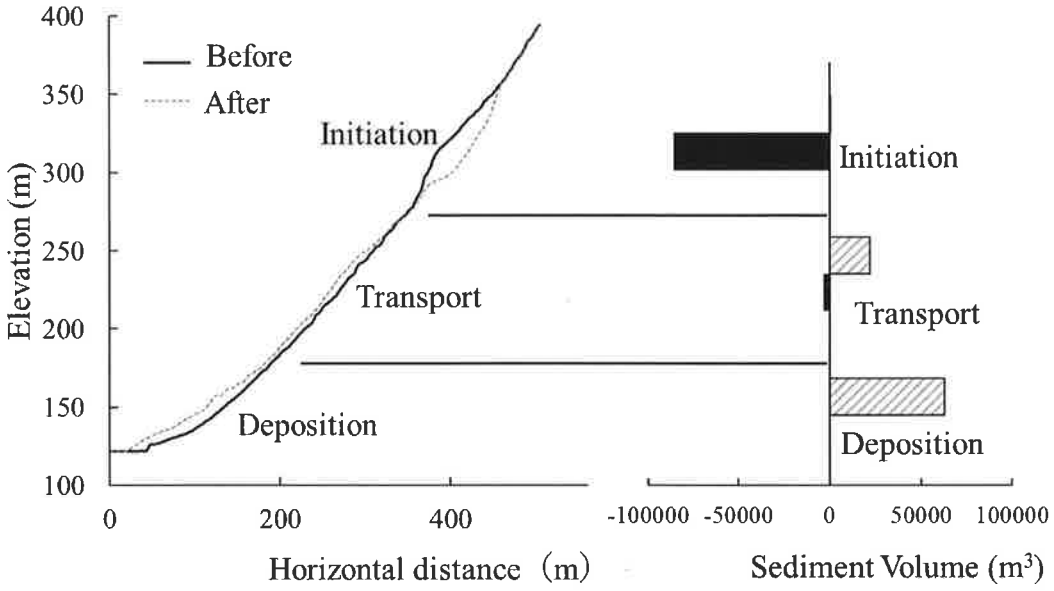

Figure 6: Longitudinal profile change and sediment production

3.3.3.3 Driftwood distribution and forest sediment runoff control function

Figure 7 shows the number of trees and their height distribution in the collapse area estimated based on the distribution of Cedar plantation forest shoot tips before the collapse. Most of the upper slope was covered with secondary broadleaf forest. However, most of the middle-downstream and sedimentation areas were covered with Cedar Forest, with average height of 22-24 m, and a few exceeding 30 m. The number of trees and their height frequency distribution are shown in Figure 7.

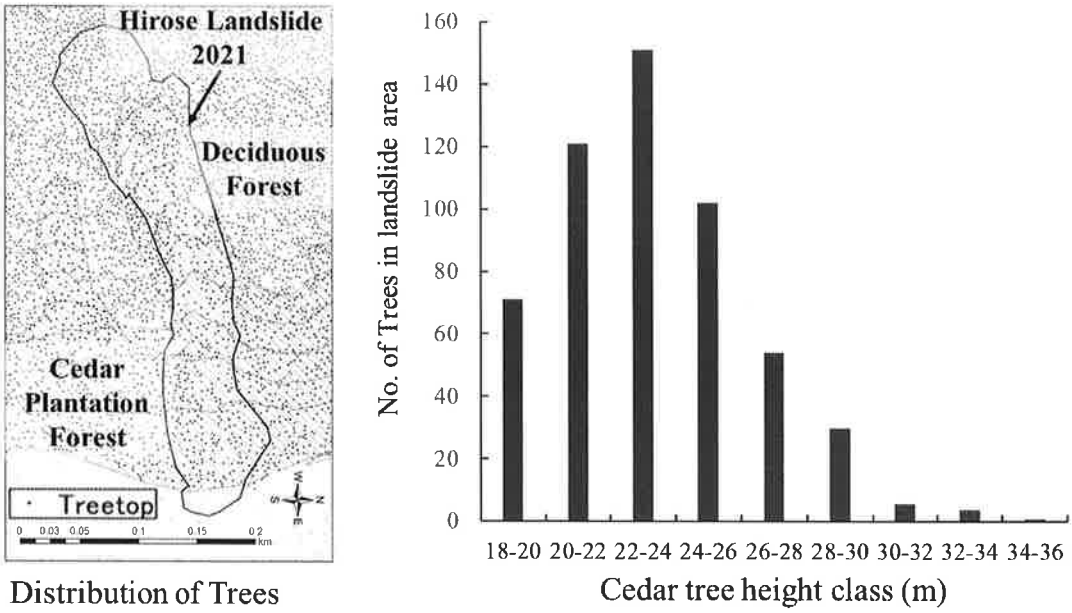

Figure 7: Tree height frequency distribution of planted Cedar Forest before the landslide

The DBH for all the 540 Cedar trees was estimated and the critical turning moment was calculated. The critical turning moment calculated by equation (1) is 59.3 kNm per tree and overall is 32067 kNm. When this value was recalculated based on the estimated tree height in 2021, 15 years later, it was found that the total turning resistance was 73069 kNm, almost double to the turning resistance of 2006.

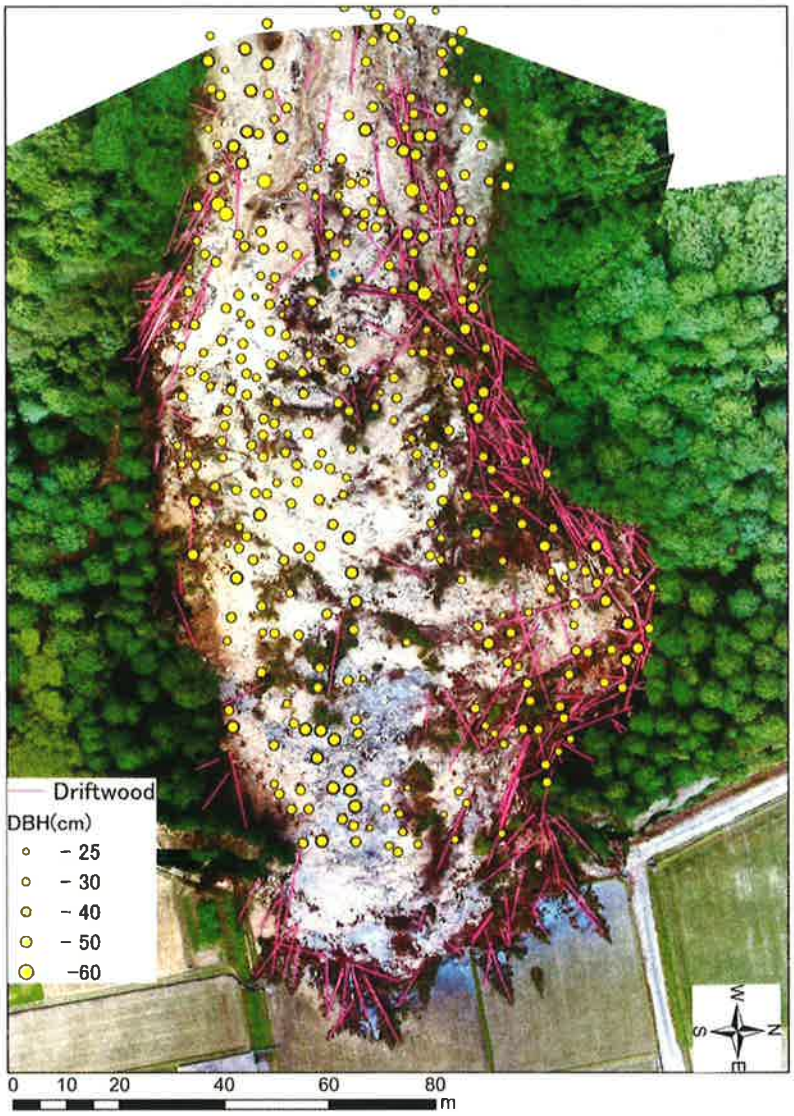

Figure 8: Landslide photo showing driftwood and Cedar trees. Yellow circles indicate the combined location and DBH (cm) of Cedar trees that were destroyed by landslide.

Figure 8 shows an orthorectified aerial photograph taken by a Drone over the deposition area. The Cedar Forest in the collapse area has been severely destroyed by the mudslide, and driftwood has accumulated as if swept up around the mudslide. The circles in the Figure 8 indicate the location and size of Cedar trees that were distributed before the collapse. The main source of the driftwood accumulated on the left bank is the Cedar Forest that was distributed along the flow path (initiation, transport, and deposit). The central part of the landslide area was sparsely forested but occupied with large-diameter sized Cedar trees. These trees were buried by the debris flow, and their tips were slightly exposed on the ground

surface. Their arrangement was consistent with the sedimentary structure of the debris flow, and they were distributed in an arc along the lobe-shaped topography (Figure 8). The number of Cedar trees that existed in the initiation, transport, and the deposit area was determined to be 540, out of which 230 trees were deposited as driftwood on the ground surface. The remaining, 310 trees, are estimated to be buried in the debris flow material and not visible.

Figure 9: Sediment accumulation by "retentiondam" like structure of driftwood observed in the sedimentation area.

Figure 9 shows the accumulation of driftwood at the end of the left bank. The roots of these driftwood has diameter of 84 cm on maximum and 46 cm on average, forming a retention dam-like structure up to 8 m high and storing a large amount of sediment behind it.

Rainfall data assessment and interviews with local residents

Figure 10 shows the daily and hourly maximum rainfall before and after the collapse. On May 20, 2021, when the landslide occurred, the rainfall was 11.5 mm and the maximum hourly rainfall was only 3 mm. Prior to this, there was rather heavy rainfall on May 17, with a daily rainfall of 105 mm and an hourly rainfall of 11.5 mm at 8:00 a.m. From then until

May 20, there was only a little amount of rainfall with a maximum daily rainfall of 10 mm. However, in early May, there was rainfall of 15-42 mm per day.

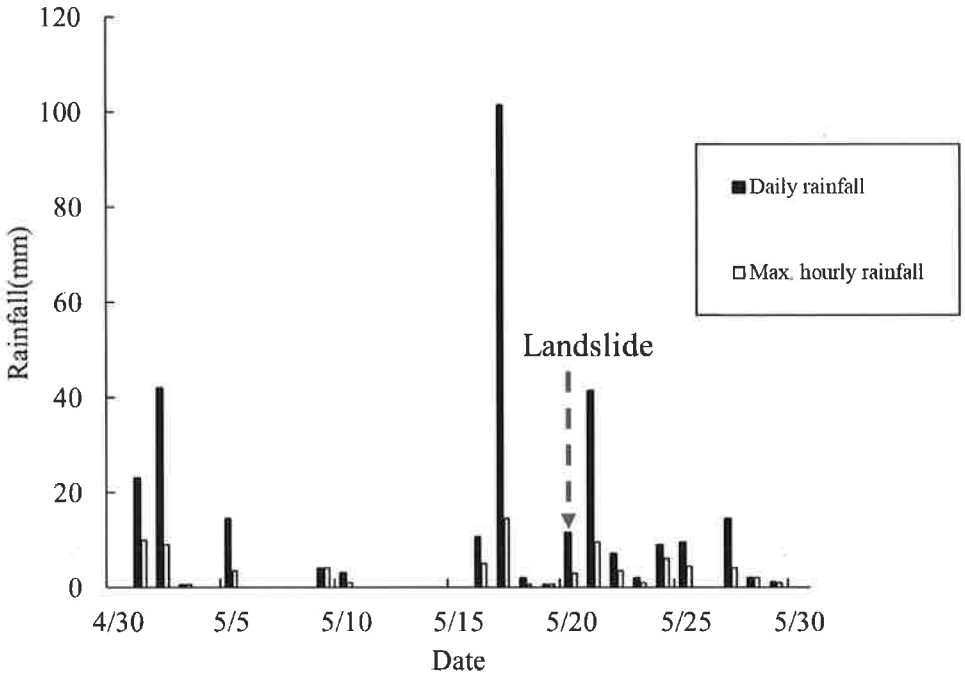

Figure 10: Daily and hourly maximum rainfall before and after the landslide (May 2021). Source: Japan Meteorological Agency (2021).

Interviews (random interaction) were conducted with the Hirose town residents regarding the occurrence of the landslide. Most of the interviewees recalled that no previous movement or cracks were noticed in the hillslope, however, they highlighted that there was intense rainfall in the area 3 days before the event. Some interviewees mentioned that the area was a bare landscape with fewer trees in the past and the plantation of Cedar trees was implemented by local government authorities. In particular, the local farmers (About 50 years old) shared his experience: "I was working on my agricultural farm in the same area just one day before (May 19), but there was nothing unusual (not even a sound). However, a few days before (May 17), we experienced heavy rainfall and trees were swaying along the head region of the landslide. On that day (May 20), I was wearing a raincoat and working around my house as there were occasional light showers occurring since morning. Just before the landslide (May 20, 2:30 pm), there was strange rumbling and crackling sound (like a loud explosion) was heard. Immediately, the collapse occurred and a huge earth mass with rocks and sediment

was knocking down the Cedar trees and flowing downwards. That event lasted within 15-20 seconds and within a short time, the dusty smoke covered this area. I also felt the smell of soil and broken wood. Then after some time, another small failure occurred with lesser sediment originating at the head section of the landslide."

The information about the reoccurrence of two separate collapses was triangulated with several other residents during the interview. It seems that a deep collapse occurred first and then some unstable slopes fall near the head region of the landslide. According to a male (80 years) respondent: "This Hirose hill slope area was once denuded and in the late 1950s and 1960s Cedar trees were planted by the government authorities together with local communities. He mentioned that the forest area had been used to harvest timber and fuelwood in the early 1950s and already collapsed twice before the Cedar trees plantation campaign was organized."

Mineral composition and physical properties of clays in collapsed sediments

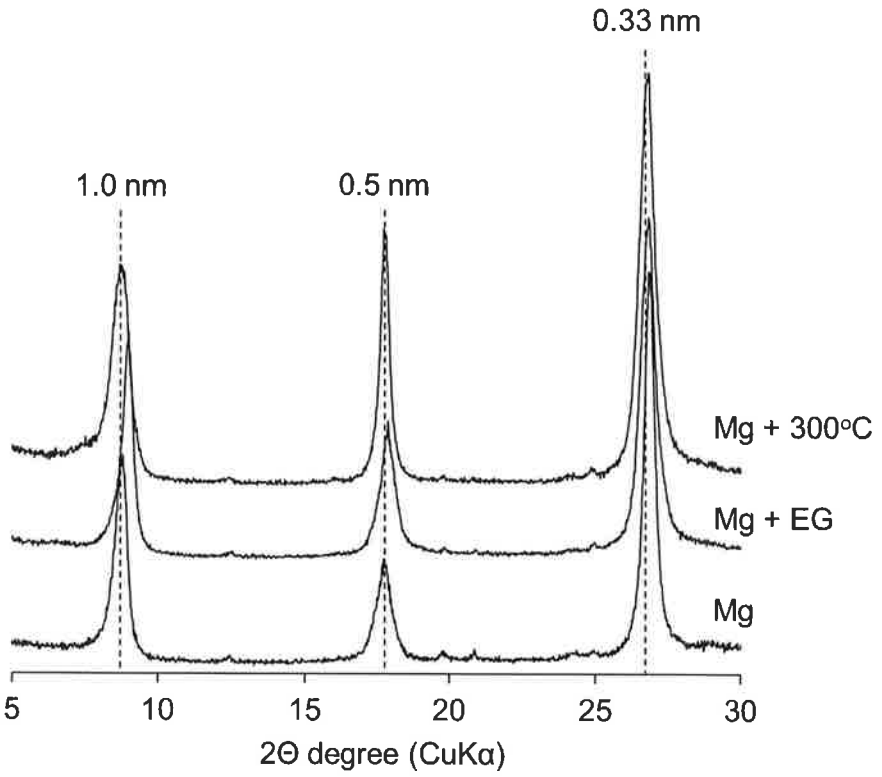

Figure 11: Results of clay mineral analysis of sampled soil.

Figure 11 shows the XRD patterns of the clay samples; the lattice plane spacing calculated from the peak positions of the XRD patterns of the Mg saturated samples were 1.0 nm, 0.5 nm, and 0.33 nm, consistent with those of illite. Furthermore, the peak at 1.0 nm, corresponding to the 001 plane of clay minerals, did not change with EG or heat treatments, which is also consistent with the characteristics of illite (Shiramizu, 2010). In addition, for hydrohaloysite, which, like illite, has a peak near 1.0 nm (1) the peak shifts from 1.0 nm to 0.7 nm due to dehydration associated with heat treatment, and (2) the peak shifts from 1.0 nm to 1.1 nm due to expansion of the interlayer by EG treatment (Joussein et al., 2005).

In summary, the mineral species is very likely illite, since the XRD pattern of this sample is consistent with that of illite, and the above peak shift was not confirmed for the 1.0 nm peak. The results of the liquid limit test are shown in Table 1. Since the liquid limit is defined as the water content ratio at 25 fall times, an approximate curve of fall times and water content ratio was developed from this table to estimate the liquid limit. The physical properties of the collapsed clay are shown in Table 2. The liquid limit was 45% and the saturated water content ratio was 65%. From the liquid limit and saturated water content ratio, the fluidization index was calculated to be 1.4, which clearly exceeds 1. Therefore, the clay was determined to have an easily fluidizable property.

Table 1: Result of liquid limit test

Number of fall	42	30	22	13
Water content (%)	39.6	43.1	46.3	47.7

Table 2: Physical property of collapsed clay

Liquid limit %	Saturated water content	Fluidization index
45	65	1.4

3.3.3.2 Discussion

Mechanism of deep-seated landslide

The deep landslide that occurred near Hirose town reached a slope failure depth of 22 m, with a total collapse area of 1.1 ha, and produced sediment volume of 86,000 m3 from the main collapsed zone. According to Hatanji (2003), deep-seated collapses that occurred

between the 1960s and 1990s varied in size from 4 to 3.7 million m3 , and the maximum depth of collapse was reported to be 17 to 100 meters. In this case, the Hirose landslide is classified as one of the relatively smallest deep-seated collapses in this region. In the Tedori River basin, a landslide occurred in 2015 during the snowmelt season in Sennindani upstream of the Ozoe River, and the volume of soil was reported to be 1.3 million m3 and the maximum depth of collapse was 45 m (Yanai, 2017). Also, in the upper reaches of the Ushikubu River in the Tedori River basin, the Betto giant Collapse (1.64 million m3 of collapsed soil) occurred in 1934 (Wang and Sassa, 2007). Hirose landslide was small in comparison to those events; however, it occurred in the lower reaches of the river near a human settlement with cultivated lands, the extent of its impact was large. The source of the collapse was a steep slope in the upper 280-360 m elevation range, and LiDAR data taken prior to the collapse showed evidence of a sliding bedrock. Interviews with nearby residents also revealed that sediment was released from the slope previously once in the 1950s. Therefore, the present collapse is predicted to be the collapse of an unstable weathered layer on the slope. According to Daimaru et al. (2013), deep-seated collapses in the middle basin of the Oigawa River are followed by a preceding collapse on both slopes, and they report that there are two types of collapses: a type in which a small-scale preceding collapse occurs at the foot of the slope that begins to expand before the collapse occurs (extrusion type) and a type in which the collapse area expands rapidly toward the upper side of the slope of the preceding collapse (expansion type). Thus, the tendency for large-scale collapses to occur after a preceding event is evident. Linear depressions (depressions roughly parallel to a mountain ridge) are explained as point where deep failures occur (Chigira, 2015). These depressions may form almost symmetrically on both sides of a mountain ridge, or they may develop on one side of a mountain ridge, or, although sometimes rare but they may form singly on a mountain ridge. Jitousono (2005) and the Volcanic and Debris Flow Team (2008) also noted that lineaments and linear depressions are key to predicting the location of a collapse. In the study area, the upper part of the landslide had a gentle slope on a ridge, and linear lineaments and depressions had developed between the ridge and the slope. The ridge-top slope had a clear crack extending from the ridge to the slope, suggesting that a subsurface fault had formed and destabilized the area. Jitousono (2005) and Jotousono et al. (2006) pointed out that if the lineament is a fault, it is likely to be fractured in deep Sub-surface, and there may be a thick layer of weathering. Takeshita and Shimizu (1997) also pointed out the need for deep

stratification of the mountain body and the existence of brittle basement rock. Rainfall takes time to pass through such thick weathered layers, and there is often a delay between the peak of rainfall and the onset of collapse (Onda et. al., 1999, Hattanji, 2003). The delay usually ranges from 20 to 150 hours, but in the case of the Hirose landslide, it took a relatively long time, 78 hours after the peak rainfall. This is thought to be caused by the time required for the groundwater table to rise due to passage through a very thick weathered layer as shown in Figure 3-A. Analysis of clay minerals exposed on the collapse surface revealed that illite was the predominant mineral. According to Maeda et al. (2011), geological characteristics of hydrothermal alteration zone landslides occur mostly in the potash feldspar and illite zones. The Kawai Mine, where the ceramic stone used to make Kutani ware is sand bedded, is located 1 km southwest of the Hirose Landslide area, and the surrounding andesite and rhyolite are widely altered. Since the liquid limit of this clay layer is smaller than the saturated water content (i.e., the fluidization index exceeds 1), it is expected to become liquid and easily fluidized as this clay layer approaches its saturated water content due to rising groundwater. It is highly likely that the clay layer that underwent this alteration was used as a slip surface and that a deep collapse occurred. Under these geological conditions, in this area where there are many lineaments and faults, it is possible that similar deep failures may occur in the future.

Quantifying the effectiveness of Cedar trees for debris flow control

Several recent large-scale landslides have been reported in which mudslides have uprooted large amounts of driftwood, which often indicated good information about discharged sediment. For example, according to Todo et al. (2015), in the 2009 landslide in northern Harima and southern Tajima, Hyogo Prefecture, when the fluid, which was a combination of driftwood and sediment, passed through a comb or grid slit, a "sieving function" has activated, allowing water to pass through the slit, while driftwood and sediment were separated and deposited on the upside of the slit. This function reduced the destructive energy of the flow, and the debris-flow reduction function was reported. Nonoyama et al. (2020) reported that mudslides generated by torrential rains that hit Hiroshima Prefecture in 2018 were deterred by the formation of lobes (tongue-shaped sedimentary landforms) due to collisions with standing trees. Even in small tree forests at the foot of mountains functioned to reduce

subsequent sediment flow and diverted towards the flat surface. Hirose landslide investigation assured that Cedar trees on the slope deterred sediment from flowing down as fallen trees intercepted the mudslide by storing sediment and eventually staying there as driftwood.

In the case of Hirose landslide, the sediment produced by the deep failure flowed down the steep slope and diffused into the alluvial cone, pushing down a well-established Cedar Forest (average diameter at breast height 48 cm, height 28 m) that was growing along the slope, and it is assumed that the flow energy was mostly reduced during this process. The traces of this can be inferred from the fact that the Cedar trees that were distributed there were deeply buried as shown in Figure 8, and their treetop ends are aligned along the top of the debris flow lobe. The amount of energy required to pull down a tree is highly correlated with its DBH (Fukami et al., 2011; Shimada and Nonoda, 2017), and a tree having a DBH of 40cm, requires approximately 80 kNm of energy to be pulled down. Therefore, we estimated the DBH from the height of 540 Cedar trees which were destroyed during collapse. By applying Shimada-Nonada formula, the strength of total lost Cedar trees was calculated. The calculated strength is approximately 73069 kNm, which has resisted the debris flow to spread down to the agricultural field in the alluvial fan. The moment of resistance to pulling down a standing tree is negatively correlated with tree density (Fukami et al., 2011), and increases exponentially with breast height diameter, meaning that it is important for disaster prevention that small diameter trees should be appropriately thinned out to create forests of large diameter trees. On the other hand, another important disaster mitigation function observed this time was that the standing trees captured the driftwood that flowed down like vertical piles and accumulated to serve as a retention-dam-like structure, storing a large amount of collapsed sediment behind them. The width of the dam reached 120 m on the left bank, and its height was up to 8 m. Driftwood spilled by mudslides is a nuisance in terms of disaster prevention, as it can get caught on bridge piers, blocking the flow of the river and causing flooding (Mizuhara, 2016). However, during the 2018 mudslide disaster in Hiroshima Prefecture, it was reported that sediment was deposited up to 1~3 m thick by driftwood dams (Nonoyama et al., 2020), which is much smaller than the Hirose Landslide. The major difference from the Hiroshima Prefecture case is that the Cedar plantation in the Hirose area had large-diameter trees (approximately 48 cm), which were able to withstand and maintain the soil pressure behind them. In the case of the debris flow in Hiroshima, a large amount of

water from torrential rains and large rocks containing large debris flowed over a long distance, whereas in the Hirose Landslide, the amount of water was less, and the distance traveled by the rocks was shorter, so the large-diameter Cedar trees probably functioned effectively as a deterrent to debris flow. It has been experimentally confirmed that in a mountain stream, driftwood included in a mudslide gets trapped when it passes through a section with standing stems, which supports the subsequent trapping of sediment and driftwood one after another, forming a channel blockage and causing the stream to divert in a short time (Hasegawa et al. 2016). Sediment stored by driftwood-dam is often considered to amplify disasters, but in open landscapes, it should be considered to examplify its contribution to disaster mitigation. As previous disasters have already demonstrated that there are no such engineering techniques that are completely safe and disaster-proof (Kato and Huang, 2021). Also considering the low cost and multifaceted benefits, one of the best ways to reduce landslide risk is to create a forest ecosystem by planting trees along slopes prone to collapse. This can be a sustainable and cost-effective ecosystem-based solution to reduce the risk of landslide disasters in similar geological settings (Moos et al., 2018). At the same time, from the perspective of disaster mitigation, it is also important to grow forests in areas such as alluvial cones, which were formed by past collapses and are likely to experience landslide in the future. It is therefore recommended to document and quantify the role of forest-based techniques to mitigate the risks of landslides in order to assess their suitability for specific locations and to ensure that they are implemented correctly.

CHAPTER 4 LANDSLIDE IN NEPAL

4.1 Geomorphological Assessment and Early Warning System of Methum Landslide in Nepal

4.1.1 Introduction

The Nepal Himalaya lies in the central part of the Himalayan range that was formed by a collision between the Indian and Eurasian plates approximately 55 million years ago (Dhakal 2015). Five physiographic regions are distinguished based on Nepal's climatic and geomorphic conditions: the Terai, Siwaliks, Hills, Middle Mountain, and High Mountain (Adhikari and Ojha 2021). Approximately 40% of the country's population lives in the hills, albeit in a scattered manner across poorly defined areas (Central Bureau of Statistics 2021). After each rainfall event during the summer monsoon season, these hill slopes suffer from soil erosion and landslides (Dahal and Hasegawa 2008). Slope failures and landmass collapses occur as a result of the combined influence of internal and external factors (Miao et al. 2021). Various internal factors that may destabilize slopes are landforms, rock structures, and rock and soil properties. External factors such as precipitation intensity, reservoir water levels, seismic events, and human activity can also trigger a slide (Wang et al. 2022). Landslides often occur due to a continual process of geomorphic evolution (Thapa 2015), and it is thus necessary to understand their geomorphological changes prior to applying landslide measures.

For landslide risk mitigation, both structural (e.g., bioengineering, retaining walls, check dams, prop walls, gabion toe walls, drainage management) and nonstructural (e.g., landslide early warning systems, awareness, capacity building, resettlement to safer areas) measures have been adopted globally (Sultana and Tan 2021; Thapa and Adhikari 2019; Lacasse et al. 2009). A country with weak economic conditions, such as Nepal, cannot allocate a budget sufficient for the construction of large infrastructure projects to control landslides, and communities are left to survive under the risk of landslides in hilly landscapes (Jones et al. 2014; Malla et al. 2020). Moreover, in cases where settlements near landslide-prone areas are unprepared, the safety of the community becomes an immediate priority (Alcántara-Ayala and Moreno 2016). This necessitates a method of landslide of prediction that would minimize landslide risk and reduce casualties by alerting vulnerable communities in advance.

Globally, early warning and monitoring systems have been developed and used to predict landslides and protect properties and livelihoods. The government of Japan in 2005 started

an early warning system in the country that relied mainly on hourly cumulative precipitation and the soil water data (Osanai et al. 2010). In Italy, a regional landslide forecasting system has been developed that integrates both temporal forecasting (which considers the rainfall amount) and spatial forecasting (which considers susceptibility maps) (Segoni et al. 2015). The Norwegian Water Resources and Energy Directorate initiated an early warning system for rainfall-induced landslides based on real-time observations of precipitation and groundwater levels (Krøgli et al. 2018). The United States of America started a debris flow early warning system in 1975 based on rainfall intensity and has since been improved and has issued multiple warnings for potential debris flows (Baum and Godt 2010).

Only limited applications of the landslide early warning system (LEWS) are known in Nepal (Dahal and Hasegawa 2008); furthermore, authorities in the Nepalese government have also largely overlooked the potential of early warning techniques for landslide risk reduction (Adhikari and Tian 2021). The LEWSs used earlier were simple and based on a single sensor, as they were designed to forecast landsides based on single metric, such as rainfall or ground displacement, and were not real-time forecasting systems. A landslide early warning system was installed during road construction to monitor potential landslides near the village of Kabilash, Chitwan district (JICA 2009). However, this system used only the rainfall threshold to predict landslides. Another LEWS was tested in Sundrawati village (Kalinchowk Rural Municipality, Dolakha district) and used a displacement sensor to predict the Mehle landslide (Thapa and Adhikari 2019). A few other LEWSs were launched on a project basis, but most of these instruments diminished once those projects were completed.

It is of utmost necessity to develop a cost-effective yet robust LEWS that uses multiple parameters to predict landslides in the country. In this context, we established a low-cost LEWS with three sensors (namely, a rainfall sensor, displacement sensor, and soil moisture sensor) to monitor the deep-seated and active landslide on a real-time basis. The LEWS has demonstrated that it can significantly reduce landslide risk to nearby inhabitants by raising an alarm. Additionally, this system can be replicated within other landslide-prone areas once the necessary thresholds of the measured parameters have been customized.

4.1.2. Materials and Methods

4.1.2.1 Study area

The Methum landslide (Figure 1) selected as the study area lies near a settlement in the Sankhu watershed (latitude 27°28' 35"– 27°32' 23" and longitude 85°16' 51"– 85° 21' 33") of the Lalitpur district in the mid-hills of Nepal. The Sankhu watershed covers approximately 33.69 square kilometers and has a population of 4,978 (2428 males and 2550 females) (Central Bureau of Statistics, 2021). The climate in this watershed is sub-temperate, with an average humidity of 50–80%. The region's average annual temperature is 14.80°C, and the annual average rainfall is 1,697 millimeters (Konjyosom Rural Municipality 2019). Major land uses in the study area include forest and non-forest (built-up, agricultural land, grassland, shrubland, water body, and barren land). The area's vegetation comprises numerous species, such as khote salla (*Pinus roxburghii*), gobre salla (*Pinus wallichiana*), katus (*Castanopsis indica*), chilaune (*Schima wallichi*), thulobanjh (*Quercus lanata*), phalant (*Quercus lamelosa*), khasru (*Quercus semicarpifloia*), and laligurash (*Rhododendron sps.*) (Divisional Forest Office, Lalitpur, 2021). Geologically, this area consists of Lesser Himalayan and Higher Himalayan rocks. Paleozoic granite (Phulchoki Group), Chandragiri limestone, the Chitlang formation, the Markhu formation, the Sopyang formation, and the Tistung formation can be observed in the Sankhu area (DMG 1994; Acharya and Paudyal 2019). Several low-grade metamorphic rocks dominate the study area, including metasandstone, phyllite, argillaceous limestone, orthoquartzite, and slate. A succession of highly weathered calcareous rocks is exposed throughout the region.

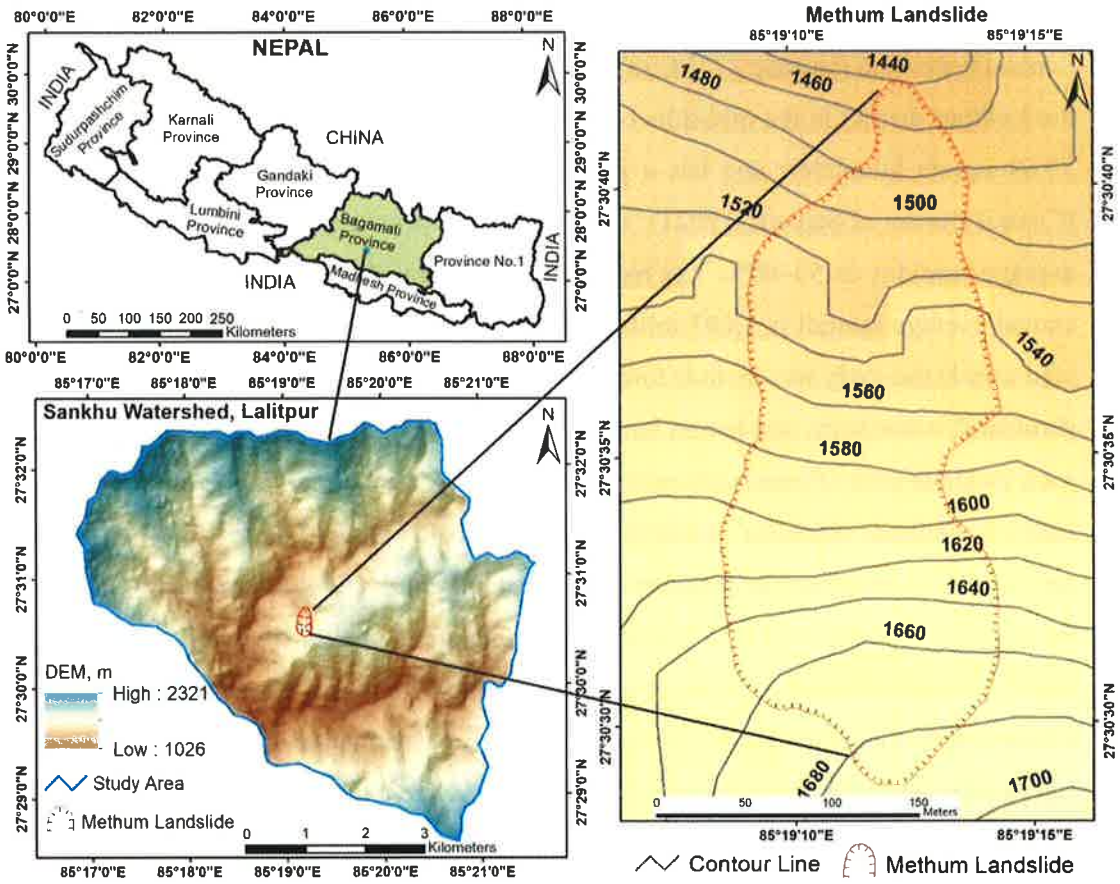

Figure 1. Study area: Methum landslide location in Sankhu watershed, Lalitpur district

4.1.2.2 Methodology

Geomorphological analysis of the Methum landslide

Geomorphology was studied with the help of aerial photographs, satellite images, and digital elevation model (DEM) data (Siart et al. 2009). Aerial photos collected in 1954 and 1972 were obtained from Nepal's Forest Research and Training Center and converted into mosaic images, which were analyzed in the ArcGIS Pro 2.7.0 Geographic Information System Environment. High-resolution satellite images for 2005 (Quickbird), 2010 (George-1), 2014 (WorldView-2), and 2020 (WorldView-3) were obtained from the Remote Sensing Technology Center (RESTEC) of Japan. AW3D high-definition terrain data for 2019 from the Maxar satellite constellation (obtained from RESTEC, Japan) were used to prepare the DEM (which has a 2 m x 2 m resolution). Using the DEM, various geomorphological

characteristics, such as longitudinal and cross-sectional profiles, and average advancing rate, were extracted.

Potential triggers of the Methum landslide

We examined three major factors that triggered (but are not necessarily limited to) this landslide: monsoon precipitation and severe earthquake tremors as natural factors and terrace farming on outward slopes as an anthropogenic preparatory factor.

To assess the respective roles played by those factors, we analyzed precipitation records, temporal earthquake events, and sloping terrace farming-related information relevant to the study area. We acquired precipitation records of three meteorological stations nearest to the study area, namely, Chapagaun, Khokana and Lele, for the 1976-2020 period from the Department of Hydrology and Meteorology (DHM), Nepal. For earthquake-related information, we assembled information gathered from peer-reviewed articles published globally and from the website hosted by the National Earthquake Monitoring and Research Center, Nepal, which were analyzed for visual interpretation. Interaction with locals and field investigation enhanced the understanding of the role that the cultivation of outward sloping terraces plays as a preparatory factor for landslide initiation and was used to support the findings. No primary data were generated for sloping terrace farming; however, the discussion was triangulated with previous studies conducted in similar geological settings. The quantitative data related to precipitation and earthquake events were analyzed and presented using Excel sheets on Windows 11 Pro.

Establishment of the landslide monitoring system

Site visits and interaction with locals confirmed that the Methum landslide had been expanding at an accelerated rate since the Gorkha Earthquake in 2015 and had been jeopardizing the settlements and a recently expanded rural road at the landslide's crown (Figure 2). As agricultural terraces were destroyed and the landslide approached their homes, three households (Ha- 27°30'29.63"N, 85°19'3.20"E, Hb- 27°30'32.88"N, 85°18'59.55"E, and Hc- 27°30'34.97"N, 85°18'58.34"E) abandoned the area in fear of new slope failures (Figure 2).

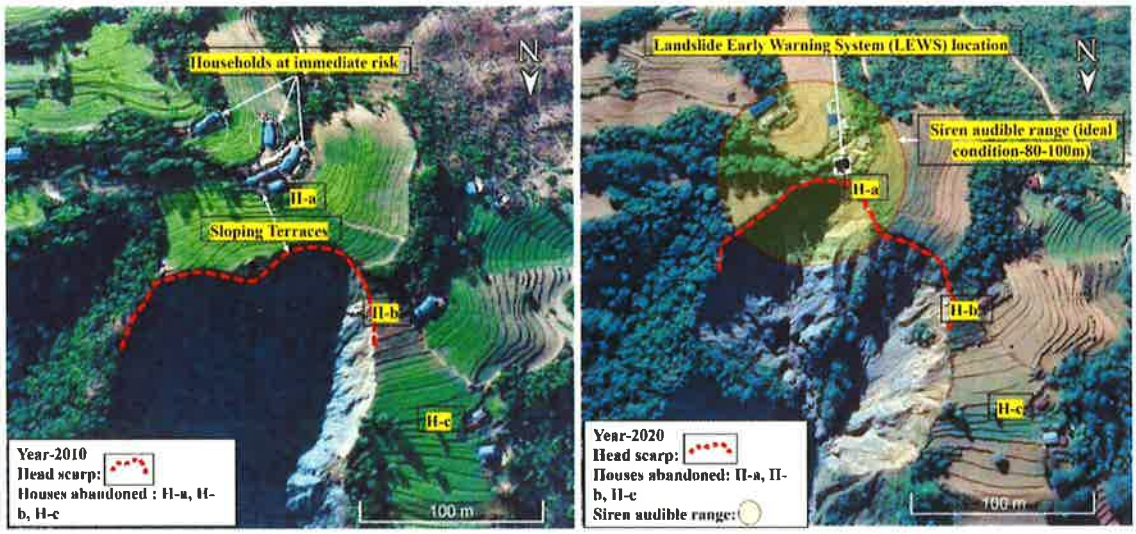

Figure 2. Methum landslide head scarp region: Household at risk and sloping terraced farms in the crown area (left photo 2010) which has already collapsed in the right photo (2020) with the LEWS station; siren audible range, and H-a, H-b, and H-c represent three abandoned houses.

In anticipation of new slope failures within the Methum landslide area, a LEWS was installed at a relatively stable site close to the head scarp (27°30'29.49"N, 85°19'3.46"E) on July 1st, 2021, to monitor landslide activity. The system comprised a precipitation sensor (rain gauge), two soil moisture sensors, a land displacement sensor (extensometer), and a data collection platform (DCP), as illustrated in Figure 3 (representative sketch), and Figure 4. The detailed specification of sensors used in the LEWS is shared in Online Resource 1 and circuit diagram of DCP is shown in Online Resource 3. The precipitation sensor (tipping bucket) was set to measure rainfall accumulated every 10 minutes; soil moisture sensors were installed at depths of 30 cm and 50 cm to detect the vertical moisture profile every 10 minutes, and a displacement sensor comprised of a wire attached to an extensometer was pegged along the potential crack zone in the crown area to measure landmass displacement (additional data are shared in Online Resource 2). A solar panel was installed on a stand facing toward the south to supply power to the battery inside the DCP system. An alarm speaker was attached to the stand facing the settlement area. Subscriber identity module (SIM) cards from two different communication companies (Nepal Telecom Corporation's Global System for Mobile [GSM] and Ncell Axiata's GSM) were used at the DCP to share the recorded data. The station was protected with wire mesh fencing, and polypropylene random copolymer

(PPR) pipe was used to protect the land displacement sensor wire that was hitched with multiple pegs along the landslide's crack zone.

This system was designed to share a real-time database with the server, designated organizations (Department of Forests and Soil Conservation, Konjyosom Rural Municipality Ward Number 2), and specific persons (nearest residents). The system was also designed to sound an alarm when the set threshold of any parameter under observation was exceeded. The thresholds for this system were calibrated with some customization referring to the warning-level limits used by the Japan International Cooperation Agency (JICA), DHM and previous research findings (JICA 2009; Dahal and Hasegawa 2008; Thapa and Adhikari 2019) and aided by researchers' experience in this field (see Table 1 below).

Table 1. The threshold set for three parameters in the LEWS (as of July 2021)

Parameter (Sensor)	Rainfall (Rain Gauge)	Displacement (Extensometer)	Soil Moisture (Props)
Threshold	1hour-60mm, 3hours-80mm, 6hours-100mm, 12hours-120mm, 24hours-140mm	≥500mm	75%
Initial reading	~ 0mm	~ 4000mm	~0%

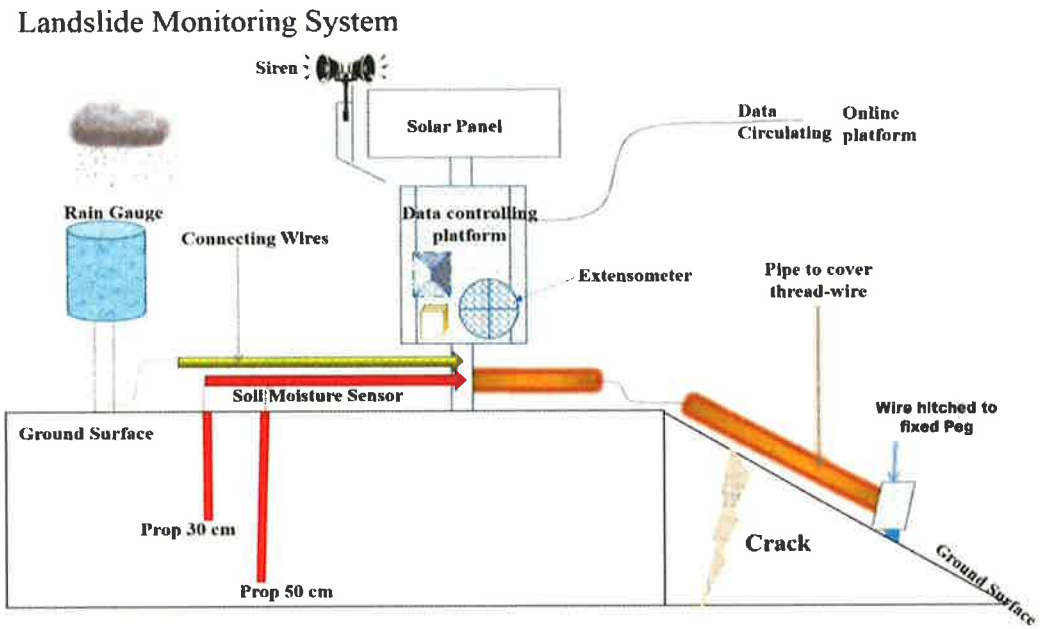

Figure 3. Representative sketch of the LEWS installed to monitor the Methum landslide.

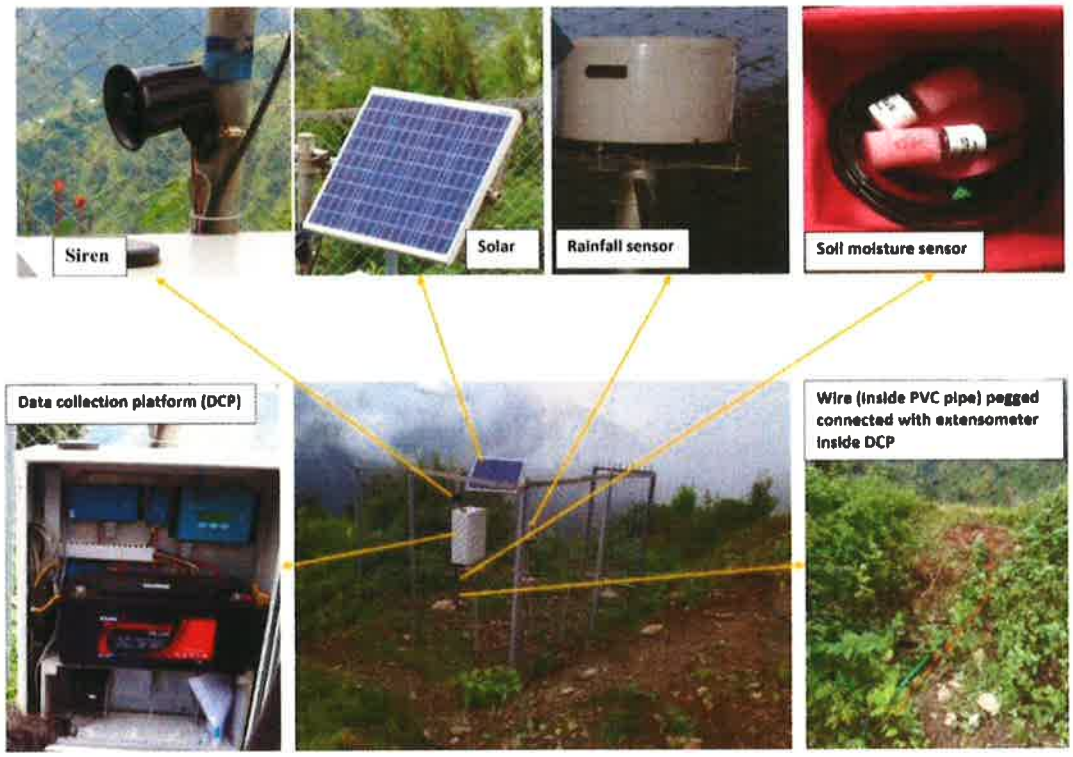

Figure 4. Landslide monitoring system showing assembled sensors and accessories (located at the stable site near crown area for monitoring the Methum landslide)

4.1.3. Results and Discussion

4.1.3.1 Results

Geomorphological assessment of the Methum landslide

An aerial photo from 1954 revealed the Methum landslide in its initial stages, with only small scar and gully like structures (Figure 5A). Vegetation was visible on the left flanks of the small collapsed area. Terraced land was also a prominent feature along the landslide's left and head regions. No significant changes were observed in the landslide's shape based on an aerial photo captured in 1972, despite the 18 years that had elapsed (Figure 5B), although the vegetation on the landslide's left flank appeared to have increased. However, it is evident from high-resolution satellite images captured in 2005, 2010, and 2020 (Figure 5C, 5D, 5E) that the small collapse structure had developed into a massive landslide, with considerable evidence of incremental failure in the upper region that expanded to both side flanks of the landslide in 2020. The 2005 image shows that multiple large ravines also appear to have formed along with the collapses. Nevertheless, in the landslide's crown zone, a few terraced landmasses appear to have remained intact up to 2010. Based on the 2020 image, it is evident that all vegetation on the slopes, in addition to several terraces that were cultivated in the landslide's crown region, moved downward (Figure 5E). By the year 2020, the landslide's crown almost approached the houses.

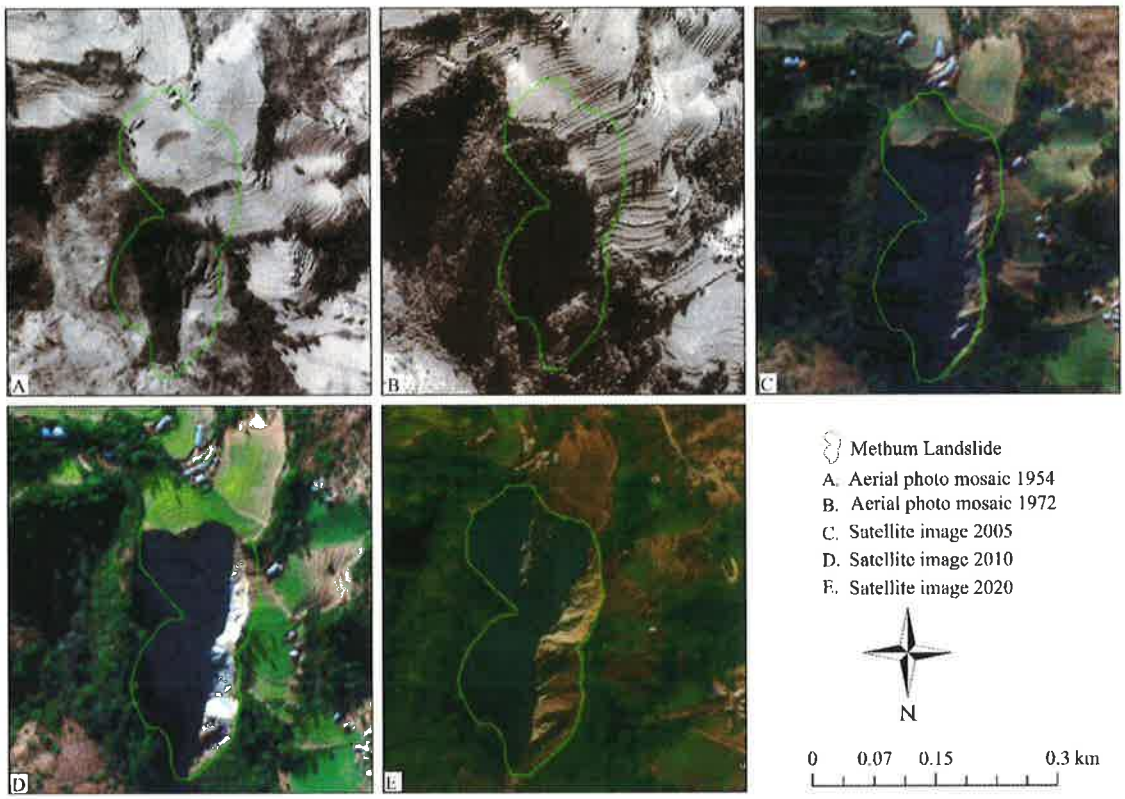

Figure 5. Temporal increment in the size of the Methum landslide scar (A, B, C, D, & E) between 1954 and 2020

The Methum landslide is an active landslide with concave longitudinal slope failure that has expanded to an area of 4.3 hectares. The landslide's main scarp is at an elevation of 1,685 m, and its toe is found at 1,455 m above sea level, with an elevation difference of 230 m. Geomorphological analysis (Figure 6) has revealed that the Methum landslide has become a large and deep-seated landslide, with a length of approximately 537 m extending from crown to toe and a breadth of approximately 170 m in its mid-section. The landslide was slow-moving in the past, but recent satellite image analysis indicated that the Methum landslide appeared to have advanced by approximately 6 m yr^{-1} between 2010 and 2019. Ravines approximately 30-35 m deep have formed in the middle section of the landslide, and steep slopes have developed at the head scarp, which seems unstable.

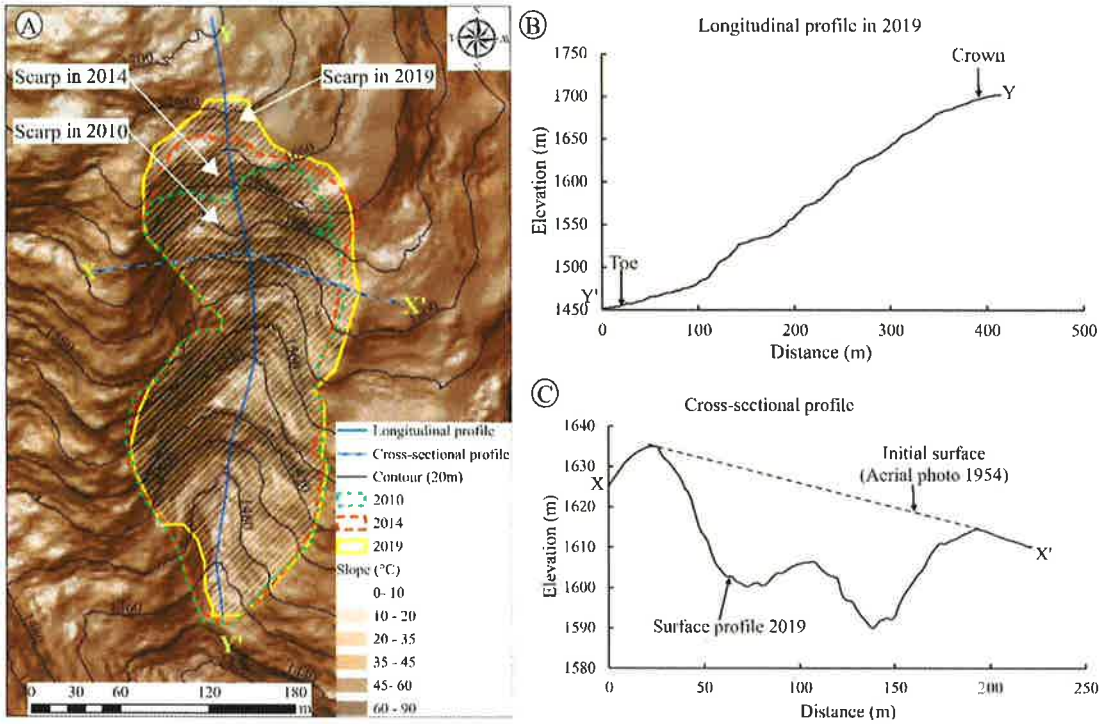

Source: Maxar Satellite imagery from 2010 and 2014, and AW3D-DEM derived from Maxar Satellite constellation, 2019.

Figure 6. Methum landslide profile: (A) representation of head scarp advancement (to south) in 2010, 2014, and 2019, (B) longitudinal profile of the landslide from toe to crown, and (C) cross-sectional profiles showing degradation of the surface topography along the middle cross-section of the landslide.

Triggering factors for the Methum landslide

During the field observation, local residents frequently remarked that past earthquakes, especially the 1934 Bihar-Nepal event, reactivated the landslide, and since then, this landslide has advanced every year. Furthermore, they mentioned that the slopes of the Methum landslide descended further whenever heavy rainfall occurred in the area. Earthquakes and monsoon rainfall are identified as the main factors triggering the occurrence of the Methum landslide. The available records for the 1976–2020 period revealed that the cumulative annual rainfall in 1985, 2002, 2014, and 2019 was higher than the area's annual average (1,697 mm) (Table 2 and Figure 7). Daily rainfall was highest on 23rd July 2002 (280 mm day^{-1}), and daily rainfall higher than 140 mm was recorded on five occasions from 1976–2020 as detailed in Table 3.

Table 2. Yearly cumulative rainfall with high intensity in the study area

Year	Cumulative yearly rainfall ($\geq$1700mmyear^{-1})
1985	1900mmyear^{-1}
1998	2274mmyear^{-1}
1999	2293.7mmyear^{-1}
2002	2329mmyear^{-1}
2004	2022mmyear^{-1}
2014	2151mmyear^{-1}
2019	1750mmyear^{-1}

Table 3. Daily cumulative rainfall with high intensity in the study area

Day	Cumulative daily rainfall ($\geq$140mmday^{-1})
5/29/1986	150.5mmday^{-1}
10/20/1987	172mmday^{-1}
7/23/2002	280mmday^{-1}
7/23/2002	200.5mmday^{-1}
7/23/2002	249.2mmday^{-1}
7/9/2004	165mmday^{-1}
7/12/2019	149.2mmday^{-1}

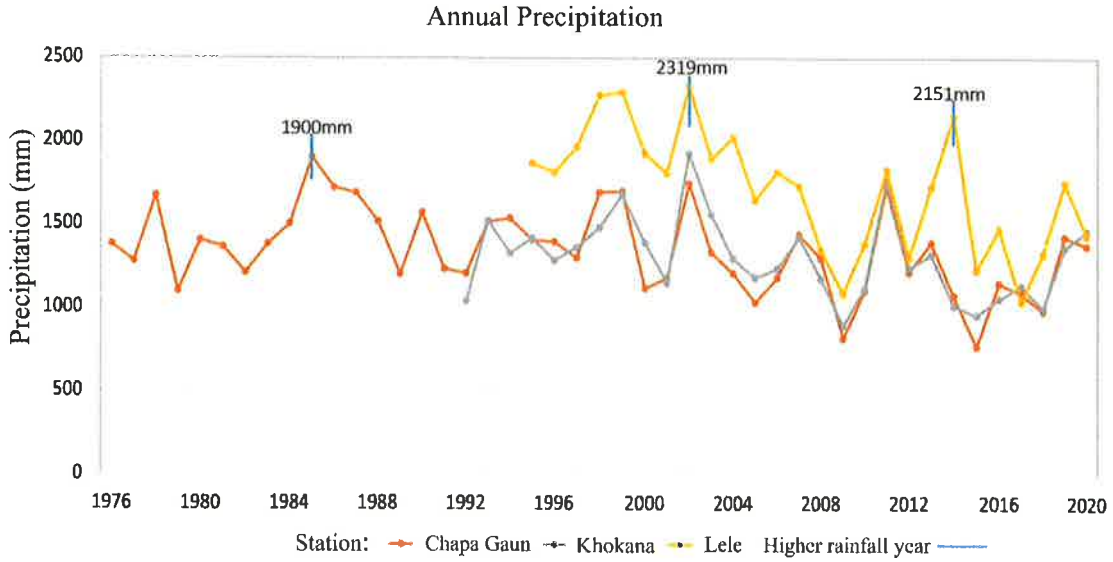

Figure 7. Precipitation data from three meteorological stations (Chapagaun, Khokana, and Lele), with vertical blue marks indicating years (1985, 2002, and 2014) that recorded higher rainfall than the annual average of 1697 mm in the study area.

Seismic activity that occurred over the last century was identified as another triggering factor for this landslide. Table 4 below presents a list of major earthquake events (local magnitude scale [ML] $\geq$ 7, that struck close to the study area during the last century in chronological order. These past earthquake events were of sufficient intensity to shake the hillslopes and trigger several landslides.

Table 4. Earthquake events occurring in proximity to the study area.

Year	1905 (Kangara-earthquake)	1934 (Bihar-Nepal earthquake)	1950 (Assam earthquake)	2015 April 25 (Gorkha earthquake)	2015 May 12 (Aftershock of Gorkha earthquake)
ML	7.8	8.1	8.6	7.8	7.3

Earthquake magnitude values in Table 4 were referred from previous scholarly archives (Bollinger et al. 2016; Okamura et al. 2015; Ader et al. 2012).

The continuation of unsuitable agricultural practices around the landslide has also contributed to landslide advancement. The field visit confirmed that the area's local

inhabitants had been farming on the outward-sloping terraces for multiple generations, producing rice, wheat, mustard, and vegetables. For agricultural crops, such as rice and wheat, local farmers plow and hoe the sloping terraces to loosen the soil, as shown in Figure 8. Most of the landslide region has a slope of more than 50%, which is more susceptible to erosion.

On such steep slopes, practicing outward-sloping terrace farming increases the susceptibility of the surface to erosion following plowing and hoeing activities. The Asian monsoon rainfall then erodes these soil surfaces, forming gullies.

Figure 8. Overview of the Methum landslide; looking from north to south: outward-sloping terraces farming practiced around the Methum landslide.

Landslide monitoring system

On August 16, 2021, one and a half months after the LEWS was installed, a new collapse occurred in the Methum landslide's head scarp region. On this occasion, this system generated an alarm that alerted locals to the landslide. The siren was heard by locals residing near the landslide crown area. On the day of the slope failure event, residents heard the first alarm at 05:35 a.m., and key individuals received alert messages notifying them about the displacement parameter that had exceeded the set threshold. The LEWS recorded 4,550 mm (initial reading 4000 mm + 550 mm) of displacement and initiated the siren on the speaker attached to the system, as intended. In this case, the displacement sensor exceeded the set threshold limit of 500 mm. Another siren was sounded at 16:55 p.m. later that same day. This alarm was triggered based on the data recorded by the rainfall sensor. By this time, the cumulative rainfall reached 66 mm hr^{-1}, which exceeded the set threshold limit of 60 mm hr^{-1}. During both alerts, the alarm sounded for 20 seconds. During this period, the monitoring system recorded the displacement of land and rainfall, as illustrated below (Figure 9).

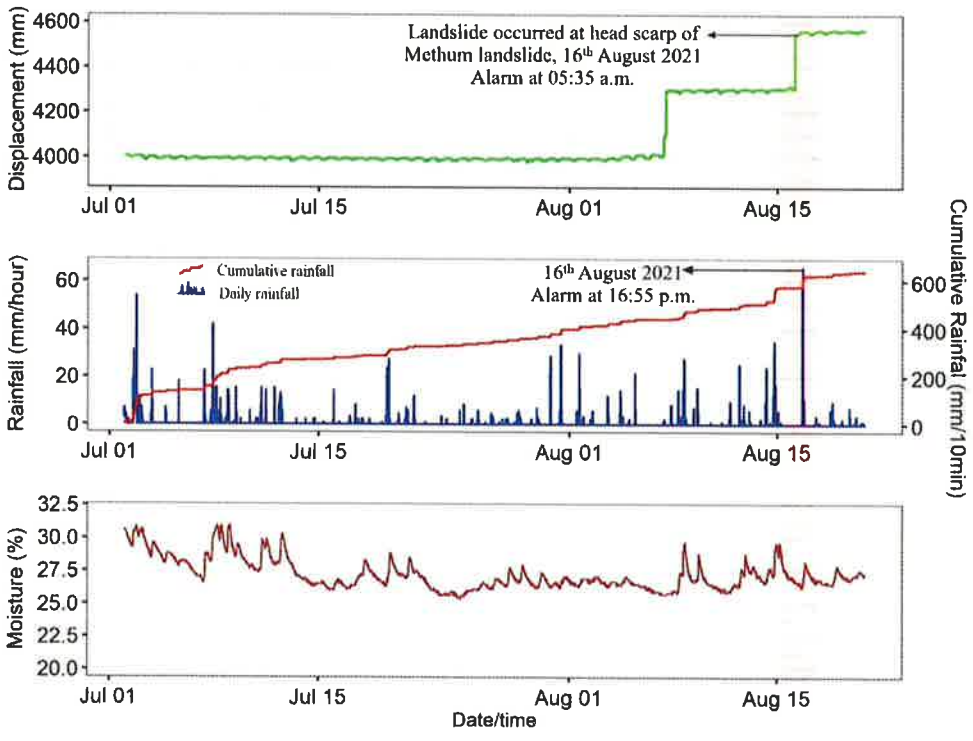

Figure 9. Displacement, rainfall, and moisture measured by LEWS for the Methum landslide.

This recent collapse occurred on the head scarp of the Methum landslide (Figure 10). The displacement sensor wire hitched with pegs was also found to have been breached along with the slide. The slide area was almost 3 m wide, and a landmass with an arc of 10 m had collapsed from the crown region of the landslide. Following this slope failure, the Methum landslide advanced toward the nearby rural road and the houses of the small community, which increased the risk of landslide in these areas.

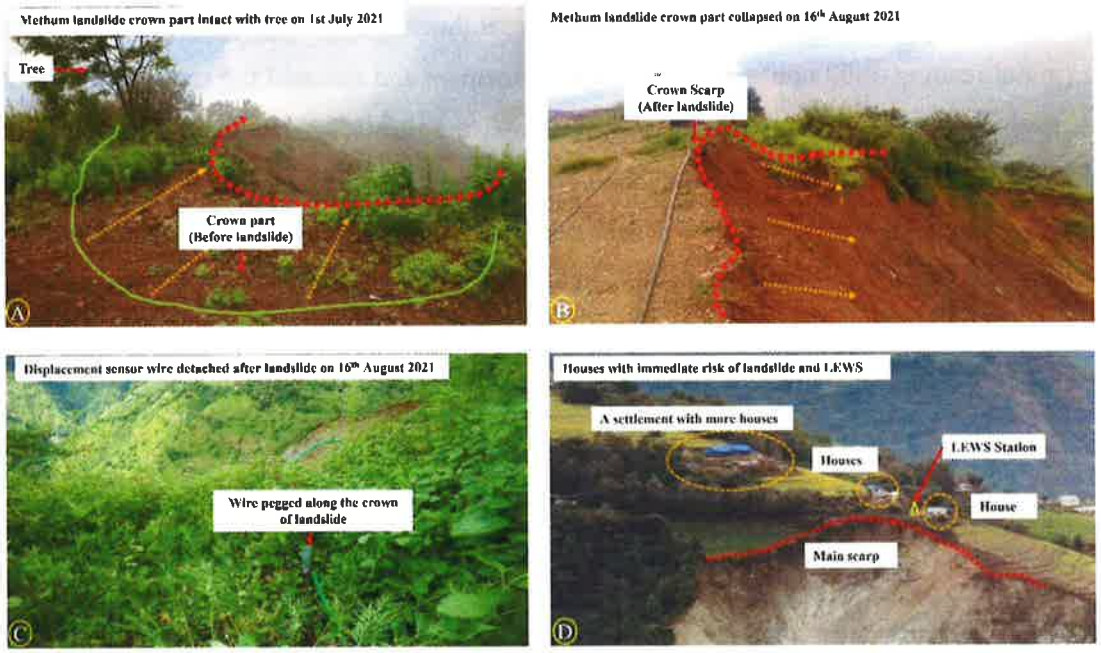

Figure 10. Methum landslide crown failure and vulnerable households: (A) head scarp of the Methum landslide as of July 1, 2021; (B) the scarp following the collapse on August 16, 2021; (C) detached wire from the displacement sensor on August 16, 2021; (D) houses and settlement above the landslide's main scarp.

4.1.3.2 Discussion

Landslide evolution and triggering factors

Geomorphological analysis reveals that the Methum landslide became a deep-seated giant landslide within the last 65 years, having developed from small gully-like structures. The available aerial photos confirmed that the landslide remained at an almost dormant stage between 1954 and 1971. However, the image from 2005 shows that its size has significantly expanded. This landslide was reactivated between 1971 and 2005. The Methum landslide

experienced continued incremental advancement from 2005 to 2021, with multiple collapses when the last displacement at the crown was also recorded by LEWS. Consequently, terraces in the crown section were disrupted, and the continuous landscape to the landslide's right and left became fragmented. This reactivation of large landslides in the Nepal Himalayas has been a major cause for concern within the communities of Nepal's mid-hills (Hasegawa et al. 2009) owing to the potential of these events to destroy communities or structures over time if left unchecked (Timilsina et al. 2017).

Both natural and anthropogenic triggering factors played a crucial role in reactivating the Methum landslide, as earlier studies have reported similar findings regarding several landslides in the hillslopes of Nepal (McAdoo et al. 2018; Gnyawali et al. 2020). Erratic rainfall during the monsoon season has emerged as the foremost natural factor that may have reactivated the Methum landslide. This area has received heavy rainfall in excess of 140 mm day^{-1} several times during the monsoon season, which is considered the potential threshold for rainfall to trigger landslides in the Nepal Himalayas (Dahal and Hasegawa 2008; Kanungo and Sharma 2014; Dikshit et al. 2019). In 2002, the study area received daily rainfall amounts of 280 mm and a cumulative yearly rainfall of 2,329 mm, which was sufficient to trigger landslides by weakening the soil surface through excessive infiltration of water. Such torrential rainfall events are sufficient to trigger landslides. For example, in 2002, monsoon rainfall triggered several landslides in many parts of Nepal (Bajracharya et al. 2017; Sharma et al. 2020).

The Nepal Himalayas is a seismically active zone that experiences recurring large-scale earthquakes, with a remarkable cluster of seismic events occurring in the 20^{th} and 21^{st} centuries. Specifically, earthquakes with seismic intensity values higher than 7 occurred in 1905, 1934, and 1950. These earthquakes generated numerous landslides and weakened the region's geology. The recent Gorkha earthquake (2015) triggered more than 19,332 coseismic landslides (Gnyawali and Adhikari 2017). The Post-Disaster Needs Assessment (PDNA) report included the Methum landslide area in the severely affected category, with an average intensity of VII on the Modified Mercalli Intensity scale (World Bank Group 2015). Although the Methum landslide was first initiated many years ago, in recent years, it remains in an active state and is advancing at an increasingly faster rate. Several further internal and external triggering factors (McColl 2015) may have influenced the reactivation of this

landslide, but owing to limited data availability, a more detailed analysis of these factors is required.

Anthropogenic factors, such as outward-sloping terrace cultivation, have also contributed to the intensified erosion in the study area. An intense tillage system has been adopted to cultivate cereal crops on sloping terraces in the area. Earlier studies have indicated that poorly managed sloping terraces cause higher erosion (West et al. 2015; Chalise et al. 2019), which leads to gully formation. Moreover, the Methum landslide surrounding the cultivated land has a slope greater than 75%, although terraces with more than a 50% slope are not recommended for cultivation (Green 1978), given the high annual degradation of sloping terraces. Many researchers have already noted that improper management of agricultural practices can lead to landslide occurrence or reactivation of old landslides and damage to villages and farms (Pandit and Balla 2004; Devkota et al. 2014). Another study estimated the average erosion rate of gently sloping terraces cultivated with rain-fed irrigation at approximately 2 mm yr^{-1} (Ghimire et al. 2013). It is estimated that the mean annual soil erosion for Nepal was 8.76, 6.55 and 7.49 t ha^{-1} yr^{-1} in 1990, 2000, and 2010, respectively (Uddin et al. 2018). The physiographic regions, namely the middle mountains, High Mountains, and High Himalayas of Nepal, have mean erosion rates of 38, 32 and 28 t ha^{-1} yr^{-1}, respectively, and barren lands have the highest erosion rate of 40 t ha^{-1} yr^{-1}, which is followed by agricultural lands at 29 t ha^{-1} yr^{-1} (Koirala et al. 2019). A recent study reported mean erosion rates of 23.2 t ha^{-1} yr^{-1} and 21.4 t ha^{-1} yr^{-1} from barren land and agricultural land, respectively, at the watershed scale in the mid-hills of Nepal (Pandey and Gurung 2022). Higher slopes and intensive tillage practices in outward sloping terraces expose soil to erosion, while creating the preparatory conditions that may trigger landslides. Torrential rainfall events in such fragile landscape conditions may have contributed to the reactivation of the Methum landslide.

While it is not possible to control rainfall and seismic activities, anthropogenic factors can be managed with appropriate assistance from experts and government authorities. Specifically, sloping terraced farming systems can be replaced with agroforestry or developed as seed orchards, which require less hoeing and plowing. Although it is cost-intensive, the reduction of tillage work and the alteration of sloping terraces into level terraces are useful strategies for reducing erosion (Mupangwa et al. 2007).

Monitoring system for landslide risk reduction

The LEWS installed for the purpose of monitoring the Methum landslide can detect landslide activities using three sensors (rainfall, displacement, soil moisture), making it a robust (Michoud et al. 2013) yet simple system. These three sensors can independently produce alarms or alert messages based on the provided threshold limit. If activity occurs on dry days, the landslide displacement sensor is mainly responsible for detecting the movement and generating alert signals, while on rainy days, all three sensors can equally and independently initiate an alarm. Moreover, on rainy days, even if the wire attached to the displacement sensor is breached or the displacement sensor becomes nonfunctional, the other two sensors—the rainfall and moisture sensors—will also produce alert alarms independently should threshold exceedance occur.

This LEWS performed effectively in the event that occurred on August 16, 2021, when alarms sounded twice during the day as rainfall and displacement thresholds were exceeded. This event increased the local communities' and other stakeholders' confidence in the LEWS. The closest inhabitants, who were among the most anxious about the prospect that a landslide disaster would occur, felt safer (Dixon et al. 2018) than they had prior to the LEWS's installation. By properly operating and sharing alarms, LEWS could mitigate the risks associated with landslides. However, sensitization is necessary to reduce overdependency on LEWS, which may cause communities to develop a false sense of security for landslide disaster (Rogers and Tsirkunov 2010).

This system has only a single-level alarm that sounds immediately after the threshold limit of any of the three sensors has been exceeded. To overcome this limitation and differentiate the state of landslide occurrence (Piciullo et al. 2018), a two-level (ordinary, escape alarm) or three-level (ordinary, pre-alarm, escape alarm) LEWS may be installed (Intrieri et al. 2013), although this will inevitably make the system more complex. In the case of multi-level alarm LEWS, the parameters need to be set to produce signals for each required level. The ordinary alarm indicates a lower increment in the observed parameter with less risk, while the pre-alarm signifies a significant increase in the parameters under observation, requiring locals to be cautious about landslide movement; and finally, the escape alarm or final alarm indicates the exceedance of the highest-threshold set, signaling locals to leave the landslide-prone area cautiously and move to safer places (Guzzetti et al. 2020). The different

level alarm may also require unique sound-producing devices for each level alarm and different messages with clear information about landslide movement to retain the credibility of the system as more false alarms could be generated. A further limitation is that the landslide's displacement will be measured only in a single direction, while movement in other directions remains undetected. Moreover, false alarm activation may occur due to disturbances along the pegged wires linked to the displacement sensor caused by animal or human movement, considering the proximity of the nearest settlement. Should false alarms occur, the locals may begin to lose trust in the system. Although this system utilizes double SIM cards to ensure reliable communication and data sharing, in the absence of the telemetry network, this system will not share any data in real time or may not generate an alarm. The system is operated using multiple sensors and electronic equipment, such as batteries, wires, and solar panels; therefore, maintenance work grounded in technical expertise is necessary at certain time intervals. Thus, the adequate sensitization of local communities and the provision that the operator (a local caretaker) be trained appropriately is of the utmost importance in reducing maintenance costs.

The threshold setting for the LEWS requires careful consideration. For this system, the rainfall thresholds set in this system were close to the threshold used in Nepal by to predict debris flow in mid-hills. While the threshold for soil moisture and displacement was set based on earlier studies and the researchers' own experiences from LEWS piloted sites. Considering the area's higher susceptibility to landslide reactivation, the threshold for the displacement sensor is 50 cm. In the case of a particular slope failure event, this low threshold will provide local inhabitants with more time to escape or to take the necessary actions. During such landslide events, in addition to the siren, an alert message will be delivered to local designated persons, assigned authorities, and local elected bodies, thus increasing real-time interaction among stakeholders and response activities if deemed essential.

Following the collapse on August 16, 2021, the landslide advanced further toward the settlement and rural road. We repaired the system by re-establishing the detached sensor wire, and two additional displacement sensors were installed to record the displacement of the landslide crown in three directions from the station. This time, the threshold for displacement was set at 300mm, as the slope of the landslide's head scarp became steeper and reached just below the rural road. This new threshold for displacement was set based on the idea that even

a 30-cm displacement would generate an alarm and increase lead time. The monitoring system's findings with lowered threshold will be presented in a future publication.

Policies conducive to the sustainability of the early warning system

The early warning system is the most important phase for landslide disaster management, as with proper forecasting, the risk of disaster could be reduced. The government of Nepal has included disaster management programs in its 10th National Development Plan for the first time (GoN/NPC 2002). While Nepal is the pioneer country in South Asia for establishing a Disaster Management Act in 1982, it has considered natural disasters to be Divine Incidents and focused on response and rehabilitation activities rather than mitigation and risk reduction. This notion was amended in 2017 when the Disaster Risk Reduction and Management Act was formulated, which included the provisions of preparedness. Nepal's Ministry of Home Affairs is the Nodal entity for disaster management at the central level; however, a number of ministries are responsible for landslide management, including the Ministry of Forest and Environment, the Ministry of Industry, Commerce and Supplies, and the Ministry of Energy, Water Resources, and Irrigation. Furthermore, provincial- and local-level governments also have the authority to coordinate disaster preparedness and response activities. The National Policy for Disaster Risk Reduction 2018 envisages the establishment of a multi-hazard early warning system. The National Strategic Plan for Disaster Risk Reduction 2018-2030 elaborates on disaster risk forecasting and early warning systems for preparedness against multiple hazards, but no specific strategies are proposed for landslides. There is a brief mention in the Guideline on Landslide Treatment and Mitigation 2016, which was developed by the former Department of Soil Conservation and Watershed Management, about the establishment of an early warning system, but no mention of any pragmatic approach to LEWSs was made. Moreover, the lack of budgetary provisions, inadequately trained experts, weak coordination among different ministries, and limited publicity of the LEWS (Kafle 2017) has undermined the scope of LEWSs to minimize the landslide risk in Nepal. Based on the experience of the present landslide warning system at the Methum landslide, it can be recommended that forecasting landslides based on rainfall, soil moisture, and land displacement are possible and feasible in terms of small-scale budgets and available technical knowledge. Upscaling this type of LEWS can contribute to mitigating landslide risk and

reducing fatalities and economic losses in the country. We encourage establishing LEWSs in landslide-prone areas where communities are at risk, but other structural treatments for landslides may not be possible immediately. It is recommended that a dedicated institution with legal, financial, and trained human resources is critical to design, implement, and manage LEWSs throughout the country. Thus, a conducive policy, specific legal instruments, financial support, and trained human resources are deemed necessary to establish and sustainably operate LEWSs in Nepal.

4.1.5 Conclusion

Landslide occurrences are common in the Nepalese mid-hills due to the combined effects of the intense Asian monsoon and seismic activities. Moreover, intense anthropogenic activities greatly impacted slope movement. The advancement of small gullies can create large-scale landslides under the continuous pressure of several triggering factors if not treated appropriately. The Methum landslide advanced significantly between 1971 and 2005. The landslide remained in an active state and posed a serious threat to nearby settlements after the 2015 Gorkha earthquake. Therefore, a low-cost LEWS was installed to monitor the active head scarp to reduce landslide risk. The LEWS installed on the Methum Landslide has communicated information relating to landmass movement to the area's inhabitants, demonstrating that it is a viable low-cost technology for landslide risk reduction at the community level. To operate the LEWS successfully, it is crucial to select stable sites, set the alarm threshold correctly, take precautions to minimize the occurrence of false alarms, build capacity, and sensitize locals. The application of LEWSs in Nepal is still in the pilot stage. Therefore, this study recommends that concerned authorities promote the technique with appropriate policy backing and popularize the use of the technology through regular budgetary programs to minimize landslide risk in vulnerable areas in the country. Replication of this system may require customizing the thresholds and parameters for each specific landslide condition and setting the audible range of the siren appropriately. Furthermore, we recommend that the LEWS should not be limited to forecasting but should also incorporate disaster response actions and encourage evacuations to safer places.

CHAPTER 5 ECOSYSTEM-BASED APPROACHES FOR LANDSLIDE RISK REDUCTION

5.1.1 Eco-DRR approaches and options.

Ecosystem-based disaster risk reduction (Eco-DRR) has been recognized as a sustainable DRR technique recently and is becoming popular in many countries globally where disasters are more frequent. World Conference on Disaster Reduction held in Kobe, Hyogo, Japan in 2005 represented by 168 states prepared the Hyogo Framework for Action (2005-2015) which highlighted the necessity of management of the ecosystem for disaster risk reduction (UNDRR, 2007). Further, the Sendai Framework for Disaster Risk Reduction 2015-2030 was adopted at the Third UN World Conference in Sendai, Japan, with 185 nations participation, on 18th March 2015, following extensive consultations and negotiations facilitated by the UN Office for Disaster Risk Reduction clearly mentioned Ecosystem-based Disaster Risk reduction approaches (WCDRR, 2015). After this Many countries adopted ECoDRR as a part of disaster risk reduction in their strategies and plans such as India, Nepal, and Japan. In this context, the Government of Nepal has prepared a Disaster risk reduction national strategic Plan of Action for 2018-2030 which envisions preparing Green Infrastructure and Ecosystem-Based Adaptation guidelines as disaster risk reduction activity. Similarly, the Government of Japan, Ministry of Environment of Japan, 2016 published a Handbook entitled "Ecosystem-based Disaster Risk Reduction in Japan" which has described different Eco-DRR approaches and possible options to achieve the objectives. Among the two approaches it is recommended to avoid exposure and the second is to reduce vulnerability. Their approaches are shown in Table 1 below:

Table 1: Ecosystem-based Disaster Risk Reduction (Eco-DRR) Approaches and Options

Approaches	Options
Avoid Exposure	Avoid developing/exploiting disaster-prone areas. (Land use plans, Zoning, safer areas, Hazard mapping, etc.)
Reduce Vulnerability	Conservation or Proper Management of Existing healthy ecosystems (Forest ecosystem, coastal ecosystem, etc.)

	2. Restoration of Degraded natural ecosystems (Such as the regeneration of forests)
	3. Creation of new (first-time) ecosystems (Protection Forest, Buffer zones)
	4. Amalgamation of Artificial structures with the above three approaches (Landslide early warning system, remote sensing)

For this, it is necessary to apply land use planning, zoning, safer areas, and hazard mapping and then avoiding developing and exploiting the disaster-prone areas could be best. However, there are areas where infrastructure already exists in hazard-prone areas. In hazard-prone areas with existing infrastructure, vulnerability reduction can be achieved through the conservation and management of the existing system, restoration of degraded ecosystems, creation of new ecosystems, and integration of artificial structures and ecosystems. The world has a total forest coverage of nearly 30 percent of its land area (FAO and UNEP, 2020). Forests provide a multitude of ecosystem services that help mitigate the risk of natural disasters. As many researchers have indicated that maintaining a healthy forest ecosystem can contribute to minimizing disasters. So, forests can be considered one of the most important ecosystems globally. However, in recent years, their loss has been increasing due to various causes, particularly deforestation. Such forest loss is in some way regarded as one of the causes of natural hazards, especially landslides. It is important to recognize the crucial role of forests in preventing landslides and other natural hazards.

Trees indeed perform engineering functions for disaster prevention in several ways. Trees can contribute to minimizing erosion and slope failures with multiple functions, such as catching, armoring, reinforcing, anchoring, supporting, reducing the velocity of water, and draining the excess water from slopes (Howell, 2001). Trees can catch eroding material sliding down slopes, with gravity or with the presence of water. Trees act as natural armor, protecting sloppy areas from surface erosion caused by runoff and rain splash. Trees enhance the soil's resilience to shear by reinforcing it with a network of roots. Through the growth of roots that penetrate probable failure planes and reach firmer layers below, trees can effectively anchor surface material. Trees provide support to the soil mass through buttressing

and arching. Trees play a crucial role in reducing the velocity of water or wind moving across the surface of the soil. This is done by the stems of vegetation offering resistance that retards the flow of water or air. The planting configuration of vegetation can enhance drainage by channeling runoff down a slope along erosion-protected lines. This helps to avoid saturation and slumping of the soil. In this way, trees prevent the initiation of landslides and protect against debris rockfall by providing a natural barrier. They effectively reduce the exposure of human houses to these hazards and minimize vulnerability.

However, the role of trees is sometimes criticized by a few researchers as their roots in the slope can enter the rock layers and weaken them to break. Once shallow failure occurs the trees themselves can add the weight of the mass along the slope. (Ammann et. al, 2009). Also, the anchorage provided by the trees is influenced by various factors, including the species selected, types of soil, and root depth. Species choice, soil type, and rooting depth (Norris et al., 2008). For instance, when the soil layer is shallow, tall trees are more susceptible to toppling during windstorms, thereby compromising the stability of the slope (Stokes et al., 2008). Researchers suggested prompt replacement of dead trees, as their decaying roots can facilitate increased water infiltration into the soil, leading to erosion and potentially triggering shallow landslides (Reubens et al., 2007; Preti, 2013). The forest ecosystem is also not considered capable of mitigating the risk of large-sized rockfalls. Forest ecosystems may have pros and cons when considering their role as slope stabilizer depending upon different factors. However, forest ecosystem provides a higher level of slope protection in comparison to other sorts of land use (Forbes et al., 2011).

5.1.2 Co-Benefits of Eco-DRR

Forest ecosystem has multiple benefits before, during, and after disasters such as they can provide basic services at all stages (Munang et al., 2013). The forest ecosystem provides multiple benefits before disasters, including aesthetic enjoyment and protection against rockfalls and debris. During disasters, forests reduce human exposure to landslide hazards. In the recovery and reconstruction phases, ecosystem services such as timber and fuelwood can be harvested. This co-benefit list includes climate change adaptation, biodiversity conservation, and contribution to livelihoods. These benefits provided by the Forest

ecosystems are evaluated as benefits provided by Eco-DRR functions. It is required to quantify and evaluate these co-benefits correctly (Dorren & Moos, 2022).

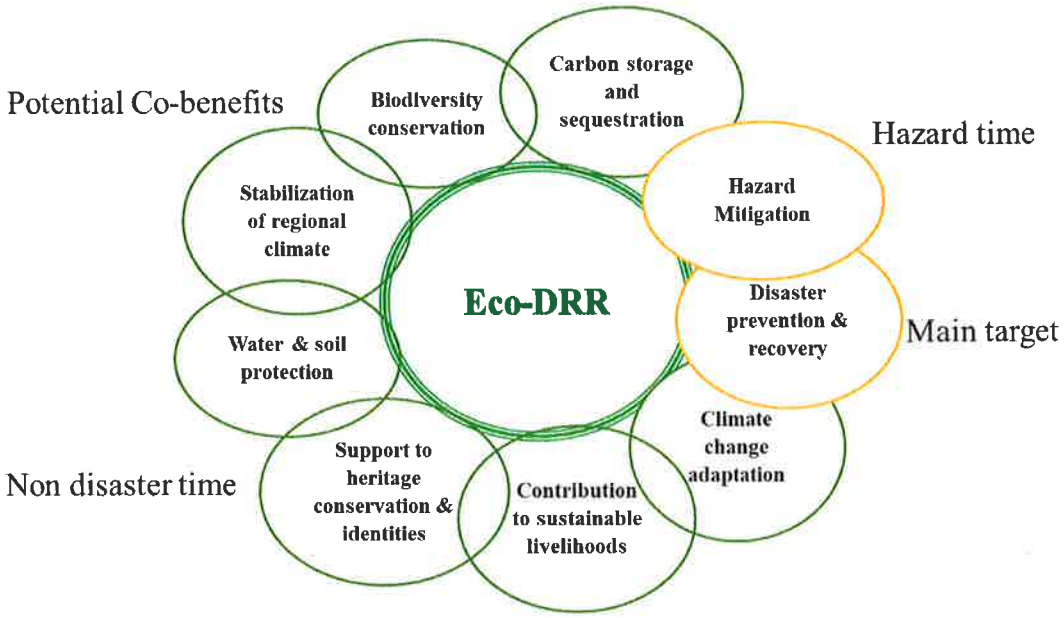

Figure 1: Main targets and co-benefits of Ecosystem-based disaster risk reduction (Source: Modified figure from Lo, V. (2016). Synthesis report on experiences with ecosystem-based approaches to climate change adaptation and disaster risk reduction. Technical Series No.85.)

5.1.3 Life span of Eco-DRR structure

Eco-DRR represents an affordable and sustainable approach to reducing disaster risks, providing advantages in terms of social, economic, and environmental aspects, consequently enhancing the value of a specific area (Oki et al., 2022). The ability of an ecosystem to operate optimally relies on its resilience, which is determined by factors such as size, density, species composition, vulnerability to hazards, and geographic location. Time and long-term planning are crucial when it comes to restoring and developing ecosystems for disaster risk reduction (DRR). Ecosystems require sufficient time to recover and reach a mature state. Moreover, in densely populated areas, the development of vegetative structures may be challenging due to limited space availability.

Indeed, civil engineering infrastructures have their own limitations when it comes to preventing disasters. They are designed with specific thresholds and may not withstand disasters beyond their capacity. Over time, these engineered structures may deteriorate, requiring increased maintenance costs to keep them functioning properly. It is crucial to recognize these limitations and factor in the long-term maintenance and potential vulnerabilities of such structures in disaster risk reduction planning. Additionally, integrating ecosystem-based approaches can provide complementary benefits and help mitigate some of the shortcomings associated with engineered structures.

Considering the time, the maintenance costs associated with ecosystem degradation are generally lower in comparison to those of engineering structures. While ecosystems may require ongoing maintenance, the expenses involved are typically less than what would be required for the construction and upkeep of engineered structures. Previous researchers have compared the lifetime of engineering structures' functioning time and vegetative structures functioning time in the past (Marongiu & Cencetti, 2013).

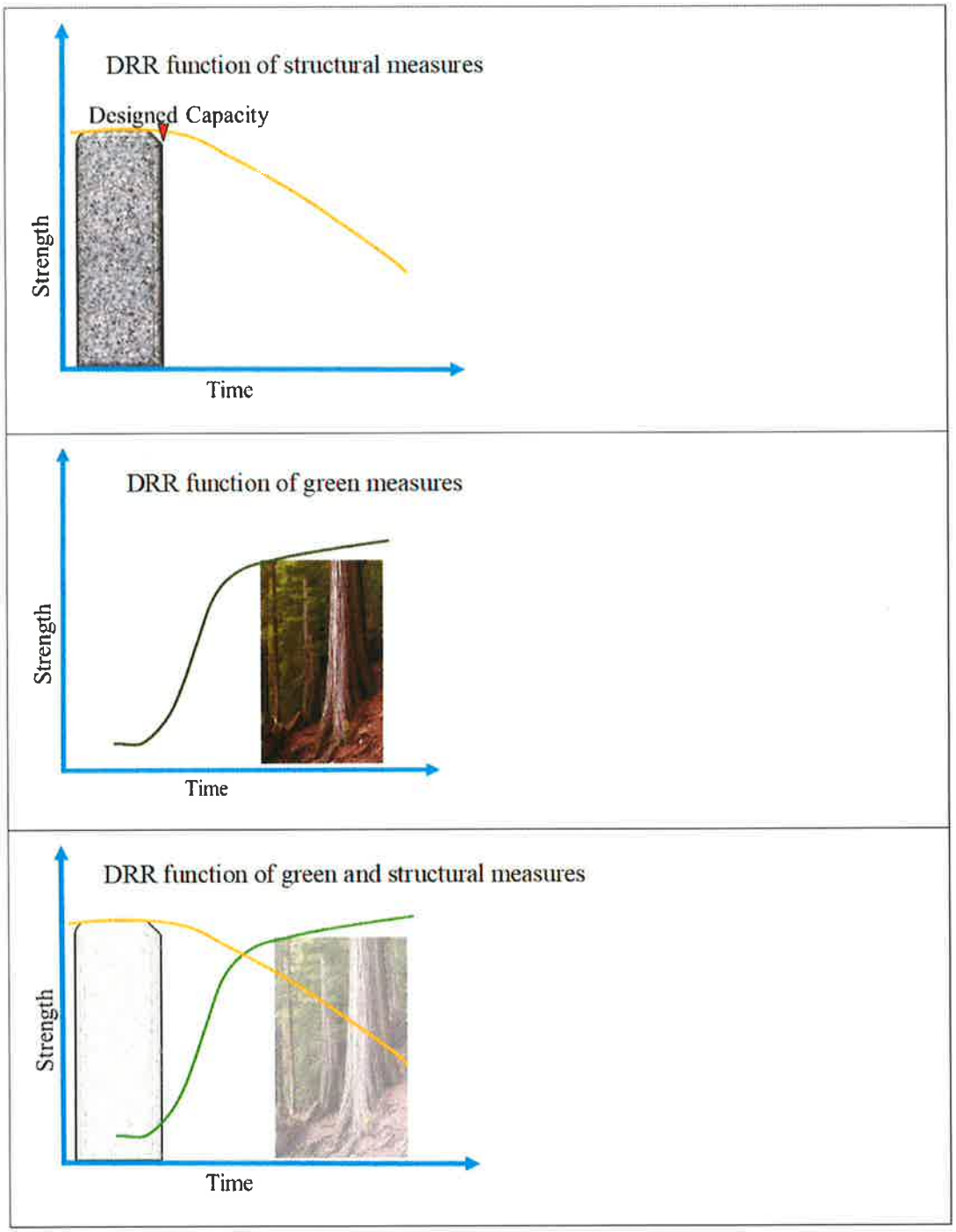

Figure 2: Lifetime of vegetative and civil engineering structures in normal condition (Adopted and modified from Natural Resource Management Handbook by Marongiu & Cencetti, 2013)

5.1.4 Integration of Eco-DRR in risk reduction strategies

Ecosystem-based solutions for disaster prevention are not a silver bullet solution to landslide disaster but of course, it is a kind of no-regret approach. There should not be Eco DRR versus Engineering DRR but needs to be a look into the broader benefits of ecosystem-based disaster risk reduction (Chandra & Dalton, 2013; Poratelli et al., 2020).

Eco-DRR plays a crucial role in preserving and revitalizing ecosystems, which is especially beneficial for countries like Japan that are currently facing challenges in land management due to a rapid decline in population and an aging society (Takeuchi et al., 2016). According to the annual report 2021, Japan has almost 12.2 million hectares (ha) of protection forests providing multiple benefits including disaster risk reduction for hundreds of years (Forestry Agency, 2021). In Nepal where most of the people live in sloppy areas and at the bottom of mid-hills and large investment in engineering infrastructure is not possible due to poor economies but sufficient forest resources are available. Nepal has almost 45% of its forest with multiple uses and is also recognized for its disaster risk reduction uses (Charmakar et al., 2021). The establishment of planted forests, with the active participation of local communities, has played a crucial role in safeguarding numerous settlements and important infrastructure from climate-related hazards in the lowland areas of Nepal (Thapa et al., 2022). Nevertheless, as ecosystem-based approaches have their limitations, it is essential to combine and integrate them with various other disaster risk reduction (DRR) measures in order to effectively enhance the social and economic resilience of society. By incorporating multiple strategies, we can create a comprehensive approach to DRR that maximizes the benefits of ecosystem-based approaches while addressing their limitations. These solutions should be integrated into broader disaster risk reduction strategies and work in harmony with other critical risk management measures, such as early warning systems and contingency plans. By incorporating ecosystem-based approaches within a comprehensive framework, we can enhance the overall effectiveness of disaster risk reduction efforts and improve the resilience of communities and infrastructure.

5.1.5 Learnings from Hirose and Sennindani landslide case studies

Sennindani landslide

Figure 3: Photographs of the Sennindani landslide in 2015 (left) and 2022 (right) (Source: Forest Management Bureau, Chugoku Forestry Agency)

The Sennindani landslide occurred at an elevation of 1400m in an area with a history of landslides, where there was sparse forest cover in the initiation zone. The landslide originated in the sparsely forested upper zone, but unfortunately, there was a lack of forest trees in the lower areas. This absence of forest at the bottom of the slope can be attributed to the steepness of the terrain. Continuous displacement, as observed in SAR data analysis, and persistent erosion caused by the Ozo river may also have contributed to the lack of a well-established forest. Additionally, aerial photographs indicate that the forested area at the bottom of the landslide might have been removed over time due to continuous erosion since 1961, as well as a shallow landslide that occurred in 2014, a few months before the main event in 2015.

As a result, all the sediment generated from the initiation zone traveled a horizontal distance of 800m downslope, reaching the Ozo river and accumulating along a 500m section. A small patch of forest trees remained intact in the middle of the landslide, effectively trapping large rocks from sliding further down. The 2015 landslide event transported approximately 1.3 million m3 of debris into the Ozo river, leading to continued sedimentation over the following years. After the landslide, the initiation and transportation zones of the landslide became barren and unstable. Therefore, human intervention became necessary to stabilize such a large-scale landslide using vegetation cover. The government decided to intervene and implement the restoration of the forest ecosystem in the area, utilizing native forest species available locally.

This serves as a typical example of integrating Eco-DRR options to restore the forest ecosystem in a landslide-affected area. However, these restoration efforts began in 2017, and it takes a considerable amount of time for the ecosystem to recover and stabilize. The progress from 2017 to 2022 demonstrates a gradual recovery and stabilization of forest species in the area.

Hirose landslide

Figure 4: Photographs of the Hirose landslide: trees fallen due to debris flow (left) and retention dam-like structure at the bottom (right) (Photo source: Yanai, S., 2021)

The Hirose landslide originated at an elevation of 380m in an area characterized by sparse vegetation, mainly consisting of broad-leaved forest species such as Quercus serrata, Alnus hirsute, Prunus serrulate, and Aria species. In the lower belt of the region, there is a cedar forest that was planted by the Forest Agency of Japan during the 1950s and 1960s.

This particular landslide is believed to have been reactivated in an area that had experienced landslides before. Interestingly, the landslide occurred twice within the span of a single day. The Hirose landslide resulted in the production of approximately 89,000 cubic meters of debris, which flowed down a slope with a gradient of 30 degrees, covering a distance of 500m and reaching agricultural land. As it traveled, the landslide caused damage to the upper slope's broadleaf forest and engulfed the cedar trees in its path within the transportation zone. While debris flows typically travel several hundred meters in sloppy landscapes, this event saw the debris flow extending only 25m beyond the forest boundary into the agricultural area.

The bottom area of the landslide encompasses highly productive paddy fields owned by the local people of Hirose town. Additionally, there are major high-tension power lines and a connecting road to another district. If the debris had flowed just a few meters further, these structures would have been destroyed. Moreover, had the landslide traveled an additional 200m downwards, all the debris could have been flushed into the Tedori River, leading to further ecological consequences in the aquatic ecosystem.

The mature cedar trees played a crucial role in impeding the outflow of debris. They resisted the debris flow when standing and created a retention dam-like structure when falling, effectively trapping a large volume of debris.

CHAPTER 6 CONCLUSION AND RECOMMENDATIONS

6.1 Conclusion

- By carefully observing geomorphological evidence, landslide evolution can be predicted, provided that temporal photographs and remote sensing data are available.
- Landslides can cause long-term environmental impacts, and in certain cases, residents may be forced to abandon their homes (In addition to life and property loss). For instance, the Sennindani landslide caused environmental problems and the Methum landslide risk forced locals to abandon houses.
- Forests can play a vital role in preventing erosion and debris flow and mitigate the risk of landslides by serving as a natural barrier. For instance, the Cedar Forest in the Hirose landslide demonstrates this.
- An early warning system can effectively alert local communities and help protect them from the destructive impacts of landslide disasters.
- The combination of ecosystem-based solutions and early warning systems can substantially reduce the risk of landslides in both Nepal and Japan.

6.2 Recommendation

- An extended investigation should be undertaken to comprehensively understand the role of hydrogeology in the occurrence of landslides, such as the Sennindani landslide, Hirose landslide, and Methum landslide.
- To gain a deeper understanding of the diverse effects of landslides, it is recommended to carry out long-term research focusing on multiple impacts.
- Continuous research and monitoring should be prioritized for both the Sennindani landslide and Methum landslide, as both landslides are supposed to be still in the active stage considering the possibility of reactivation.
- Academia and implementing agencies should focus on generating compelling evidence to showcase the forest ecosystem as an effective and sustainable technique for Ecosystem-based disaster risk reduction.

- The necessary width to protect a certain volume of debris from landslides needs to be assessed to recommend the necessary safe forest zone width in sloppy areas.
- The combination of ecosystem-based solutions and landslide early warning systems can substantially reduce the risk of landslides.

REFERENCES

1.Panwar, V., & Sen, S. (2019). Economic Impact of Natural Disasters: An Empirical Re-examination. *Margin: The Journal of Applied Economic Research*, *13*(1), 109–139. https://doi.org/10.1177/0973801018800087

2.Khan, M. T. I., Anwar, S., Sarkodie, S. A., Yaseen, M. R., & Nadeem, A. M. (2023). Do natural disasters affect economic growth? The role of human capital, foreign direct investment, and infrastructure dynamics. *Heliyon*, *9*(1), e12911. https://doi.org/10.1016/j.heliyon.2023.e12911

3.*UN News*. (2021, September 1). *Climate and weather-related disasters surge five-fold over 50 years, but early warnings save lives—WMO report.* https://news.un.org/en/story/2021/09/1098662

4.Mokhtari, M., Faridi, P., Masoodi, M., Ahmadi, S. M., Mokhtari, M., Faridi, P., Masoodi, M., & Ahmadi, S. M. (2023). *Perspective Chapter: A Global View of Natural Hazards Related Disasters*. IntechOpen. https://doi.org/10.5772/intechopen.111582

5.*Annual Disaster Statistical Review 2016: The numbers and trends - World | ReliefWeb*. (2017, November 21). https://reliefweb.int/report/world/annual-disaster-statistical-review-2016-numbers-and-trends

6.Emberson, R., Kirschbaum, D. B., Amatya, P., Tanyas, H., & Marc, O. (2022). Insights from the topographic characteristics of a large global catalog of rainfall-induced landslide event inventories. *Natural Hazards and Earth System Sciences*, *22*(3), 1129–1149. https://doi.org/10.5194/nhess-22-1129-2022

7.*Asian Disaster Reduction Center（ADRC）*. (2022). Natural Disaster Databook 2021 An Analytical Overview. Retrieved May 26, 2023, from https://www.adrc.asia/publications/databook/DB2021_e.php

8.Cui, P., Lin, Y., & Chen, C. (2012). Destruction of vegetation due to geo-hazards and its environmental impacts in the Wenchuan earthquake areas. *Ecological Engineering*, *44*, 61–69. https://doi.org/10.1016/j.ecoleng.2012.03.012

9.Highland, L.M., & Bobrowsky, Peter, 2008, The landslide handbook—A guide to understanding landslides: Reston, Virginia, U.S. *Geological Survey Circular* 1325, 129 p. Retrieved May 26, 2023, from https://www.usgs.gov/programs/landslide-hazards.

10.Zhang, J., Lu, M., Zhang, L., & Xue, Y. (2021). Assessing indirect economic losses of landslides along highways. *Natural Hazards*, *106*(3), 2775–2796. https://doi.org/10.1007/s11069-021-04566-3

11.Winter, M. G., & Bromhead, E. N. (2012). Landslide risk: Some issues that determine societal acceptance. *Natural Hazards*, *62*(2), 169–187. https://doi.org/10.1007/s11069-011-9987-1

12.Bromhead, E. N. (1997). The treatment of landslides. *Proceedings of the Institution of Civil Engineers - Geotechnical Engineering*, *125*(2), 85–96. https://doi.org/10.1680/igeng.1997.29231

13.Swanston, D.N., & Schuster, R. L. (1989). Long-Term Landslide Hazard Mitigation Programs: Structure and Experience from Other Countries. *Environmental & Engineering Geoscience*, *xxvi*(1), 109–133. https://doi.org/10.2113/gseegeosci.xxvi.1.109

14.Rey, F., Bifulco, C., Bischetti, G. B., Bourrier, F., De Cesare, G., Florineth, F., Graf, F., Marden, M., Mickovski, S. B., Phillips, C., Peklo, K., Poesen, J., Polster, D., Preti, F., Rauch, H. P., Raymond, P., Sangalli, P., Tardio, G., & Stokes, A. (2019). Soil and water bioengineering: Practice and research needs for reconciling natural hazard control and ecological restoration. *Science of The Total Environment*, *648*, 1210–1218. https://doi.org/10.1016/j.scitotenv.2018.08.217

15.Adhikari, B. R., & Tian, B. (2021). Spatiotemporal Distribution of Landslides in Nepal. In S. Eslamian & F. Eslamian (Eds.), *Handbook of Disaster Risk Reduction for Resilience: New Frameworks for Building Resilience to Disasters* (pp. 453–471). Springer International Publishing. https://doi.org/10.1007/978-3-030-61278-8_20

16.Kwong, A. K. L., Wang, M., Lee, C. F., & Law, K. T. (2004). A review of landslide problems and mitigation measures in Chongqing and Hong Kong: Similarities and differences. *Engineering Geology*, *76*(1), 27–39. https://doi.org/10.1016/j.enggeo.2004.06.004

17.Popescu, M. E., & Sasahara, K. (2009). Engineering Measures for Landslide Disaster Mitigation. In K. Sassa & P. Canuti (Eds.), *Landslides – Disaster Risk Reduction* (pp. 609–631). Springer. https://doi.org/10.1007/978-3-540-69970-5_32

18.moos, J. (1999). Roadside Bio-engineering: site handbook. His Majesty's Government of Nepal, Department of Roads. Retrieved May 29, 2023, from

https://dor.gov.np/home/publication/gesu-publication/force/roadside-bio-engineering-site-handbook-2-76-1-12.

19. Estrella, M., Saalismaa, N. (Eds.), 2013. Ecosystem-based disaster risk reduction (Eco-DRR): An overview, in: The Role of Ecosystems in Disaster Risk Reduction. United Nations University Press, Shibuya-ku, Tokyo.

20. Moos, C., Bebi, P., Schwarz, M., Stoffel, M., Sudmeier-Rieux, K., & Dorren, L. (2018). Ecosystem-based disaster risk reduction in mountains. *Earth-Science Reviews*, *177*, 497–513. https://doi.org/10.1016/j.earscirev.2017.12.011

21. Wamsler, C., & Pauleit, S. (2016). Making headway in climate policy mainstreaming and ecosystem-based adaptation: Two pioneering countries, different pathways, one goal. *Climatic Change*, *137*(1), 71–87. https://doi.org/10.1007/s10584-016-1660-y

22. Kato, S., & Huang, W. (2021). Land use management recommendations for reducing the risk of downstream flooding based on a land use change analysis and the concept of ecosystem-based disaster risk reduction. *Journal of Environmental Management*, *287*, 112341. https://doi.org/10.1016/j.jenvman.2021.112341

23. Dhyani, S., Lahoti, S., Khare, S., Pujari, P., & Verma, P. (2018). Ecosystem based Disaster Risk Reduction approaches (EbDRR) as a prerequisite for inclusive urban transformation of Nagpur City, India. *International Journal of Disaster Risk Reduction*, *32*, 95–105. https://doi.org/10.1016/j.ijdrr.2018.01.018

24. Feagin, R. A., Mukherjee, N., Shanker, K., Baird, A. H., Cinner, J., Kerr, A. M., Koedam, N., Sridhar, A., Arthur, R., Jayatissa, L. p., Lo Seen, D., Menon, M., Rodriguez, S., Shamsuddoha, Md., & Dahdouh-Guebas, F. (2010). Shelter from the storm? Use and misuse of coastal vegetation bioshields for managing natural disasters. *Conservation Letters*, *3*(1), 1–11. https://doi.org/10.1111/j.1755-263X.2009.00087.x

25. Uy, N., & Shaw, R. (2012). The Role of Ecosystems in Climate Change Adaptation and Disaster Risk Reduction. In N. Uy & R. Shaw (Eds.), *Ecosystem-Based Adaptation* (Vol. 12, pp. 41–59). Emerald Group Publishing Limited. https://doi.org/10.1108/S2040-7262(2012)0000012009

26. Chaudhary, M. T., & Piracha, A. (2021). Natural Disasters—Origins, Impacts, Management. *Encyclopedia*, *1*(4), Article 4. https://doi.org/10.3390/encyclopedia1040084

27.Carlowicz, M. (1996). Natural hazards need not lead to natural disasters. *Eos, Transactions American Geophysical Union*, *77*(16), 149–153. https://doi.org/10.1029/96EO00100

28.Alexander, D. E. (1995). A Survey of the Field of Natural Hazards and Disaster Studies. In A. Carrara & F. Guzzetti (Eds.), *Geographical Information Systems in Assessing Natural Hazards*. (pp. 1–19). Springer Netherlands. https://doi.org/10.1007/978-94-015-8404-3_1

29.Felbermayr, G., & Gröschl, J. (2014). Naturally negative: The growth effects of natural disasters. *Journal of Development Economics*, *111*, 92–106. https://doi.org/10.1016/j.jdeveco.2014.07.004

30.Keim, M. E. (2008). Building Human Resilience: The Role of Public Health Preparedness and Response As an Adaptation to Climate Change. *American Journal of Preventive Medicine*, *35*(5), 508–516. https://doi.org/10.1016/j.amepre.2008.08.022

31.https://www.unisdr.org/files/7817_UNISDRTerminologyEnglish.pdf

32.Lavell, A., Oppenheimer, M., Diop, C., Hess, J., Lempert, R., Li, J., Muir-Wood, R., Myeong, S., Moser, S., Takeuchi, K., Cardona, O. D., Hallegatte, S., Lemos, M., Little, C., Lotsch, A., & Weber, E. (2012). Climate change: New dimensions in disaster risk, exposure, vulnerability, and resilience. In *Managing the Risks of Extreme Events and Disasters to Advance Climate Change Adaptation: Special Report of the Intergovernmental Panel on Climate Change* (pp. 25–64). Cambridge University Press. https://doi.org/10.1017/CBO9781139177245.004

33.Pelling, M. (2001) Natural disasters? In N. Castree and B. Braun (eds) *Social Nature*. Blackwell, London. pp. 170– 188.

34.Zacharias, M. A., & Gregr, E. J. (2005). Sensitivity and Vulnerability in Marine Environments: An Approach to Identifying Vulnerable Marine Areas. *Conservation Biology*, *19*(1), 86–97. https://doi.org/10.1111/j.1523-1739.2005.00148.x

35.Adger, W. N. (2006). Vulnerability. *Global Environmental Change*, *16*(3), 268–281. https://doi.org/10.1016/j.gloenvcha.2006.02.006

36.Manyena, S. B. (2006). The concept of resilience revisited. *Disasters*, *30*(4), 434–450. https://doi.org/10.1111/j.0361-3666.2006.00331.x

37. *Varnes, D.J. 1978. Slope movements: types and processes. R.L. Schuster, R.J. Krizek (Eds.), Landslide Analysis and Control, National Academy of Sciences, Special Report 176, Transportation Research Board, Washington D.C. (1978), pp. 11-33. Avaiale from https://scholar.google.com/scholar_lookup?title=Slope%20movements%3A%20types%20and%20processes&publication_year=1978&author=D.J.%20Varnes*

38. Song, C., Yu, C., Li, Z., Pazzi, V., Del Soldato, M., Cruz, A., & Utili, S. (2021). Landslide geometry and activity in Villa de la Independencia (Bolivia) revealed by InSAR and seismic noise measurements. *Landslides*, *18*(8), 2721–2737. https://doi.org/10.1007/s10346-021-01659-9

39. Lan, H., Liu, X., Li, L., Li, Q., Tian, N., & Peng, J. (2022). Remote Sensing Precursors Analysis for Giant Landslides. *Remote Sensing*, *14*(17), Article 17. https://doi.org/10.3390/rs14174399

40. Song, C., Yu, C., Li, Z., Utili, S., Frattini, P., Crosta, G., & Peng, J. (2022). Triggering and recovery of earthquake accelerated landslides in Central Italy revealed by satellite radar observations. *Nature Communications*, *13*(1), Article 1. https://doi.org/10.1038/s41467-022-35035-5

41. Geertsema, M., Highland, L., & Vaugeouis, L. (2009). Environmental Impact of Landslides. In K. Sassa & P. Canuti (Eds.), *Landslides – Disaster Risk Reduction* (pp. 589–607). Springer. https://doi.org/10.1007/978-3-540-69970-5_31

42. Turner, A. K. (2018). Social and environmental impacts of landslides. *Innovative Infrastructure Solutions*, *3*(1), 70. https://doi.org/10.1007/s41062-018-0175-y

43. Kondratyeva, L. M., Makhinov, A. N., Andreeva, D. V., & Bashkurova, A. S. (2020). Changes in Water Quality in the Bureiskoe Reservoir Caused by a Large Landslide. *Water Resources*, *47*(2), 257–268. https://doi.org/10.1134/S0097807820020086

44. Schuster, R.L., & Highland, L.M. (2007). Overview of the Effects of Mass Wasting on the Natural Environment. *Environmental & Engineering Geoscience*, *13*(1), 25–44. https://doi.org/10.2113/gseegeosci.13.1.25

45. Tanyaş, H., Kirschbaum, D., Görüm, T., van Westen, C. J., Tang, C., & Lombardo, L. (2021). A closer look at factors governing landslide recovery time in post-seismic periods. *Geomorphology*, *391*, 107912. https://doi.org/10.1016/j.geomorph.2021.107912

46. Anderson, M. G., & Holcombe, E. (2013). *Community-Based Landslide Risk Reduction: Managing Disasters in Small Steps*. World Bank Publications.

47. Dai, F. C., Lee, C. F., & Ngai, Y. Y. (2002). Landslide risk assessment and management: An overview. *Engineering Geology*, *64*(1), 65–87. https://doi.org/10.1016/S0013-7952(01)00093-X

48. Margottini, C., Canuti, P., & Sassa, K. (Eds.). (2013). *Landslide Science and Practice: Volume 7: Social and Economic Impact and Policies*. Springer. https://doi.org/10.1007/978-3-642-31313-4

49. Dikshit, A., Satyam, D. N., & Towhata, I. (2018). Early warning system using tilt sensors in Chibo, Kalimpong, Darjeeling Himalayas, India. *Natural Hazards*, *94*(2), 727–741. https://doi.org/10.1007/s11069-018-3417-6

50. Abraham, M. T., Satyam, N., Pradhan, B., Segoni, S., & Alamri, A. (2022). Developing a prototype landslide early warning system for Darjeeling Himalayas using SIGMA model and real-time field monitoring. *Geosciences Journal*, *26*(2), 289–301. https://doi.org/10.1007/s12303-021-0026-2

51. Thapa, P. S., Adhikari, B. R., Shaw, R., Bhattarai, D., & Yanai, S. (2023). Geomorphological analysis and early warning systems for landslide risk mitigation in Nepalese mid-hills. *Natural Hazards*, *117*(2), 1793–1812. https://doi.org/10.1007/s11069-023-05929-8

52. McVittie, A., Cole, L., Wreford, A., Sgobbi, A., & Yordi, B. (2018). Ecosystem-based solutions for disaster risk reduction: Lessons from European applications of ecosystem-based adaptation measures. *International Journal of Disaster Risk Reduction*, *32*, 42–54. https://doi.org/10.1016/j.ijdrr.2017.12.014

53. Sandholz, S., Lange, W., & Nehren, U. (2018). Governing green change: Ecosystem-based measures for reducing landslide risk in Rio de Janeiro. *International Journal of Disaster Risk Reduction*, *32*, 75–86. https://doi.org/10.1016/j.ijdrr.2018.01.020

54. Teich, M., Accastello, C., Perzl, F., Berger, F., Teich, M., Accastello, C., Perzl, F., & Berger, F. (2022). Protective Forests for Ecosystem-based Disaster Risk Reduction (Eco-DRR) in the Alpine Space. In *Protective Forests as Ecosystem-based Solution for Disaster Risk Reduction (Eco-DRR)*. IntechOpen. https://doi.org/10.5772/intechopen.99505

55. Shinohara, Y., & Kume, T. (2022). Changes in the factors contributing to the reduction of landslide fatalities between 1945 and 2019 in Japan. *Science of The Total Environment*, *827*, 154392. https://doi.org/10.1016/j.scitotenv.2022.154392

56. Dolojan, N. L. J., Moriguchi, S., Hashimoto, M., & Terada, K. (2021). Mapping method of rainfall-induced landslide hazards by infiltration and slope stability analysis. *Landslides*, *18*(6), 2039–2057. https://doi.org/10.1007/s10346-020-01617-x

57. Parvin, G. A., Fujita, K., Shaw, R., & Rahman, Md. H. (2022). Cross-Cutting Issues in Landslide Hazard of Japan: Forest Management, Climate Change, Demographic Change and Aging Society. In R. Sarkar, R. Shaw, & B. Pradhan (Eds.), *Impact of Climate Change, Land Use and Land Cover, and Socio-economic Dynamics on Landslides* (pp. 471–491). Springer Nature. https://doi.org/10.1007/978-981-16-7314-6_21

58. Valagussa, A., Marc, O., Frattini, P., & Crosta, G. B. (2019). Seismic and geological controls on earthquake-induced landslide size. *Earth and Planetary Science Letters*, *506*, 268–281. https://doi.org/10.1016/j.epsl.2018.11.005

59. Chen, C.-W., Iida, T., & Yamada, R. (2017). Effects of active fault types on earthquake-induced deep-seated landslides: A study of historical cases in Japan. *Geomorphology*, *295*, 680–689. https://doi.org/10.1016/j.geomorph.2017.07.030

60. Kadomura, H. (1980). Erosion by Human Activities in Japan. *GeoJournal*, *4*(2), 133–144. https://doi.org/10.1007/BF00160740

61. Amatya, S. C. (2020). Challenges of Landslide Disaster for Development in Nepal. *Journal of Development Innovations*, *4*(1), Article 1.

62. Adhikari, B. R., & Tian, B. (2021). Spatiotemporal Distribution of Landslides in Nepal. In S. Eslamian & F. Eslamian (Eds.), *Handbook of Disaster Risk Reduction for Resilience: New Frameworks for Building Resilience to Disasters* (pp. 453–471). Springer International Publishing. https://doi.org/10.1007/978-3-030-61278-8_20

63. Dahal, R. K., & Hasegawa, S. (2008). Representative rainfall thresholds for landslides in the Nepal Himalaya. *Geomorphology*, *100*(3), 429–443. https://doi.org/10.1016/j.geomorph.2008.01.014

64. Dahal, R. K. (2022). Earthquake-Induced Landslides in the Nepal Himalaya. In I. Towhata, G. Wang, Q. Xu, & C. Massey (Eds.), *Coseismic Landslides: Phenomena,*

Long-Term Effects and Mitigation (pp. 59–82). Springer Nature. https://doi.org/10.1007/978-981-19-6597-5_3

65.K.C., S. (2013). Community Vulnerability to Floods and Landslides in Nepal. *Ecology and Society*, *18*(1). https://www.jstor.org/stable/26269258

66.Bellugi DG, Milledge DG, Cuffey KM, et al (2021) Controls on the size distributions of shallow landslides. Proceedings of the National Academy of Sciences 118:e2021855118. https://doi.org/10.1073/pnas.2021855118

67.Bennett GL, Miller SR, Roering JJ, Schmidt DA (2016) Landslides, threshold slopes, and the survival of relict terrain in the wake of the Mendocino Triple Junction. Geology 44:363–366. https://doi.org/10.1130/G37530.1

68.Borrelli L, Conforti M, Mercuri M (2019) LiDAR and UAV System Data to Analyse Recent Morphological Changes of a Small Drainage Basin. ISPRS International Journal of Geo-Information 8:536. https://doi.org/10.3390/ijgi8120536

69.Chen P, Shi W, Liu Y, Cao X (2022) Slip rate deficit partitioned by fault-fold system on the active Haiyuan fault zone, Northeastern Tibetan Plateau. Journal of Structural Geology 155:104516. https://doi.org/10.1016/j.jsg.2022.104516

70.Chigira M, Tsou C-Y, Matsushi Y, et al (2013) Topographic precursors and geological structures of deep-seated catastrophic landslides caused by Typhoon Talas. Geomorphology 201:479–493. https://doi.org/10.1016/j.geomorph.2013.07.020

71.Dai FC, Deng JH, Tham LG, et al (2004) A large landslide in Zigui County, Three Gorges area. Can Geotech J 41:1233–1240. https://doi.org/10.1139/t04-049

72.Daimaru H, Kurokawa U, Murakami W, Matsuura S (2013) Topographic features of deep-seated landslides inferred from multi-temporal geographical information in Senzu district, central Japan. Journal of the Japan Landslide Society 50, 24–33. https://doi.org/10.3313/jls.50.24

73.Dang MH, Umeda S, Yuhi M (2014) Long-term riverbed response of lower Tedori River, Japan, to sediment extraction and dam construction. Environ Earth Sci 72:2971–2983. https://doi.org/10.1007/s12665-014-3202-0

74.Deng H, Zhong CY, WU L, Tu GX (2021) Process analysis of causes of Luanshigang landslide in the Dadu River, China. Environ Earth Sci 80:737. https://doi.org/10.1007/s12665-021-10069-y

75.Du Y, Xu Q, Zhang L, et al (2017) Recent Landslide Movement in Tsaoling, Taiwan Tracked by TerraSAR-X/TanDEM-X DEM Time Series. Remote Sensing 9:353. https://doi.org/10.3390/rs9040353

76.Fujii Y, Hori S (2003) Internal structure of the Jinnosuke-dani landslide, observable on the Betto valley wall. Journal of the Japan Landslide Society 40, 311–315. https://doi.org/10.3313/jls.40.4_311 (In Japanese abstract in English)

77.Geospatial Information Authority of Japan. Available online: https://maps.gsi.go.jp/#5/36.104611/140.084556/&base=std&ls=std&disp=1&vs=c1g1j0h0k0l0u0t0z0r0s0m0f1. Accessed 15 December 2022

78.Giordan D, Adams MS, Aicardi I, et al (2020) The use of unmanned aerial vehicles (UAVs) for engineering geology applications. Bull Eng Geol Environ 79:3437–3481. https://doi.org/10.1007/s10064-020-01766-2

79.James MR, Robson S (2012) Straightforward reconstruction of 3D surfaces and topography with a camera: Accuracy and geoscience application. Journal of Geophysical Research: Earth Surface 117:. https://doi.org/10.1029/2011JF002289

80.Jebur MN, Pradhan B, Tehrany MS (2015) Using ALOS PALSAR derived high-resolution DInSAR to detect slow-moving landslides in tropical forest: Cameron Highlands, Malaysia. Geomatics, Natural Hazards and Risk 6:741–759. https://doi.org/10.1080/19475705.2013.860407

81.Kjekstad O, Highland L (2009) Economic and Social Impacts of Landslides. In: Sassa K, Canuti P (eds) Landslides – Disaster Risk Reduction. Springer, Berlin, Heidelberg, pp 573–587. https://doi.org/10.1007/978-3-540-69970-5_30

82.Lan H, Liu X, Li L, et al (2022) Remote Sensing Precursors Analysis for Giant Landslides. Remote Sensing 14:4399. https://doi.org/10.3390/rs14174399

83.Li W, Zhan W, Lu H, et al (2023) Precursors to large rockslides visible on optical remote-sensing images and their implications for landslide early detection. Landslides 20:1–12. https://doi.org/10.1007/s10346-022-01960-1

84.Marui H, Koizumi Y (2014) Case Study on the Kokkawa Landslide Caused by Snowmelt. In: Shan W, Guo Y, Wang F, et al. (eds) Landslides in Cold Regions in the Context of Climate Change. Springer International Publishing, Cham, pp 253–261. https://doi.org/10.1007/978-3-319-00867-7_18

85.Matsuura S, Asano S, Okamoto T, et al (1998) Estimation of the Intensity of Meltwater Flowing out from the Bottom of a Snow Pack Prior to Hachimantai-Sumikawa landslide and its Probability Analysis Using AMeDAS Data Set. Landslides 35:20-28_1. https://doi.org/10.3313/jls1964.35.2_20

86.Michinaka H, Hiramatsu Y, (2010). Detection of Landslide Displacement at the Hakusan volcano from Interferometric Analysis of ALOS/PALSAR data. Journal of the Geodetic Society of Japan 56, 179–194. https://doi.org/10.11366/sokuchi.56.179

87.Miyagi T, Prasad GB, Tanavud C, et al (2004) Landslide Risk Evaluation and Mapping - Manual of Aerial Photo Interpretation for Landslide Topography and Risk Management. *Report of the National Research Institute for Earth Science and Disaster Prevention* **2004**, 66, 75-137.

88.National Research Institute for Earth Science and Disaster Resilience. Japan Seismic Hazard Information Station (J-SHIS) Map. Available online: https://www.j-shis.bosai.go.jp/map/ Accessed 2 December 2022

89.Nishii R, Matsuoka N, Daimaru H, Yasuda M (2013) Precursors and triggers of an alpine rockslide in Japan: the 2004 partial collapse during a snow-melting period. Landslides 10:75–82. https://doi.org/10.1007/s10346-012-0353-5

90.Ogita S, Sagara W, Higaki D (2017) Shapes and Mechanisms of Large-Scale Landslides in Japan: Forecasting Analysis from an Inventory (WCoE 2014–2017). In: Sassa K, Mikoš M, Yin Y (eds) Advancing Culture of Living with Landslides. Springer International Publishing, Cham, pp 315–324. https://doi.org/10.1007/978-3-319-59469-9_26

91.Okamoto T, Matsuura S, Larsen JO, et al (2018) The response of pore water pressure to snow accumulation on a low-permeability clay landslide. Engineering Geology 242:130–141. https://doi.org/10.1016/j.enggeo.2018.06.002

92.Osawa H, Matsushi Y, Matsuura S, et al (2018) Seasonal transition of hydrological processes in a slow-moving landslide in a snowy region. Hydrological Processes 32:2695–2707. https://doi.org/10.1002/hyp.13212

93.Wang F, Okuno T, Matsumoto T (2007) Deformation characteristics and influential factors for the giant Jinnosuke-dani landslide in the Haku-san Mountain area, Japan. Landslides 4:19–31. https://doi.org/10.1007/s10346-006-0049-9

94. Williams R, (2012). DEMs of Difference. Available at: https://www.researchgate.net/publication/310596075_DEMs_of_Difference. Accessed on 2 February 2023

95. Yang W, Liu L, Shi P (2020) Detecting precursors of an imminent landslide along the Jinsha River. Natural Hazards and Earth System Sciences 20:3215–3224. https://doi.org/10.5194/nhess-20-3215-2020

96. Yuya K, Yoshihiro H (2017) Landslide displacement detection around Hakusan volcano, central Japan, from InSAR analysis of ALOS-2/PALSAR-2 data. Science Reports of Kanazawa University (Web) 61, 39–47.

97. Bandoh, H., Kida, I., and Ueda, H. (2011) Olfactory Responses to Natal Stream Water in Sockeye Salmon by BOLD fMRI. *PLOS ONE*, **6** (1), e16051. Available at: 10.1371/journal.pone.0016051

98. Benda, L. (1990) The influence of debris flows on channels and valley floors in the Oregon Coast Range, U.S.A. *Earth Surface Processes and Landforms*, **15** (5), 457–466. Available at: doi.org/ 10.1002/esp.3290150508

99. Bhat, D.R., Osawa, S., Wakai, A., Sasahara, K., Bh, N.P., ary, Cai, F., Ochiai, H., and Tanaka, N. (2021) Rigorous Analysis of Stress-Dependent Landslide Movements with Groundwater Fluctuations Applicable to Disaster Prevention in Monsoon Asia. *Journal of Disaster Research*, **16** (4), 658–673. Available at: doi.org/ 10.20965/jdr.2021.p0658

100. Dadson, S.J., Hovius, N., Chen, H., Dade, W.B., Lin, J.-C., Hsu, M.-L., Lin, C.-W., Horng, M.-J., Chen, T.-C., Milliman, J., and Stark, C.P. (2004) Earthquake-triggered increase in sediment delivery from an active mountain belt. *Geology*, **32** (8), 733–736. Available at: doi.org/10.1130/G20639.1

101. Dang, M.H., Umeda, S., and Yuhi, M. (2014) Long-term riverbed response of lower Tedori River, Japan, to sediment extraction and dam construction. *Environ Earth Sci*, **72** (8), 2971–2983. Available at: doi.org/10.1007/s12665-014-3202-0

102. Esposito, G., Carabella, C., Paglia, G., and Miccadei, E. (2021) Relationships between Morphostructural/Geological Framework and Landslide Types: Historical Landslides in the Hilly Piedmont Area of Abruzzo Region (Central Italy). *Land*, **10** (3), 287. Available at:doi.org/ 10.3390/land10030287

103.Ezcurra, E., Barrios, E., Ezcurra, P., Ezcurra, A., Vanderplank, S., Vidal, O., Villanueva-Almanza, L., and Aburto-Oropeza, O. (2019) A natural experiment reveals the impact of hydroelectric dams on the estuaries of tropical rivers. *Science Advances*, **5** (3), eaau9875. Available at: doi.org/10.1126/sciadv.aau9875

104.Fujita, T., Yokoyama, R., Kato, Y., Inoue, O., and Harada, M. (2022) To what extent has Ayu (Plecoglossus altivelis)'s spawning environment been clarified? *Ecology and Civil Engineering*, **24** (2), 217–234. Available at: doi.org/10.3825/ece.21-00021

105.Geertsema, M., Highland, L., and Vaugeouis, L. (2009) Environmental Impact of Landslides, in *Landslides – Disaster Risk Reduction* (eds.Sassa, K., and Canuti, P.), Springer, Berlin, Heidelberg, pp. 589–607. Available at: doi.org/10.1007/978-3-540-69970-5_31

106.Gregory, R.S., and Levings, C.D. (1998) Turbidity Reduces Predation on Migrating Juvenile Pacific Salmon. *Transactions of the American Fisheries Society*, **127** (2), 275–285. Available at: doi.org/10.1577/1548-8659(1998)127<0275:TRPOMJ>2.0.CO;2

107.Guzzetti, F., Mondini, A.C., Cardinali, M., Fiorucci, F., Santangelo, M., and Chang, K.-T. (2012) Landslide inventory maps: New tools for an old problem. *Earth-Science Reviews*, **112** (1), 42–66. Available at: doi.org/10.1016/j.earscirev.2012.02.001

108.Hai, M.D., Umeda, S., and Yuhi, M. (2019) Morphological Changes of the Lower Tedori River, Japan, over 50 Years. *Water*, **11** (9), 1852. Available at: doi.org/10.3390/w11091852

109.Hovius, N., Stark, C.P., Hao-Tsu, C., and Jiun-Chuan, L. (2000) Supply and Removal of Sediment in a Landslide-Dominated Mountain Belt: Central Range, Taiwan. *The Journal of Geology*, **108** (1), 73–89. Available at: doi.org/10.1086/314387

110.Ishida R. 1962. On the spawnning of the Ayu, Plecoglossus altivelis T. and S. -III. Relationships between the size of spawners and the depth of water of the spawnning ground. *Bulletin of the Japanese Society of Scientific Fisheries*, **28** (2), 399-404. Available at: doi.org/10.2331/suisan.28.399

111.Ishida R., 1990. 6. The Structure of Spawning Ground of Ayu, Plecoglossus altivelis. *Aquaculture*, **38** (2), 207–208. Available at: doi.org/10.11233/aquaculturesci1953.38.207

112.Johnson, A.C., Swanston, D.N., and McGee, K.E. (2000) Landslide Initiation, Runout, and Deposition Within Clearcuts and Old-Growth Forests of Alaska1. *JAWRA Journal of the American Water Resources Association*, **36** (1), 17–30. Available at: doi.org/10.1111/j.1752-1688.2000.tb04245.x

113.Kanbara J, Imamori N (2020) Outline of measures for sediment disaster by the Sabo department of MLIT, Japan. *Landslides*, **17** (11), 2503–2513. Available at: doi.org/10.1007/s10346-020-01554-9

114.Kawagoe, S., Kazama, S., and Ranjan Sarukkalige, P. (2009) Assessment of snowmelt triggered landslide hazard and risk in Japan. *Cold Regions Science and Technology*, **58** (3), 120–129. Available at:doi.org/10.1016/j.coldregions.2009.05.004

115.Kemp, P., Sear, D., Collins, A., Naden, P., and Jones, I. (2011) The impacts of fine sediment on riverine fish. *Hydrological Processes*, **25** (11), 1800–1821. Available at: doi.org/10.1002/hyp.7940

116.Kinki Chugoku Forest Management Bureau (2021) Report on Technical Review Meeting on the Collapsed Land upstream of Tedori River. Available at: https://www.rinya.maff.go.jp/kinki/tisan/tetorigawa/211223.htm.Accessed 10 Jan 2023.

117.Kobiyama M, de Almeida Mota A, Grison F, Nery Giglio J. 2011. Landslide influence on turbidity and total solids in Cubatão do Norte River, Santa Catarina, Brazil. *Natural Hazards* **59**: 1077–1086. Available at: doi.org/10.1007/s11069-011-9818-4.

118.Korup, O. (2006) Effects of large deep-seated landslides on hillslope morphology, western Southern Alps, New Zealand. *Journal of Geophysical Research: Earth Surface*, **111** (F1). Available at:doi.org/10.1029/2004JF000242

119.Larsen, M.C., and Simon, A. (1993) A Rainfall Intensity-Duration Threshold for Landslides in a Humid-Tropical Environment, Puerto Rico. *Geografiska Annaler: Series A, Physical Geography*, **75** (1–2), 13–23. Available at: doi.org/10.1080/04353676.1993.11880379

120.Lazar, A.N., Butterfield, D., Futter, M.N., Rankinen, K., Thouvenot-Korppoo, M., Jarritt, N., Lawrence, D.S.L., Wade, A.J., and Whitehead, P.G. (2010) An assessment of the fine sediment dynamics in an upland river system: INCA-Sed modifications

and implications for fisheries. *Science of The Total Environment*, **408** (12), 2555–2566. Available at: https://doi.org/10.1016/j.scitotenv.2010.02.030

121.Ministry of Land, Infrastructure, Transport and Tourism (2011) National land numerical information download service. Available at: http://nlftp.mlit.go.jp/ksj/. Accessed 1 Jan 2023.

122. Ministry of Land, Infrastructure, Transport and Tourism_(2020) White Paper on Land, Infrastructure, Transport and Tourism in Japan. Available at: https://www.mlit.go.jp/en/statistics/white-paper-mlit-index.html___Accessed 2 February 2022.

123.Petley, D. (2012) Global patterns of loss of life from landslides. *Geology*, **40** (10), 927–930. Available at: https://doi.org/10.1130/G33217.1

124.Rudolf-Miklau, F., and Suda, J. (2013) Design Criteria for Torrential Barriers, in *Dating Torrential Processes on Fans and Cones: Methods and Their Application for Hazard and Risk Assessment* (eds.Schneuwly-Bollschweiler, M., Stoffel, M., and Rudolf-Miklau, F.), Springer Netherlands, Dordrecht, pp. 375–389. Available at: doi.org/10.1007/978-94-007-4336-6_26

125.Sassa, K. (2005) Landslide disasters triggered by the 2004 Mid-Niigata Prefecture earthquake in Japan. *Landslides*, **2** (2), 135–142. Available at: doi.org/10.1007/s10346-005-0054-4

126.Sato, R., Ganzawa, Y., Yanai, S., and Momose, T. (2020) Evaluation of sediment movement in the Tedori River using the luminescence method. *Journal of Japan Society of Civil Engineers, Ser. B2 (Coastal Engineering)*, **76**, I_1405-I_1410. Available at: doi.org/10.2208/kaigan.76.2_I_1405

127.Schuster, R.L., and Highland, L.M. (2007) Overview of the Effects of Mass Wasting on the Natural Environment. *Environmental & Engineering Geoscience*, **13** (1), 25–44. Available at: doi.org/10.2113/gseegeosci.13.1.25

128.Schuster, R.L., and Highland, L.M. (2007) The Third Hans Cloos Lecture. Urban landslides: socioeconomic impacts and overview of mitigative strategies. *Bull Eng Geol Environ*, **66** (1), 1–27. Available at: doi.org/10.1007/s10064-006-0080-z

129.Sidle, R.C., Pearce, A.J., O'Loughlin, C.L., 1985. Hillslope stabil-ity and landuse. Water Resour. Monogr., vol. 11 American Geo-physical Union, Washington, DC 140 pp

(16) (PDF) Characteristics of channel steps and reach morphology in headwater streams, Southeast Alaska. Available from: https://www.researchgate.net/publication/223226050_Characteristics_of_channel_steps_and_reach_morphology_in_headwater_streams_Southeast_Alaska. Accessed 7 Apr 2023.

130. Takase, K., and Fujihara, Y. (2019) Evaluation of the effects of irrigation water on groundwater budget by a hydrologic model. *Paddy Water Environ*, **17** (3), 439–446. Available at: 10.1007/s10333-019-00739-w

131. Tanaka, K., Segawa, M., Fujiwara, Y., Takase, K., Maruyama, T., and Chono, S. (2017) High-turbidity Water from Landslides Affects Groundwater Recharge of Paddy Fields in the Tedori River Alluvial Fan. *Journal of Japan Society of Hydrology and Water Resources*, **30**, 173–180. Available at: doi.org 10.3178/jjshwr.30.173

132. Thapa, P.S., Chaudhary, S., and Dasgupta, P. (2022) Contribution of integrated watershed management (IWM) to disaster risk reduction and community development: Lessons from Nepal. International *Journal of Disaster Risk Reduction*, **76**, 103029. Available at: 10.1016/j.ijdrr.2022.103029

133. Varnes, D.J. (1978) Slope Movement Types and Processes. *Transportation Research Board Special Report*, (176). Available at: http://onlinepubs.trb.org/Onlinepubs/sr/sr176/176-002.pdf Accessed 15 Jan 2023.

134. Wang, F., Okuno, T., and Matsumoto, T. (2007) Deformation characteristics and influential factors for the giant Jinnosuke-dani landslide in the Haku-san Mountain area, Japan. *Landslides*, **4** (1), 19–31. Available at: doi.org/10.1007/s10346-006-0049-9

135. Yamamoto, Y., Hino, H., and Ueda, H. (2010) Olfactory Imprinting of Amino Acids in Lacustrine Sockeye Salmon. *PLOS ONE*, **5** (1), e8633. Available at: https://doi.org/10.1371/journal.pone.0008633

136. Yanai S. (2018). Characteristics of the landslide that occurred at Mt. Hakusan in May 2015 and its impact on the downstream system. INTERPRAEVENT 2018 in the Pacific Rim In [Symposium] (pp.124-131).

137. Yanai, S. (2018). Characteristics of a Landslide Occurred in May 2015 in Mt. Hakusan and its Influence on Downstream System. In INTERPRAENENT 2018 in

the Pacific Rim In [Symposium] (pp.124-131). http://www.interpraevent.at/palm-cms/upload_files/Publikationen/Tagungsbeitraege/2018_1_124.pdf. Accessed 2 Mar 2022.

138.Yoshioka, Y., Nakamura, K., Horino, H., and Kawashima, S. (2016) Numerical assessments of the impacts of climate change on regional groundwater systems in a paddy-dominated alluvial fan. *Paddy Water Environ*, **14** (1), 93–103. Available at: doi.org/10.1007/s10333-015-0481-3

139.Yoshioka, Y., Nakamura, K., Takimoto, H., Sakurai, S., Nakagiri, T., Horino, H., and Tsuchihara, T. (2020) Multiple-indicator study of the response of groundwater recharge sources to highly turbid river water after a landslide in the Tedori River alluvial fan, Japan. *Hydrological Processes*, **34** (16), 3539–3554. Available at: doi.org/10.1002/hyp.13796

140.Asada, H, Minagawa, T, Koyama, A and Ichiyanagi, H. 2020. Analysis of Factors Contributing to Surface Failure on Slopes Caused by the July 2017 Torrential Rainfall in Northern Kyushu, Japan. Applied Ecological Engineering. 23. 185-196.

141.Chigira, M. 2015. Prediction of deep collapse locations and future research development. Applied Geology. 56. 200- 209.

142.Daimaru, H, Kurokawa, U, Murakami, W and Matsuura, J. 2013. Geomorphological characteristics of deep-fall occurrence slopes in the Sento area based on multitemporal geographic information. Journal of the Landslide Engineering Society of Japan. 50. 24-33.

143.Ellen, S, D and Fleming, R, W. 1987. Mobilization of debris flows from soil slips, San Fransisco Bay region, California, Geological Society of America Reviews in Engineering Geology. 7. 31-40.

144.Fukami, Y, Kitahara, Y, Ono, H, Toudou, C and Yamase, K. 2011. Stand Pull-down Test under Different Conditions of Soil Moisture. Journal of Forest Science Society of Japan. 93. 8-13.

145.Hasegawa, Y, Satomi, Y and Mizuyama, T. 2016. Experiments on the Formation and Failure of a River Channel Blockage by a Mudflow Containing Driftwood. Journal of Erosion Control Society of Japan. 69. 19-23.

146.Hatanji, T. 2003. Characteristics of rainfall-induced deep failures, Journal of Erosion Control Society of Japan. 55 (6). 74-77. Ishikawa Prefecture. 1987.Fundamental Land Classification Survey, Tsurugi. Jitousono, T. 2005. Deep Failure. Journal of Erosion Control Society of Japan. 58. 60-66.

147.Jitousono, T, Shimokawa, E and Teramoto Y. 2006. Proposal of a Prediction Method for Deep Failure Sites. Journal of Erosion Control Society of Japan. 59. 5-12.

148.Joussein, E, Petit, S, Churchman, J, Theng, B, Righi, D and Delvaux, B. 2005. Halloysite clay minerals-a review. Clay minerals. Clay minerals. 40. 383-426. Kaibori, M, Hasegawa, Y, Yamashita, Y, Sakita, H, Nakai, S, Kuwata, S, Hiramatsu, S, Jitousono T, Irasawa, M, Shimizu, S, Imaizumi, F, Nakatani, K, Kashiwabara, Y, Kato, N, Torita, E, Hirakawa, Y, Yoshinaga, S, Tanaka, K and Hayashi, S. 2018. Landslide Disasters in Hiroshima Prefecture Caused by Heavy Rainfall in July, 2008. Journal of Erosion Control Society of Japan. 71. 49-60. Japan Meteorological Agency. Ishikawa Prefecture Hakusan River Area Meteorological Data (viewed August 20, 2021) (https://www.data.jma.go.jp/obd/stats/etrn/index. php?prec_no=56&block_no=0973&year=2021&month= 05&day=20&view=g_pre).

149.Joussein, E, Petit, S, Churchman, J, Theng, B, Righi, D and Delvaux, B. 2005. Halloysite clay minerals–a review. Clay minerals. 40. 383-426.

150.Kato, S and Huang, W. 2021. Land use management recommendations for reducing the risk of downstream flooding based on a land use change analysis and the concept of ecosystem-based disaster risk reduction. Journal of Environmental Management. 287. 112341.

151.Kitahara, Y. 2010. Collapse prevention function of forest root systems. Water Science. 53. 11-37.

152.Kotani, J and Sengi, Y. 2006. Estimation of site index and stem quality in old Cryptomeria japonica plantations by factors of site environment. Ishikawa Prefectural Forest Experiment Report. 38. 16-20.

153.Maeda, H, Natani, H, Uematsu, S and Kono, K. 2011. Geological characteristics of hydrothermal alteration zone landslides: Example of Ikutawara-minami landslide area, Hokkaido. Journal of the Landslide Engineering Society of Japan. 48. 139-146.

154.Matsumura, K, Fujita, S, Yamada, T, Gonda, Y, Numamoto, S, Tutsumi, D, Nakatani, K, Imaizumi, F, Shimada, T, Kaibori, M, Suzuki, K, Tokunaga, H, Kashiwabara, Y,

Nagano, E, Yokoyama, O, Suzuki, T, Takezawa, N, Ohno, R, Nagayama, T, Ikejima, T, Tsuchiya, S. 2012. Landslides in the Kii Peninsula caused by Typhoon No.12 in September 2011. Journal of Erosion Control Society of Japan. 64. 43-53.

155.Mizuhara, K. 2016. A Study on Disasters Caused by Driftwood Associated with Mudslides and Measures to Prevent and Mitigate Them. Water Science 60. 1-46.

156.Mizuyama, T, Kurihara, J and Suzuki, H. 1990. Impact energy absorption effect of standing trees. Journal of Erosion Control Society of Japan. 42(6). 24-28.

157.Moos, C, Bebi, P, Schwarz, Stoffel, M, Sudmeier-Rieux, K and Dorren, L. 2018. Ecosystem-based disaster risk reduction in mountains. Earth-Science Reviews.177. 497–513.

158.Nonoyama, K, Ikeyama, T and Yamane, M. 2020. Effects of forests on sediment discharge reduction in mudslides caused by the July 2008 heavy rain disaster in Hiroshima Prefecture, Japan. Water Science. 64. 21-42.

159.Onda, Y, Komatsu, Y, Tsujimura, M and Fujiwara, J. 1999. Prediction of the time of collapse occurrence from the difference of delay time of rainfall-runoff peak. Journal of Erosion Control Society of Japan. 51. 48-52.

160.R core team. 2021. R: A language and environment for statistical computing. R Foundation for Statistical Computing, Vienna, Austria. https://www.R-project.org/.

161.Shimada, H and Nonoda, T. 2017. Pull-down resistance of cedar and cypress stands in the central region of Mie Prefecture. Journal of the Japanese Society of Arboricultural Engineering. 43(1). 138-143.

162. Shiramizu, H. 2010. Clay Mineralogy - Basics of Clay Science. Asakura Shoten.

163.Takeshita, K and Shimizu, A. 1997. Deep Failure of the Left Bank of the Aburatani River, Sakamoto Village, Kumamoto Prefecture, Japan (Preliminary Report). Journal of Erosion Control Society of Japan. 50. 77-80.

164.Todo, C, Yamase, K, Tanigawa,H, Ohashi, M, Ikeno, H, Dan'ura,M and Hirano, Y. 2015. Special Issue on "Disaster Prevention Revegetation and Landslide Disaster "Effect of Thinning on Maximum Pull-down Resistance Moment of Japanese Cedar. Journal of the Japanese Society for Afforestation Engineering. 41. 308-314.

165.Volcanic and Debris Flow Team, Sediment Management Research Group, Public Works Research Institute. 2008. Manual for Identifying Streams at Risk of Deep Failure (Draft). Public Works Research Institute data.4115.

166. Wang, F, and Sassa, K. 2007. Initiation and Traveling Mechanisms of the May 2004 Landslide-Debris Flow at Bettou-Dani of the Jinnosuke-Dani Landslide, Haku-San Mountain, Japan. Soils and Foundations, 47(1), 141–152.

167. Yamashita, Y, Ishikawa, Y and Kusano, S. 1992. Soil properties of collapsed areas at the source of debris flow, Japan. Journal of the Japanese Society of Arboricultural Engineering. 44 (5). 19-25.

168. Yanai, S and Igarashi, Y. 1990. History of the Slope Failure and Paleoenvironment on the Marine Terrace of Hidaka District, Central Hokkaido. The Quaternarily Research. 29. 319–336.

169. Yanai, S. 2017. Landslide and turbid water in the headwaters area of Mt. Hakusan in May 2015. Water Science 61. 75–91.

170. Acharya M, Paudyal KR (2019) Geological setting of the Chandragiri-Chitlang Range, southwest of Kathmandu Valley, central Nepal. Journal of Nepal Geological Society 58:199–207. https://doi.org/10.3126/jngs.v58i0.24605

171. Ader T, Avouac J-P, Liu-Zeng J, Lyon-Caen H, Bollinger L, Galetzka J, Genrich J, Thomas M, Chanard K, Sapkota SN, Rajaure S, Shrestha P, Ding L, Flouzat M (2012) Convergence rate across the Nepal Himalaya and interseismic coupling on the Main Himalayan Thrust: Implications for seismic hazard. Journal of Geophysical Research: Solid Earth 117(B4). https://doi.org/10.1029/2011JB009071

172. Adhikari BR, Ojha RB (2021) Geology and Physiography. In: Ojha RB, Panday D (eds) The Soils of Nepal. Springer International Publishing, Cham, pp 29–39. https://doi.org/10.1007/978-3-030-80999-7_4

173. Adhikari BR, Tian B (2021) Spatiotemporal distribution of landslides in Nepal. In: Eslamian S, Eslamian F (eds) Handbook of disaster risk reduction for resilience. Springer: Cham, pp 453–471. https://doi.org/10.1007/978-3-030-61278-8_20

174. Alcántara-Ayala I, Moreno AR (2016) Landslide risk perception and communication for disaster risk management in mountain areas of developing countries: a Mexican foretaste. J Mt Sci 13(12):2079–2093. https://doi.org/10.1007/s11629-015-3823-0

175. Bajracharya SR, Shrestha MS, Shrestha AB (2017) Assessment of high-resolution satellite rainfall estimation products in a streamflow model for flood prediction in the Bagmati basin, Nepal. Journal of Flood Risk Management 10(1):5–16. https://doi.org/10.1111/jfr3.12133

176.Baum RL, Godt JW (2010) Early warning of rainfall-induced shallow landslides and debris flows in the USA. Landslides 7(3):259–272. https://doi.org/10.1007/s10346-009-0177-0

177.Bollinger L, Tapponnier P, Sapkota SN, Klinger Y (2016) Slip deficit in central Nepal: omen for a repeat of the 1344 AD earthquake? Earth, Planets and Space 68(1):12. https://doi.org/10.1186/s40623-016-0389-1

178.Central Bureau of Statistics (2021) Preliminary Report of National Population Census. National Planning Commission, Government of Nepal. https://censusnepal.cbs.gov.np/Home/Details?tpid=5&tfsid=17. Accessed 9 April 2022.

179.Chalise D, Kumar L, Kristiansen P (2019) Land Degradation by Soil Erosion in Nepal: A Review. Soil Systems 3(1):12. https://doi.org/10.3390/soilsystems3010012

180.Dahal RK, Hasegawa S (2008) Representative rainfall thresholds for landslides in the Nepal Himalaya. Geomorphology 100(3):429–443. https://doi.org/10.1016/j.geomorph.2008.01.014

181.Devkota BD, Paudel P, Kubota T, Deepak KC (2014) Landslide and Flood Hazards Consequences and Community Based Management Initiatives in Nepal Himalaya. In Proceedings of the Interpraevent International Symposium, Nara, Japan, 25–28. http://www.interpraevent.at/palm-cms/upload_files/Publikationen/Tagungsbeitraege/2014_1_198.pdf Accessed 20 May 2022.

182.Dhakal S (2015) Evolution of Geomorphologic Hazards in Hindu Kush Himalaya. In: Nibanupudi HK, Shaw R (eds) Mountain Hazards and Disaster Risk Reduction. Springer Japan, Tokyo, pp 53–72. https://doi.org/10.1007/978-4-431-55242-0_4

183.Dikshit A, Sarkar R, Pradhan B, Acharya S, Dorji K (2019) Estimating Rainfall Thresholds for Landslide Occurrence in the Bhutan Himalayas. Water 11(8):1616. https://doi.org/10.3390/w11081616

184.Dixon N, Smith A, Flint JA, Khanna R, Clark B, Andjelkovic M (2018) An acoustic emission landslide early warning system for communities in low-income and middle-income countries. Landslides 15(8):1631–1644. https://doi.org/10.1007/s10346-018-0977-1

185.DMG (1994) Geological Map of Nepal. Department of Mines and Geology, Government of Nepal. https://dmgnepal.gov.np/. Accessed 14 April 2022.

186.Ghimire SK, Higaki D, Bhattarai TP (2013) Estimation of Soil Erosion Rates and Eroded Sediment in a Degraded Catchment of the Siwalik Hills, Nepal. Land 2(3):370–391. https://doi.org/10.3390/land2030370

187.Gnyawali KR, Adhikari BR (2017) Spatial Relations of Earthquake Induced Landslides Triggered by 2015 Gorkha Earthquake Mw = 7.8. In: Mikoš M, Casagli N, Yin Y, Sassa K (eds) Advancing Culture of Living with Landslides. Springer International Publishing, Cham, pp 85–93. https://doi.org/10.1007/978-3-319-53485-5_10

188.Gnyawali KR, Zhang Y, Wang G, Miao L, Pradhan AMS, Adhikari BR, Xiao L (2020) Mapping the susceptibility of rainfall and earthquake triggered landslides along China–Nepal highways. Bull Eng Geol Environ 79(2):587–601. https://doi.org/10.1007/s10064-019-01583-2

189.GoN/NPC (2002) Tenth periodic plan. Government of Nepal, National Planning Commission, Singha Durbar, Kathmandu, Nepal. [online] Available at: https://www.npc.gov.np/en/category/periodic_plans. Accessed 18 Jul 2022

190.Green R (1978) The construction and management of bench terracing system in the hill areas of Nepal. His Majesty's Government of Nepal, Integrated Watershed Management Torrent Control and Land Use Development Project. Ministry of Forest, Department of Soil and Water Conservation, Kathmandu, Nepal. 69 pp.

191.Guzzetti F, Gariano SL, Peruccacci S, Brunetti MT, Marchesini I, Rossi M, Melillo M (2020) Geographical landslide early warning systems. Earth-Science Reviews 200:102973. https://doi.org/10.1016/j.earscirev.2019.102973

192.Hasegawa S, Dahal RK, Yamanaka M, Bhandary NP, Yatabe R, Inagaki H (2009) Causes of large-scale landslides in the Lesser Himalaya of central Nepal. Environ Geol 57(6):1423–1434. https://doi.org/10.1007/s00254-008-1420-z

193.Intrieri E, Gigli G, Casagli N, Nadim F (2013) Brief communication "Landslide Early Warning System: toolbox and general concepts." Natural Hazards and Earth System Sciences 13(1):85–90. https://doi.org/10.5194/nhess-13-85-2013

194.JICA (2009) The study on disaster risk management for Narayangharh, Mugling highway. Japan International Cooperation Agency. Final report, Volume I, Summary, Nippon koei co., Ltd. pp 4-11. http://open_jicareport.jica.go.jp/pdf/11922242_01.pdf

195.Jones S, Oven KJ, Manyena B, Aryal K (2014) Governance struggles and policy processes in disaster risk reduction: A case study from Nepal. Geoforum 57:78–90. https://doi.org/10.1016/j.geoforum.2014.07.011

196.Kafle S (2017) Disaster Early Warning Systems in Nepal: Institutional and Operational Frameworks. Geography and Natural Resources 2017, 7:2. https://doi.org/10.4172/2167-0587.1000196

197.Kanungo DP, Sharma S (2014) Rainfall thresholds for prediction of shallow landslides around Chamoli-Joshimath region, Garhwal Himalayas, India. Landslides 11(4):629–638. https://doi.org/10.1007/s10346-013-0438-9

198.Koirala P, Thakuri S, Joshi S, Chauhan R (2019) Estimation of Soil Erosion in Nepal Using a RUSLE Modeling and Geospatial Tool. Geosciences 9(4):147. https://doi.org/10.3390/geosciences9040147

199.Konjyosom Rural Municipality (2019) Konjyosom Rural Municipality Profile. Konjyosom Rural Municipality Office. https://www.konjyosommun.gov.np/publications. Accessed 14 April 2022.

200.Krøgli IK, Devoli G, Colleuille H, Boje S, Sund M, Engen IK (2018) The Norwegian forecasting and warning service for rainfall- and snowmelt-induced landslides. Natural Hazards and Earth System Sciences 18(5):1427–1450. https://doi.org/10.5194/nhess-18-1427-2018

201.Lacasse S, Nadim F, Lacasse S, Nadim F (2009) Landslide Risk Assessment and Mitigation Strategy. In: Sassa K, Canuti P (eds) Landslides – Disaster Risk Reduction. Springer, Berlin, Heidelberg, pp 31–61. https://doi.org/10.1007/978-3-540-69970-5_3

202.Malla SB, Dahal RK, Hasegawa S (2020) Analyzing the disaster response competency of the local government official and the elected representative in Nepal. Geoenvironmental Disasters 7(1):15. https://doi.org/10.1186/s40677-020-00153-z

203.McAdoo BG, Quak M, Gnyawali KR, Adhikari BR, Devkota S, Rajbhandari PL, Sudmeier-Rieux K (2018) Roads and landslides in Nepal: how development affects

environmental risk. Natural Hazards and Earth System Sciences 18(12):3203–3210. https://doi.org/10.5194/nhess-18-3203-2018

204.McColl ST (2015) Landslide Causes and Triggers. In: Landslide Hazards, Risks, and Disasters. Elsevier, pp 17–42. https://doi.org/10.1016/B978-0-12-396452-6.00002-1

205.Miao F, Wu Y, Li L, Liao K, Xue Y (2021) Triggering factors and threshold analysis of baishuihe landslide based on the data mining methods. Nat Hazards 105(3):2677–2696. https://doi.org/10.1007/s11069-020-04419-5

206.Michoud C, Bazin S, Blikra LH, Derron M-H, Jaboyedoff M (2013) Experiences from site-specific landslide early warning systems. Natural Hazards and Earth System Sciences 13(10):2659–2673. https://doi.org/10.5194/nhess-13-2659-2013

207.Mupangwa W, Twomlow S, Walker S, Hove L (2007) Effect of minimum tillage and mulching on maize (Zea mays L.) yield and water content of clayey and sandy soils. Physics and Chemistry of the Earth, Parts A/B/C 32(15):1127–1134. https://doi.org/10.1016/j.pce.2007.07.030

208.Okamura M, Bhandary NP, Mori S, Marasini N, Hazarika H (2015) Report on a reconnaissance survey of damage in Kathmandu caused by the 2015 Gorkha Nepal earthquake. Soils and Foundations 55(5):1015–1029. https://doi.org/10.1016/j.sandf.2015.09.005

209.Osanai N, Shimizu T, Kuramoto K, Kojima S, Noro T (2010) Japanese early-warning for debris flows and slope failures using rainfall indices with Radial Basis Function Network. Landslides 7(3):325–338. https://doi.org/10.1007/s10346-010-0229-5

210.Pandey P, Gurung A (2022) Soil loss and erosion potential estimation of Jhimruk watershed, Nepal. Environ Earth Sci 81(20):496. https://doi.org/10.1007/s12665-022-10602-7

211.Piciullo L, Calvello M, Cepeda JM (2018) Territorial early warning systems for rainfall-induced landslides. Earth-Science Reviews 179:228–247. https://doi.org/10.1016/j.earscirev.2018.02.013

212.Pandit K, Balla MK (2004) Indigenous knowledge of terrace management in Paundi Khola watershed, Lamjung district, Nepal. Himalayan Journal of Sciences 2(3):33–36. https://doi.org/10.3126/hjs.v2i3.228

213.Rogers D and Tsirkunov V (2010) Costs and benefits of early warning systems. Global Assessment Report on Disaster Risk Reduction. The World Bank, 17pp.

https://documents1.worldbank.org/curated/pt/609951468330279598/pdf/693580ESW0P1230aster0Risk0Reduction.pdf. Accessed 29 April 2022.

214.Segoni S, Lagomarsino D, Fanti R, Moretti S, Casagli N (2015) Integration of rainfall thresholds and susceptibility maps in the Emilia Romagna (Italy) regional-scale landslide warning system. Landslides 12(4):773–785. https://doi.org/10.1007/s10346-014-0502-0

215.Sharma S, Khadka N, Hamal K, Baniya B, Luintel N, Joshi BB (2020) Spatial and Temporal Analysis of Precipitation and Its Extremities in Seven Provinces of Nepal (2001-2016). Applied Ecology and Environmental Sciences :64–73. https://doi.org/10.12691/aees-8-2-4

216.Siart C, Bubenzer O, Eitel B (2009) Combining digital elevation data (SRTM/ASTER), high resolution satellite imagery (Quickbird) and GIS for geomorphological mapping: A multi-component case study on Mediterranean karst in Central Crete. Geomorphology 112(1):106–121. https://doi.org/10.1016/j.geomorph.2009.05.010

217.Sultana N, Tan S (2021) Landslide mitigation strategies in southeast Bangladesh: Lessons learned from the institutional responses. International Journal of Disaster Risk Reduction 62:102402. https://doi.org/10.1016/j.ijdrr.2021.102402

218.Thapa PB (2015) Occurrence of landslides in Nepal and their mitigation options. Journal of Nepal Geological Society 49(1):17–28. https://doi.org/10.3126/jngs.v49i1.23138

219.Thapa PS, Adhikari BR (2019) Development of community-based landslide early warning system in the earthquake-affected areas of Nepal Himalaya. J Mt Sci 16(12):2701–2713. https://doi.org/10.1007/s11629-019-5586-5

220.Timilsina M, Bhandary NP, Dahal RK, Yatabe R (2017) Large-Scale Landslide Inventory Mapping in Lesser Himalaya of Nepal Using Geographic Information System. In: Yamagishi H, Bhandary NP (eds) GIS Landslide. Springer Japan, Tokyo, pp 97–112. https://doi.org/10.1007/978-4-431-54391-6_6

221.Uddin K, Abdul Matin M, Maharjan S (2018) Assessment of Land Cover Change and Its Impact on Changes in Soil Erosion Risk in Nepal. Sustainability 10(12):4715. https://doi.org/10.3390/su10124715

222. Wang X, Xiao Y, Shi W, Ren J, Liang F, Lu J, Li H, Yu X (2022) Forensic analysis and numerical simulation of a catastrophic landslide of dissolved and fractured rock slope subject to underground mining. Landslides 19(5):1045–1067. https://doi.org/10.1007/s10346-021-01842-y

223. West AJ, Arnold M, AumaÎtre G, Bourlès DL, Keddadouche K, Bickle M, Ojha T (2015) High natural erosion rates are the backdrop for present-day soil erosion in the agricultural Middle Hills of Nepal. Earth Surf Dynam 3(3):363–387. https://doi.org/10.5194/esurf-3-363-2015

224. World Bank Group (2015) Nepal - Earthquake post disaster needs assessment: sector reports. Washington, D.C.: World Bank Group.pp.25-27. https://documents.worldbank.org/en/publication/documents-reports/documentdetail/546211467998818313/nepal-earthquake-post-disaster-needs-assessment-sector-reports. Accessed 11 May 2022.

225. Hyogo Framework for Action 2005-2015: Building the resilience of nations and communities to disasters - full text | *UNDRR*. (2007, November 15). https://www.undrr.org/publication/hyogo-framework-action-2005-2015-building-resilience-nations-and-communities-disasters

226. Third UN World Conference on Disaster Risk Reduction (WCDRR)—Resilient people. Resilient planet. (2015). Retrieved June 16, 2023, from https://www.wcdrr.org/

227. FAO and UNEP. (2020). *The State of the World's Forests 2020: Forests, biodiversity and people*. FAO and UNEP. https://doi.org/10.4060/ca8642en

228. Lo, V. (2016). Synthesis report on experiences with ecosystem-based approaches to climate change adaptation and disaster risk reduction. Technical Series No.85. Secretariat of the Convention on Biological Diversity, Montreal, 106 pages

229. Marongiu, I., & Cencetti, T. (2013). *Natural Resource Management—Handbook. "Soil Bio-engineering techniques for Slope protection and Stabilization."*.

230. Poratelli, F., Accastello, C., Freppaz, M., & Brun, F. (2020). Integrated grey-green management of avalanche risk: Economic and ecologic evidences from the Western Italian Alps. *International Journal of Disaster Risk Reduction*, *46*, 101502. https://doi.org/10.1016/j.ijdrr.2020.101502

231.Dorren, L., & Moos, C. (2022). Towards quantitative evidence of Eco-DRR in mountains: A concise review. *Ecological Engineering*, *175*, 106485. https://doi.org/10.1016/j.ecoleng.2021.106485

232.Howell, J. (2001) Application of bio-engineering in slope stabilization: experience from Nepal. In: Tianchi L, Chalise SR, Upreti BN (eds) Landslide hazard mitigation in the Hindu Kush-Himalayas. International Centre for Integrated Mountain Development (ICIMOD), Kathmandu, pp 147–161.

233.Ammann M, Böll A, Rickli C, Speck T, Holdenrieder O (2009) Significance of tree root decomposition for shallow landslides. For Snow Landsc Res 82(79–94):79

234.Norris, J. E., Greenwood, J. R., Achim, A., Gardiner, B. A., Nicoll, B. C., Cammeraat, E., & Mickovski, S. B. (2008). Hazard Assessment of Vegetated Slopes. In J. E. Norris, A. Stokes, S. B. Mickovski, E. Cammeraat, R. van Beek, B. C. Nicoll, & A. Achim (Eds.), *Slope Stability and Erosion Control: Ecotechnological Solutions* (pp. 119–166). Springer Netherlands. https://doi.org/10.1007/978-1-4020-6676-4_5

235.Stokes, A., Norris, J. E., van Beek, L. P. H., Bogaard, T., Cammeraat, E., Mickovski, S. B., Jenner, A., Di Iorio, A., & Fourcaud, T. (2008). How Vegetation Reinforces Soil on Slopes. In J. E. Norris, A. Stokes, S. B. Mickovski, E. Cammeraat, R. van Beek, B. C. Nicoll, & A. Achim (Eds.), *Slope Stability and Erosion Control: Ecotechnological Solutions* (pp. 65–118). Springer Netherlands. https://doi.org/10.1007/978-1-4020-6676-4_4

236.Reubens, B., Poesen, J., Danjon, F., Geudens, G., & Muys, B. (2007). The role of fine and coarse roots in shallow slope stability and soil erosion control with a focus on root system architecture: A review. *Trees*, *21*(4), 385–402. https://doi.org/10.1007/s00468-007-0132-4

237.Preti, F. (2013). Forest protection and protection forest: Tree root degradation over hydrological shallow landslides triggering. *Ecological Engineering*, *61*, 633–645. https://doi.org/10.1016/j.ecoleng.2012.11.009

238.Munang, R., Thiaw, I., Alverson, K., Liu, J., & Han, Z. (2013). The role of ecosystem services in climate change adaptation and disaster risk reduction. *Current Opinion in Environmental Sustainability*, *5*(1), 47–52. https://doi.org/10.1016/j.cosust.2013.02.002

239.Dalton, J.; Murti, R. ; Chandra, A. (2013) . Utilizing Integrated Water Resource Management Approaches to Support Disaster Risk Reduction. In The Role of Ecosystems in Disaster Risk Reduction; Sudmeier-Rieux, K., Estrella, M., Eds.; United Nations University Press: Bonn, Germany, 2013

240.Forestry Agency (2021). Annual Report on Forest and Forestry in Japan. Ministry of Agriculture, Forestry and Fisheries, Japan. Retrieved June 17, 2023, from https://www.maff.go.jp/e/data/publish/attach/pdf/index-96.pdf

241.Forbes, K., Broadhead, J., Bischetti, G. B., Brardinoni, F., Dykes, A., Gray, D., Imaizumi, F., Kuriakose, S. L., Osman, N., Petley, D., Stokes, A., & Verbist, B. (2011). *Forests and landslides The role of trees and forests in the prevention of landslides and rehabilitation of landslide-affected areas in Asia*. Retrieved June 17, 2023, from https://www.semanticscholar.org/paper/Forests-and-landslides-The-role-of-trees-and-in-the-Forbes-Broadhead/79d0040c9910f642ac5b0db605b317bb4e21e76e

242.Takeuchi, K., Nakayama, N., Teshima, H., Takemoto, K., & Turner, N. (2016). Ecosystem-Based Approaches Toward a Resilient Society in Harmony with Nature. In F. G. Renaud, K. Sudmeier-Rieux, M. Estrella, & U. Nehren (Eds.), *Ecosystem-Based Disaster Risk Reduction and Adaptation in Practice* (pp. 315–333). Springer International Publishing. https://doi.org/10.1007/978-3-319-43633-3_14

243.Thapa, P. S., Chaudhary, S., & Dasgupta, P. (2022). Contribution of integrated watershed management (IWM) to disaster risk reduction and community development: Lessons from Nepal. *International Journal of Disaster Risk Reduction*, *76*, 103029. https://doi.org/10.1016/j.ijdrr.2022.103029

244.Oki, Y., Kitazato, H., Fujii, T., & Yasukawa, S. (2022). Habitat mapping for human well-being: A tool for reducing risk in disaster-prone coastal environments and human communities. *Geological Society, London, Special Publications*, *505*(1), 271–282. https://doi.org/10.1144/SP505-2021-26

245.UN-ISDR (2004). Terminology of Disaster Risk Reduction. Geneva: United Nations International Strategy for Disaster Reduction.

LIST OF FIGURES

Figures used in Section 3.1 (Chapter 3)

Figures used in Section 3.2 (Chapter 3)

Figures used in Section 3.3 (Chapter 3)

Figures used in Section 4.1 (Chapter 4)

Figures used in Section 5.1 (Chapter 5)

LIST OF TABLES

Tables used in Section 3.1 (Chapter 3)

Tables used in Section 3.2 (Chapter 3)

Tables used in Section 3.3 (Chapter 3)

Tables used in Section 4.1 (Chapter 4)

Tables used in Section 5.1 (Chapter 5)

ABBREVIATIONS

ALOS PALSAR	Advanced Land Observing Satellite
DCP	Data Collection Platform
DEM	Digital elevation model
DRR	Disaster Risk reduction
ECO-DRR	Ecosystem-based disaster risk reduction
GIS	Geographical Information System
GSI	Geospatial Information Authority of Japan
Hr	Hour
Mo	Month
Yr	Year
IDW	Inverse distance weighted
JAXA	Japan Aerospace Exploration Agency
kNm	kilonewton meter
LEWS	Landslide Early warning system
LIDAR	Light Detection and Ranging
MLITT	Ministry of Land, Infrastructure, Transport and Tourism
Mo	Month
NTU	Nephelometric Turbidity Units
PALSAR	Phased Array Type L-band Synthetic Aperture Radar
SAR	Synthetic Aperture Radar
UAV	Unmanned Aerial Vehicle
XRD	X-ray diffraction analysis

LIST OF PUBLICATIONS

Published articles.

Thapa, P.S., Adhikari, B.R., Shaw, R. et al. Geomorphological analysis and early warning systems for landslide risk mitigation in Nepalese mid-hills. Nat Hazards (2023). https://doi.org/10.1007/s11069-023-05929-8

Thapa, P.S., Hanzawa, K., Katsumi, N., et al. Characteristics of Deep-seated Landslide and Debris-flow Prevention Function of Cedar Forest -Learnings from Hirose Landslide, Ishikawa Prefecture, Japan. Bulletin of Ishikawa Prefectural University. Vol. 06, pp (1-12) (2023). Available at: https://ishikawa-pu.repo.nii.ac.jp/?action=pages_view_main&active_action=repository_view_main_item_detail&item_id=215&item_no=1&page_id=13&block_id=21

Oral Presentations

Thapa P.S., Adhikari B.R., Shaw, R., Bhattarai, D., Yanai, S. Geomorphological analysis of landslide and early warning system for landslide risk mitigation in Nepalese mid-hills. Nepal Geological Society 35th Himalaya-Karakorum-Tibet Workshop. 2-4 November 2022, Hotel Pokhara Grande, Pokhara, Nepal. Abstract published: Journal of Nepal Geological Society, 2022, Vol. 64 (Sp. Issue), p 134.

Yanai S., Thapa, P.S., Katsumi, N., Momose, T. The role of the tephra layer in the landslides caused by the 2018 Hokkaido Eastern Iburi Earthquake, Japan. Nepal Geological Society 35th Himalaya-Karakorum-Tibet Workshop, Abstract published: Journal of Nepal Geological Society, 2022, Vol. 64 (Sp. Issue) p155. 2-4 November 2022, Hotel Pokhara Grande, Pokhara, Nepal.

Thapa P.S., Murakami, W., Daimaru, H., Yanai, S. Evaluation of Geomorphological Precursors and Triggering Factors of a Large-Scale Landslide in Mt. Hakusan, Central Japan. INTERPRAEVENT 2023 International Symposium Natural Disasters Occurrence, Reduction, and Restoration in Mountain Regions：17-18 April 2023, National Chung Hsing University, Taiwan.

Poster Presentations

Yanai, S., Thapa, P.S., Furuichi, T. Dating analysis of the landslides caused by the 2018 Hokkaido Eastern Iburi Earthquake. 17-18 April 2023, National Chung Hsing University, Taiwan.

Suzuki, M., Thapa, P.S., Katsumi, N., Daimaru, H., and Yanai, S. Revegetation after slope failure by the 2018 Hokkaido Eastern Iburi earthquake. 134th Annual Meeting of the Japanese Forest Society, 2023. Vol.134, p 209. Available at: https://www.forestry.jp/content/images/2023/03/%E7%AC%AC134%E5%9B%9E%E6%A3%AE%E6%9E%97%E5%AD%A6%E4%BC%9A%E5%A4%A7%E4%BC%9A%E5%AD%A6%E8%A1%93%E8%AC%9B%E6%BC%94%E9%9B%86.pdf

Under review article

Thapa P.S., Murakami, W., Daimaru, H., Yanai, S. Evaluation of Geomorphological Precursors and Triggering Factors of a Large-Scale Landslide in Mt. Hakusan, Central Japan. Landslides (2023). **Manuscript Number**: LASL-D-23-00304.

Thapa, P.S., Daimaru, H., Ichion, E. and Yanai, S. Impacts of sediment transported downstream from the 2015 deep-seated landslide in Mt. Hakusan, Japan. Earth Surface Processes and Landforms (2023). **Manuscript ID**: ESP-23-0216.

Future submissions (*Planned to submit soon*)

Thapa, P.S., Daimaru, H., Yanai, S. Analysis of an ecosystem-based approach to the restoration of a Sennindani 2015 Landslide, Mt. Hakusan, Central Japan. International Journal of Disaster Risk Reduction or Engineering Ecology (2023).